

# INTERACTION OF PLANNING REGIONS IN CORTEX

Thesis by

Chess Stetson

In Partial Fulfillment of the Requirements

for the Degree of

Doctor of Philosophy

California Institute of Technology

Pasadena, California

2012

(Defended January 31, 2012)

© 2012

Robert Chess Abernathy Stetson

All rights reserved

## **Dedication**

**JSCS, RBCS, AKA, KAS, GAS, RJS**

## **Acknowledgement**

I would like to thank my advisor, Richard Andersen, for the opportunity to do this work, and for his guidance and the excellent laboratory environment he has provided. I would also like to thank my committee, Erik Winfree, Shinsuke Shimojo, Masakazu Konishi, and Ralph Adolphs for their guidance. I would like to thank Andrew Robertson, Arnulf Graf, Benjamin Novak, Benjamin Flusberg, Bijan Pesaran, Boris Revechkis, Cevat Ustun, David Eagleman, Erik Schomburg, Eunjung Hwang, Giulio Rottaro, Gloria Sheng, Grant Mulliken, Igor Kagan, Igor Fineman, Jeremy Emken, Kelsie Pejsa, Lindsay Bremner, Linus Schumacher, Markus Hauschild, Melanie Wilke, Nicole Sammons, Read Montague, Tobi Delbrueck, Tessa Yao, Viktor Shcherbatyuk, Vivian Yang, Xoana Troncosco, Xu Cui, and Yaser Abu-Mostafa for many productive and enjoyable discussions. I also feel very grateful for support from the Sloan Swartz Foundation and the National Institutes of Health, and for my time thus far as a member of the Caltech community.

# **Interaction of Planning Regions in Cortex**

**Thesis by Chess Stetson**

**In Partial Fulfillment of the Requirements of Doctor of Philosophy**

**California Institute of Technology**

**Pasadena, California**

**2012**

**Advisor: Prof. Richard A. Andersen**

## **Abstract**

To what extent do parietal and frontal areas involved in action planning interact as a monkey plans a movement? This report seeks an answer using the timing relationships between action potentials, local field potentials (LFPs) and behavioral events as a monkey plans reaches and eye movements to remembered targets. Both parietal reach region (PRR) and dorsal premotor cortex (PMd) show similar profiles of activity characteristic of action planning. In some cases, both premotor and intraparietal areas show decision-making activity far earlier than previously anticipated, even before the onset of the trial. However, despite their similarities in action planning, PMd responds tens of milliseconds sooner to targets and movement instructions. These results suggest that PMd precedes PRR, apparently contrary to a common heuristic about the chain of processing from sensation to action. On the other hand, during periods of steady state, as the monkey anticipates information or plans a movement, the apparent

directionality of fronto-parietal interaction may reverse. Coherent phase-locking between action potentials and local field potentials (LFPs), which has been implicated in directional influence between brain regions, is highly significant from PRR to PMd, but not vice-versa. Spikes in PRR cohere with LFPs in PMd between 15–25 Hz, whereas spikes in PMd do not cohere with LFPs in PRR at any frequency. This uni-directional spike-LFP coherence varies over the course of the trial, achieving a peak in magnitude and frequency, on average, during the planning period. The phase-locking component of the coherence shows weak but significant variation according to the particular action being planned. The cross-cortical coherence also varies significantly with cortical anatomy. Coherence is stronger between spikes in PRR and LFPs in its anatomical target PMd than between PRR and other recording areas within and beyond the arcuate sulcus (associated with saccades, and not known to be connected with PRR). The asymmetry of spike - LFP coherence, its task-dependence, and variation over cortical territory add to a growing body of knowledge implicating the intraparietal sulcus as the center of a network of beta-band activity characteristic of action planning. This highly specific beta-band oscillation links frontal and parietal planning regions at the single cell level. Overall, these results suggest an interplay between premotor and parietal regions, with influence shifting back and forth according to the phase of behavior.

## Table of Contents

Acknowledgement .....	iii
Abstract .....	iv
Table of Contents .....	vi
List of Figures .....	viii
Abbreviations and Lexicon .....	x
<b>1 Introduction .....</b>	<b>1</b>
1.1 Cross-cortical influence .....	1
1.2 Functional connectivity .....	4
1.3 Measures of connectivity and influence .....	6
1.4 Locality of the LFP .....	10
1.5 Functionally similar, anatomically distinct .....	12
<b>2 Evoked Responses .....</b>	<b>21</b>
2.1 Visually evoked responses .....	21
2.2 Timing of responses to spatial and effector instructions .....	25
<b>3 Effector Decisions in Frontal and Parietal Cortices .....</b>	<b>31</b>
3.1 Effector decisions during the planning period .....	31
3.2 Effector decisions in PM and IPS during blind choice .....	33

<b>4</b>	<b>Oscillatory Properties of Frontal and Parietal Cortices</b> .....	41
4.1	LFP and spiking spectra .....	41
4.2	Development of LFP power within the task .....	43
4.3	Spike-LFP coherence within individual cortical regions .....	51
<b>5</b>	<b>Interaction of Signals Across Cortex</b> .....	60
5.1	Spike-spike interactions .....	60
5.2	LFP-LFP coherence .....	61
5.3	Cross-cortical spike-LFP coherence .....	70
5.4	Meaning of the PRR-PMd spike-LFP coherence asymmetry .....	82
<b>6</b>	<b>Comments on Recurrent Networks</b> .....	90
6.1	Consequences of a single $\beta$ -band input into a recurrent network .....	90
6.2	Coherence and mutual information .....	92
6.3	Connectivity between PRR and PMd .....	95
<b>7</b>	<b>Conclusion</b> .....	97
<b>8</b>	<b>Appendix: Methods for Neurophysiology</b> .....	106
<b>9</b>	<b>References</b> .....	111

## List of Figures

Figure 1.1.1 .....	2
Figure 1.2.1 .....	5
Figure 1.4.1 .....	11
Figure 1.5.1 .....	13
Figure 1.5.2 .....	14
Figure 1.5.3 .....	16
Figure 1.5.4 .....	17
Figure 1.5.5 .....	18
Figure 1.5.6 .....	20
Figure 2.1.1 .....	22
Figure 2.1.2 .....	24
Figure 2.2.1 .....	26
Figure 2.2.2 .....	27
Figure 2.2.3 .....	29
Figure 3.1.1 .....	32
Figure 3.2.1 .....	36
Figure 3.2.2 .....	38
Figure 4.1.1 .....	42
Figure 4.1.2 .....	43
Figure 4.2.1 .....	44
Figure 4.2.2 .....	46
Figure 4.2.3 .....	48
Figure 4.2.4 .....	50
Figure 4.3.1 .....	52
Figure 4.3.2 .....	54
Figure 4.3.3 .....	56
Figure 4.3.4 .....	59
Figure 5.1.1 .....	60
Figure 5.2.1 .....	63
Figure 5.2.2 .....	64
Figure 5.2.3 .....	67
Figure 5.2.4 .....	68
Figure 5.3.1 .....	73
Figure 5.3.2 .....	77
Figure 5.3.3 .....	79

Figure 5.3.4 .....	81
Figure 5.3.5 .....	86
Figure 6.1.1 .....	91
Figure 6.2.1 .....	94
Figure 6.4.1 .....	96
Summary figure 7.1 .....	97
Summary figure 7.2 .....	98
Summary figure 7.3 .....	99
Summary figure 7.4 .....	99
Summary figure 7.5 .....	100
Summary figure 7.6 .....	101
Summary figure 7.7 .....	102
Summary figure 7.8 .....	103
Summary figure 7.9 .....	104

## Abbreviations and Lexicon

$\alpha$  (Alpha) — 8–13Hz

$\beta$  (Beta) — 13–30Hz

$\gamma$  (Gamma) — 30–100Hz

effector — either a reach or saccade

FEF (frontal eye fields) — region around the nadir of the arcuate sulcus, associated with eye movements

LFP (local field potential) — low-pass filtered, oscillatory activity recorded from sharp electrodes, thought to represent a sum of inputs or local processing within a cortical region

LIP (lateral Intraparietal) — a region in the lateral bank of the intraparietal sulcus, known to correlate with the directionality of upcoming movements, particularly saccades

PRR (parietal reach region) — a region on the caudal aspect of the medial bank of the intraparietal sulcus, activated in advance of reaching movements

PMd (dorsal premotor cortex) — a brain region rostral to the primary motor strip, medial to the arcuate sulcus, thought to be involved in the preparation of reaching movements.

saccade — a ballistic movement of the eye

S.E.M — standard error of the mean

# 1 Introduction

## 1.1 Cross-cortical influence

Decades of single-unit neurophysiology have revealed a wealth of knowledge about the function of individual cortical areas, yet we know relatively little of how they interact. In particular, do separate patches of cortex with the same functional properties act together? Consider the dorsal premotor area (PMd) and parietal reach region (PRR), which both show evidence of planning activity, but are separated by other cortical areas with lower-level and more stereotyped sensory and motor properties. Do PRR and PMd interact as an animal plans an action?

A popular heuristic for understanding reach planning in cortex dictates that sensory information enters the striate cortex in the occipital lobe, travels forward, and eventually reaches the motor areas to produce an action (fig. 1.1.1). This idea has its roots in the so-called “dorsal and ventral stream” hypothesis [Goodale and Milner, 1992; Ungerleider and Mishkin, 1982], which implies an ever higher-level representation (“perception”) as information travels anteriorly. Neurons along the dorsal stream, starting in the visual cortex and continuing through the parietal lobe, have been shown to encode information about where a target is or how an upcoming action will be performed. The dorsal/ventral stream framework was proposed as a way of distinguishing large classes of cells involved in two different kinds of perception (“where” or “how” in dorsal, “what” in ventral). A seemingly natural addition is to think of the dorsal stream as extending beyond perceptual areas toward motor areas in the frontal lobe, thereby closing the perception-action loop (see fig. 1.1.1; Dwight et al., 2011; Mulliken, 2008).

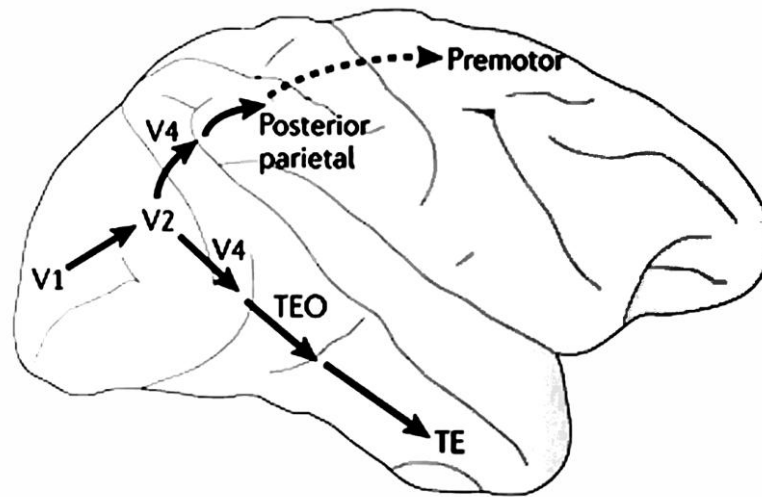


**Figure 1.1.1:** A heuristic for cortical communication. The classic picture from Goodale and Milner [1992], has been augmented with a parieto-frontal projection to close the perception-action loop (adapted from Dwight et al. [2011]). The “where/how” perception pathway, ending in posterior parietal cortex of the macaque, influences premotor cortex to produce actions.

A somewhat different notion was proposed by Fuster in 1995, though with reference largely to the interaction between primary sensory and motor areas. Nevertheless, as in the dorsal stream hypothesis, sensory information travels up a hierarchy from simple processing areas to higher-level association areas, then onward to prefrontal cortex, and down to the motor cortex where actions are generated. However, feedback connections exist at every stage, and also connect equivalent levels of the hierarchy, so that low-level sensory areas are also directly connected to low-level motor areas. Within this feedback framework, some motor areas could show evidence of visual input before certain higher-level sensory areas. However, as in the dorsal stream pictured in fig.

1.1.1, the Fuster model implies a causal hierarchy, such that higher level areas may drive lower-level areas in the absence of sensory input [Rao and Ballard, 1999] or motor output.

The aforementioned general frameworks (feed-forward vs. recurrent) could be distinguished in part by responses of single neurons to visual input. But which cortical area drives the other when no visual input is present? Understanding directions of influence in general will require recognizing the forest, rather than just the trees. Knowing the properties of single neurons alone will not suffice. Distinguishing between these large-scale networks requires a study of many neurons' interaction

So-called higher-level cortical areas, such as PRR and PMd, can predict a monkey's future movements. This predictive capacity in PRR and PMd neurons persists even at times when inputs are neither present, nor outputs permitted, such as when a monkey plans an action to a remembered target. How might PRR and PMd interact during this kind of planning?

## 1.2 Functional connectivity

The simplified frameworks for cortical interaction described in section 1.2 do no justice to the complexity of anatomical connectivity in cortex [Felleman and Van Essen, 1991].

Instead, these heuristics may be more appropriate for understanding *functional* connectivity. The byzantine anatomical connections between areas may be unwieldy, yet the brain may also organize large classes of cells into functional sub-networks, as a way of modularizing computation. That is, among a large group of anatomically connected regions, different subsets may be functionally connected at different times. Consider tapping your toes and humming in rhythm, and later walking and chewing gum completely asynchronously.

Indeed, synchrony may be the key to functional connectivity. Two theories for synchronous functional connectivity are outlined in fig. 1.1.2. Spikes can either adopt a preferred phase (fig. 1.2.1.A) or frequency (fig. 1.2.1.B), with the goal of arriving at a local peak in the sub-threshold membrane potential in a downstream target and generating a further spike.

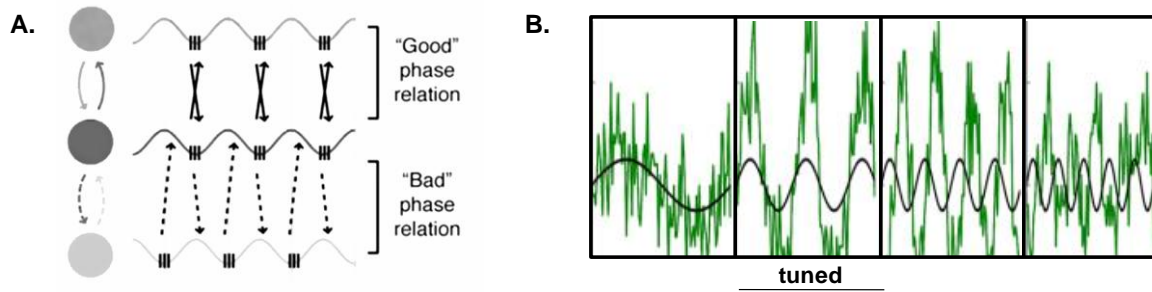


**Figure 1.2.1:** Candidate mechanisms for functional connectivity. **A.** Spikes may synchronize at an advantageous phase for the purpose of establishing communication (adapted from Womelsdorf et al. [2008]). **B.** Spikes may adopt a preferred frequency in order to isolate downstream targets (adapted from Akam and Kullman [2010]). Neural activity (green) is greater at the preferred frequency (“tuned”) but filtered out at higher frequencies, resulting in a lower amplitude and a phase offset. In both cases, communicating spikes will line up with the peaks in the sub-threshold membrane potential of downstream targets.

The entrainment-by-phase and by-frequency hypotheses imply somewhat different mechanisms. In order to for one area to entrain another by frequency, the first need only start firing at the tuned frequency of the second. In contrast, to entrain two areas at a particular phase, the correct phase must be provided independently to one or both regions. Despite their differences, both mechanisms would be expected to result in prominent and synchronous oscillatory activity across cortical tissue.

In general, local field potentials (LFPs) exhibit a  $1/f^n$  frequency profile in the brain, the natural result of a random point-process, such as spikes, integrated or convolved with a slow waveform, such as an excitatory post-synaptic potential. However, significant

deviations from this frequency profile exist in the brain, and seem to be associated with specific brain areas and tasks. Notably, theta (2–8 Hz) oscillations in the hippocampus have been associated with navigation [Huxter et al., 2003]. Gamma (30–100 Hz) oscillations are particularly strong in the visual cortices [Gray and Singer, 1989], and are strongly modulated by attention [Fries et al., 2001]. Beta-band (12–25 Hz) oscillations, while less well studied, are strong in the intraparietal sulcus [Brovelli et al., 2004], and can code for movement plans, including the direction [Hwang and Andersen, 2009] and the effector [Scherberger et al., 2005] for in an upcoming movement. The purpose of these oscillations may be to synchronize cortical networks to form functional links [Buzsaki, 2006].

### **1.3 Measures of connectivity and influence**

The intent of this research is the use of electrical recordings in multiple brain regions to determine influence and connectivity, by comparing and correlating these recordings in the time and frequency domain. The most basic measure of influence at our disposal is a comparison of evoked responses in two regions in the time domain. In two regions A and B, known to be connected, A is likely upstream of B if it responds earlier to a stimulus.

Other time-domain measures, such as the cross-correlation, can likewise be used to interpret influence. A consistent timing offset between two regions could be interpreted to represent a causal interaction. Cross-correlation, or spike-triggered averaging, can be used when one region is thought to influence another at a delay. The Granger causality, an autoregressive measure which is asymmetric in time, summarizes a delayed

correlative effect into a single number [Granger, 1969; Baccala and Sameshima, 2001]. These correlative and autoregressive measures would be useful for revealing any process in which an input affects an output at a delay, for example, a spike in one region creating a downstream post-synaptic potential in a second after axonal propagation.

Functional connectivity, on the other hand, may not take the simple form of a signal in A smeared out in time and added to B. As discussed in 1.1.3, two regions could be co-modulated at a given frequency and phase-offset, for the purpose of creating a functional channel. Or one region might only influence another at a given frequency, as in the case of the filtering network. To test for these kinds of interaction, a time-domain measure might not be appropriate. Cross-correlation would produce an oscillatory plot, not easily understood as a single measure of connectivity. A more appropriate measure would assess the interaction directly in the frequency domain, by calculating the consistency of phase offset. The coherence provides such a measure,

$$C(S, L) = \frac{\langle S\bar{L} \rangle}{\langle |S| \rangle \langle |L| \rangle} . \quad (1)$$

S and L are the Fourier transforms of time-domain signals s and l, and  $\bar{L}$  is the complex conjugate of L. A useful feature of the coherence is that normalizes for the average power of the two signals. Thus, oscillatory components in both signals, which may be unrelated but are high enough in power to induce spurious noise in the time domain measures, will be eliminated in the coherence. The coherence may also be partialized, in order to remove the effects of a third signal [Gersch and Goddard, 1970]:

$$P(S, L_2|L_1) = \frac{C(S, L_2) - C(S, L_1)C(L_1, L_2)}{\sqrt{1 - C(S, L_1)^2}\sqrt{1 - C(L_1, L_2)^2}} . \quad (2)$$

While normalized for average power, the coherence responds to co-fluctuations in amplitude on an epoch-by-epoch basis. Correlations in amplitude at the frequency of interest might be an important component of the interaction between two regions, as in the filtering interaction suggested in fig. 1.2.1.B. However, if phase-locking alone is sought, a measure which eliminates power correlations would be desirable. An unconventional variant of the coherence averages over the power on an epoch-by-epoch basis, isolating only phase-locking between regions:

$$C_p(S, L) = \left\langle \frac{S\bar{L}}{|S||L|} \right\rangle \quad (3)$$

This variant is explored in section 5.3. Still another variant of a phase-locking measure is the spike-triggered version [Vinck et al., 2011], which will reveal phase interactions at a given frequency, but is centered on individual spikes rather than on arbitrary windows of spiking:

$$P_l(l, s) = \left\langle FFT(l_s) \right\rangle \quad (4)$$

Also worthy of mention is the frequency-domain Granger-causality, and the partial-directed coherence [Baccala and Sameshima]. These are autoregressive measures, where the autoregressive components in time are transformed into the frequency domain. Frequency-domain Granger causality [Baccala and Sameshima, 2001; Brovelli et al., 2004], or partial directed coherence, imposes the time asymmetry required for an interpretation of causality while maintaining frequency-domain specificity, potentially allowing this measure to reveal influences at different frequencies which actually go in the opposite direction from one another. The Granger causality measures how much A predicts B apart from what B predicts about itself, and the partial directed coherence

transforms this into the frequency domain. In other words, how much do deviations in amplitude and phase of a certain frequency component in A predict deviations at the same frequency in B? However, unlike the coherence, it does not normalize over the power at each frequency before the autoregressive step. Therefore, a relationship at one frequency is subject to noise from others. Also, the partial Granger causality is difficult to interpret between two signals polluted by different amounts of noise. If A drives B at a small time lag (much less than the period of the signal of interest), and C equals A with copious noise added, then B may actually become a better predictor of C than C is of itself. For this reason, partial directed causality is difficult to interpret when applied to spikes and LFPs. LFPs may very well be caused by the sum of spiking in many cells, yet an individual cell will not be highly predictive of the LFP, and will in fact be predictable of the LFP, making the LFP appear to cause the spike.

We would be remiss not to mention the most basic measure of communication, the mutual information [Shannon, 1948]. Between two signals, spike train  $s_1$  and  $s_2$ , the mutual information describes the reduction in uncertainty one has about  $s_1$  knowing  $s_2$ , and vice-versa:

$$mI(s_1, s_2) = \sum_{s_1, s_2} p(s_1, s_2) \log\left(\frac{p(s_1, s_2)}{p(s_1)p(s_2)}\right) \quad (5)$$

Despite the general applicability of the mutual information [Mulliken et al., 2008], its interpretation can sometimes be difficult in neuroscience applications where artifacts may be induced due to practical requirements, such as aliasing from windowing spike counts.

Section 6 discusses the relationship of mutual information (eq. 5) to the cross-cortical spike-LFP coherence (eq. 1). Section 5.2 describes partial directed causality as applied to LFP-LFP interactions, and section 5.3 uses phase-locking (eq. 4) to look for trial-by-trial variations in phase and magnitude of coherence. However, the bulk of this manuscript will be devoted to an understanding of the conventional coherence (eq. 1) between spikes and LFPs. The spike-LFP coherence makes few assumptions, and permits phase-locking (fig. 1.2.1.A), frequency-matching (fig. 1.2.1.B), and causal interpretations of the interaction.

## **1.4 Locality of the LFP**

The local field potential (LFP) is a low-pass filtered (usually  $< 300$  Hz) version of the electrical potential recorded on a sharp electrode. It has perhaps been surprising to see in recent years that the LFP has strong behavioral and perceptual correlates [Pesaran et al., 2002; Wilke et al., 2006]. Some have even suggested that it represents a fundamental computational tool for the brain, coupling neurons via direct electrical feedback [Anastassiou et al., 2011]. While the biophysical properties of the LFP are not yet fully understood, it is thought to have a small spatial extent, on the order of tens or hundreds of microns [Katzner, 2009]. Figure 1.4.1 shows an experiment comparing EEG to LFPs and membrane potentials in rat cortex. The traces show the similarity in LFPs and membrane potentials, which is not reflected in the larger-scale EEG.

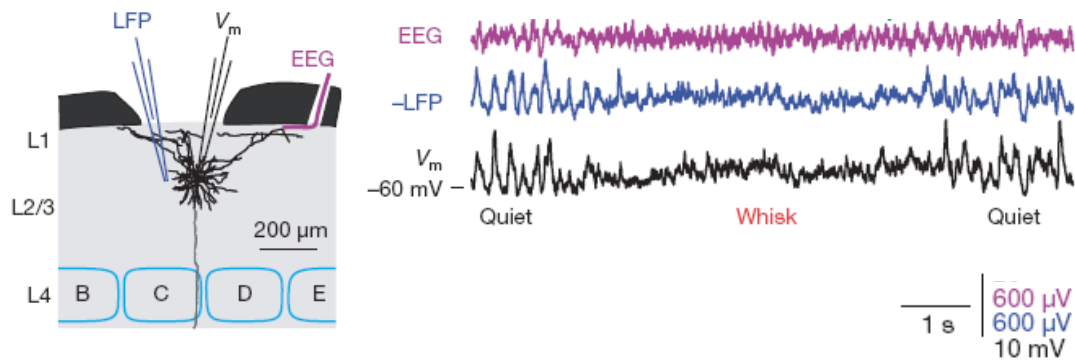


**Figure 1.4.1:** Adapted from Poulet and Petersen [2008]. Whole-cell patch clamp and simultaneous extracellular recordings were made in rat somatosensory barrel cortex. Throughout the experiments, LFPs correlated more strongly with membrane potential  $V_m$  than did subdural EEG.

Naturally, when neighboring cortical patches feature correlated LFPs, the spatial scale of the LFP becomes larger [Linden et al., 2011]. However, the working understanding in this manuscript is that LFPs represent a sum of local neural activity, with a physical size scale on the order of tens to hundreds of microns. Whether the source of the LFP is more heavily influenced by synaptic activity or cortical inputs [Mitzdorf, 1985], or is a simple average of local membrane potentials, awaits further study.

## 1.5 Functionally similar, anatomically distinct

A surprising property of the cerebral cortex is that vastly separated parts of the cortex behave the same way. Homologous locations in the two cerebral hemispheres, linked by the corpus callosum, have similar properties. Yet it is also remarkable to note the functional similarity between cortical patches in different lobes of the brain. Nowhere is this phenomenon clearer than between the intraparietal sulcus (IPS) and the premotor cortices (PM, fig. 1.5.1), both of which show similar planning activity [Chafee and Goldman-Rakic, 1998].

Planning denotes the preparation of a particular kind of movement to a spatial target, in the absence of visual stimuli. This report will exclusively deal with spatial and effector movement tasks, in which the monkey, starting from fixation, plans a movement to a spatial target by either reaching with his arm or saccading with his eyes (fig. 1.5.2).

Critically, following any instructions given, the animal is required to maintain fixation for a period of time during which there are no visual inputs. The lack of visual stimulus means that any persistent activity in these areas which predicts the upcoming action is not due to a sensory instruction. Even when the monkeys freely decide on how to move, without any explicit instruction, cellular activity during the planning period predicts the monkey's future action, suggesting that movement plans are represented in these regions as they are formed. This manuscript primarily deals with subsets of IPS and PM: the parietal reach region (PRR), an area generally on the medial bank of the intraparietal sulcus and known to be biased toward reaching movements [Snyder et al., 1997], and the dorsal premotor cortex (PMd), an area in the frontal lobe between the arcuate sulcus and the primary motor strip known to be involved in producing reaches [Cisek and Kalaska, 2005; Graziano, 2002]. Retrograde tracer studies have shown these areas to be

anatomically connected [Colby et al., 1988; Caminiti et al., 1999; Tanne-Gariepy et al., 2002]. Note that we also discuss a larger set of areas, including lateral intraparietal (LIP) and frontal eye fields (FEF) in section 3.2. Figure 1.5.1 shows approximate recording locations for PMd and PRR, superimposed over T-1 MRI slices from the approximate depth of the average recording.

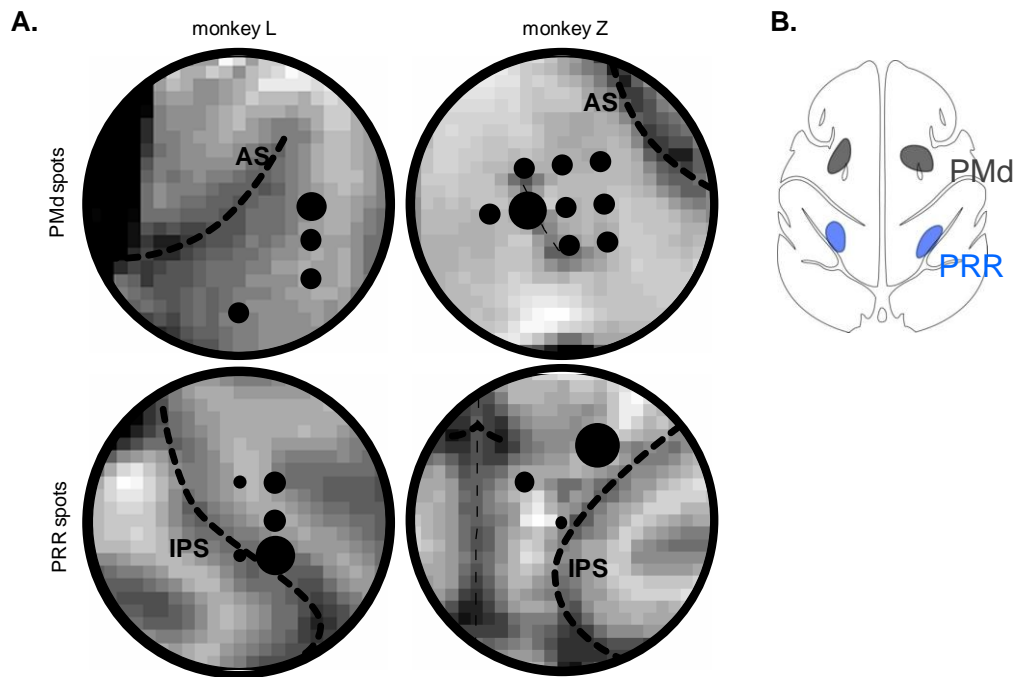


**Figure 1.5.1:** Reach-biased planning regions in frontal and parietal lobes. **A.** Dots superimposed on T-1 MRI slices from the approximate average depth of recording. Dotted lines represent approximate locations of the AS (arcuate sulcus) and IPS (intraparietal sulcus). **B.** Icon of the recording regions, as used in later figures

In order to determine whether PRR and PMd show evidence of communication as the monkey plans an action, the monkeys in this study performed a task in which they planned either a reach or a saccade to a remembered target in the right or left hemispace. Figure 1.5.2 shows a diagram of the task. The monkey held a central target for around one second, after which a peripheral target appeared and then disappeared. Still maintaining fixation, the monkey waited for around another second, and then made either a reach or a saccade (eye movement) to the location of the peripheral target (see Methods). The critical manipulation is the planning period, during which a representation of the target remains in working memory, and during which effector instructions may also be stored (in the case of effector instructed trials, see Methods), or an effector choice may develop [Cui and Andersen, 2007].

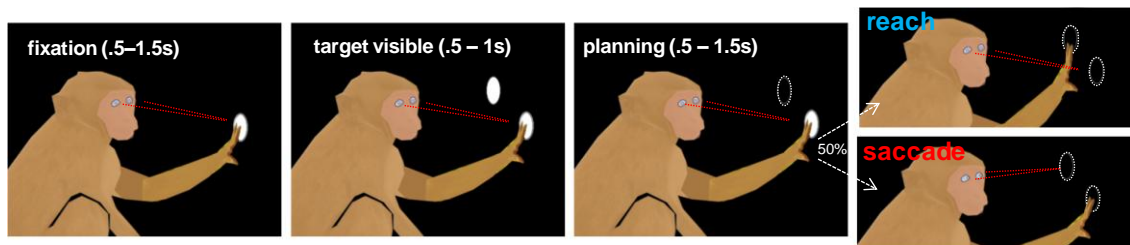


**Figure 1.5.2:** A spatial and effector task. Each monkey performed a memory-reach/saccade task in which he held a central illuminated fixation spot with his hand and eyes as a peripheral target appeared and disappeared. After a planning period, he made either a reach or saccade to the remembered target (reaches or saccades were either chosen, or instructed via a 50 ms color change in the target, with 50% probability; see Methods).

The recorded data show that PRR and PMd both exhibit visual responses and spatial selectivity (fig. 1.5.3) during planning. The bottom row shows a canonical cell type, recorded in the right PRR, with visual onset activity selective for the ipsilateral visual hemispace (blue), followed by persistent activity that continues for the entire duration of the memory period. When a contralateral target is presented, this cell does not fire during the memory period (orange). The second from the bottom row shows a more unusual cell, with persistent activity apparently preferring the opposite hemifield from the direction of the visual response. The top two rows were recorded on the same day, and show cells with small visual responses (but significant anticipatory activity in PMd) during the memory period. Both prefer the contralateral visual hemispace, and maintain the same visual tuning when the target is off as when it is on. The left PRR cell shows increased activity during movement, whereas the left PMd cell shows offset-related activity. Figure 1.5.4 summarizes the amount and directionality of the planning period directional tuning in PRR and PMd. In addition to visual tuning, these areas also exhibit pronounced effector-tuning.

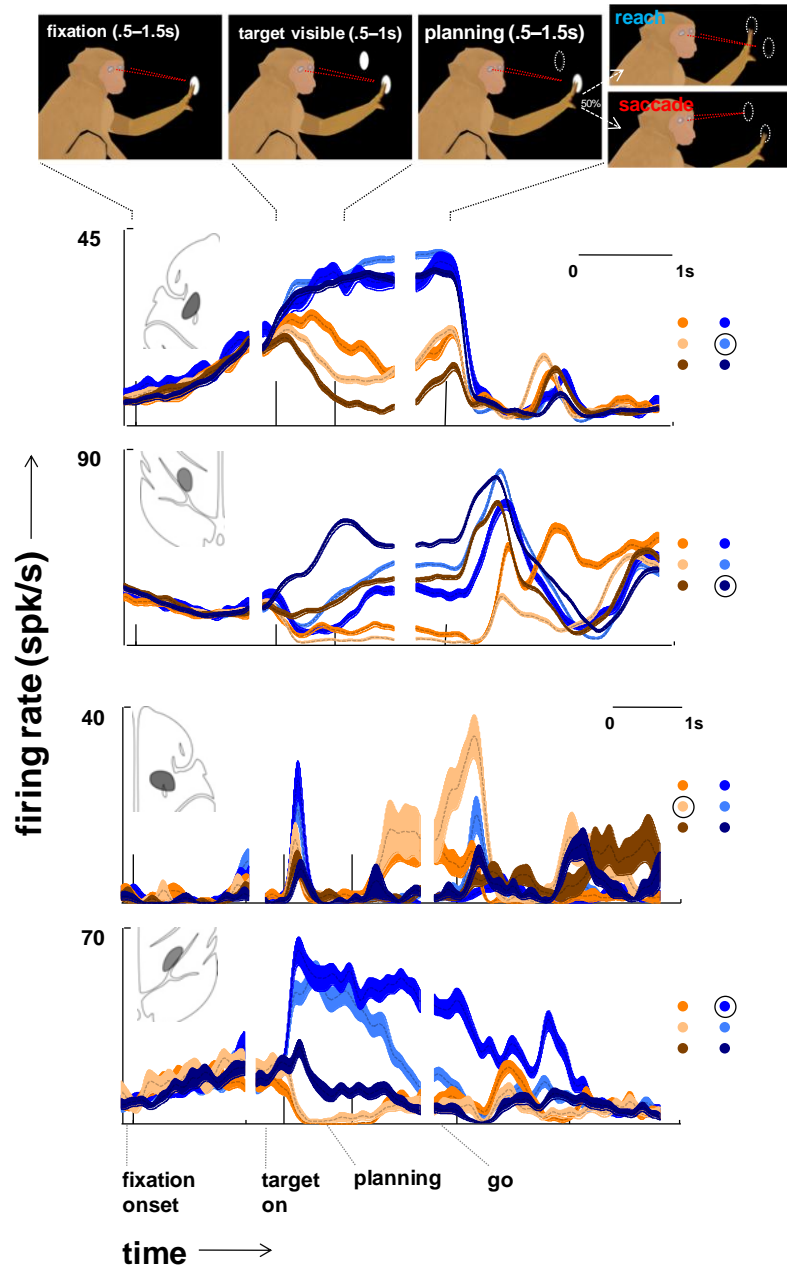


**Figure 1.5.3:** Direction tuning during the planning period. Each trace represents an average of spiking activity in a given reach direction, indicated by the color (variants of blue for contralateral, variants of orange for ipsilateral). Vertical lines indicate transitions between trial states. Insets show target location, and the location corresponding to the maximum firing rate for each cell is circled.

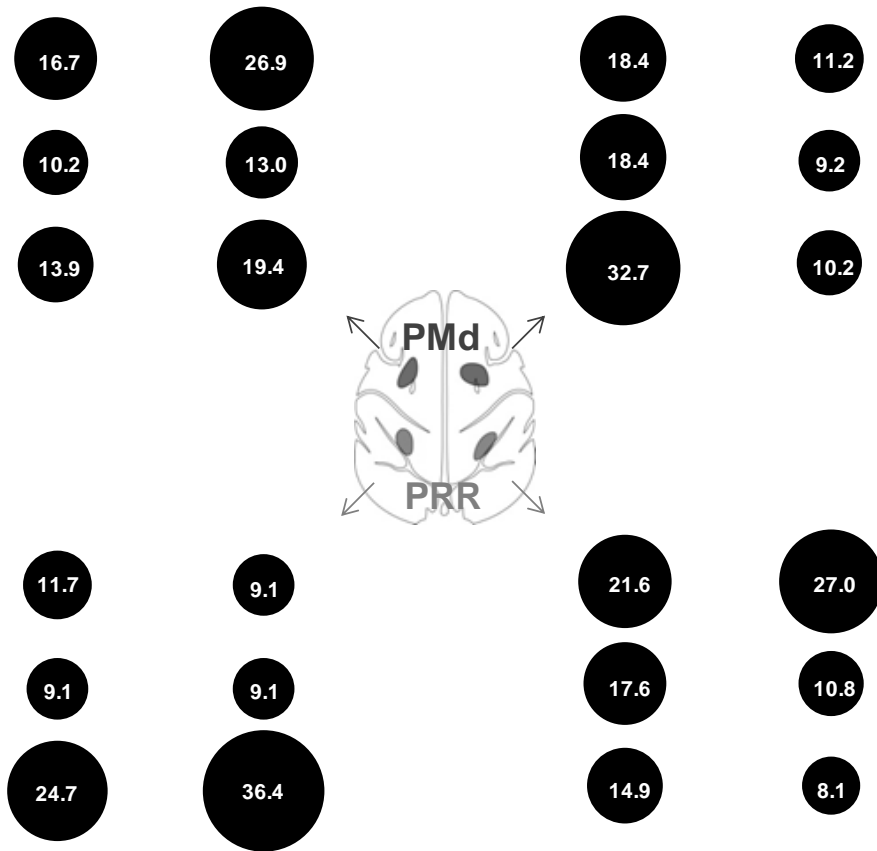


**Figure 1.5.4:** Cohort for both monkeys. The area of the dot represents the percentage of multi-unit spikes preferring that spatial location (as in the insets, fig. 1.5.3). The outside line represents 10%. Overall, PRR and PMd show selectivity for the contralateral visual hemispace. Note that both monkeys (monkey L and R) used the right hand.

The example cells in fig. 1.5.5 are the same as those in fig. 1.5.3 (top rows), but with spatial directions averaged into ipsilateral and contralateral bins, and with saccade trials added. Again, it is still clear that both cells prefer the visual space contralateral to the recording locations. However, they seem to fire somewhat less for reaches in that

direction, compared to saccades. One interesting thing about this cell, which is particularly apparent when its firing patterns are displayed this way, is the consistency in firing rate it seems to show for its preferred direction and effector throughout the planning period, neither accumulating nor diminishing in activity.

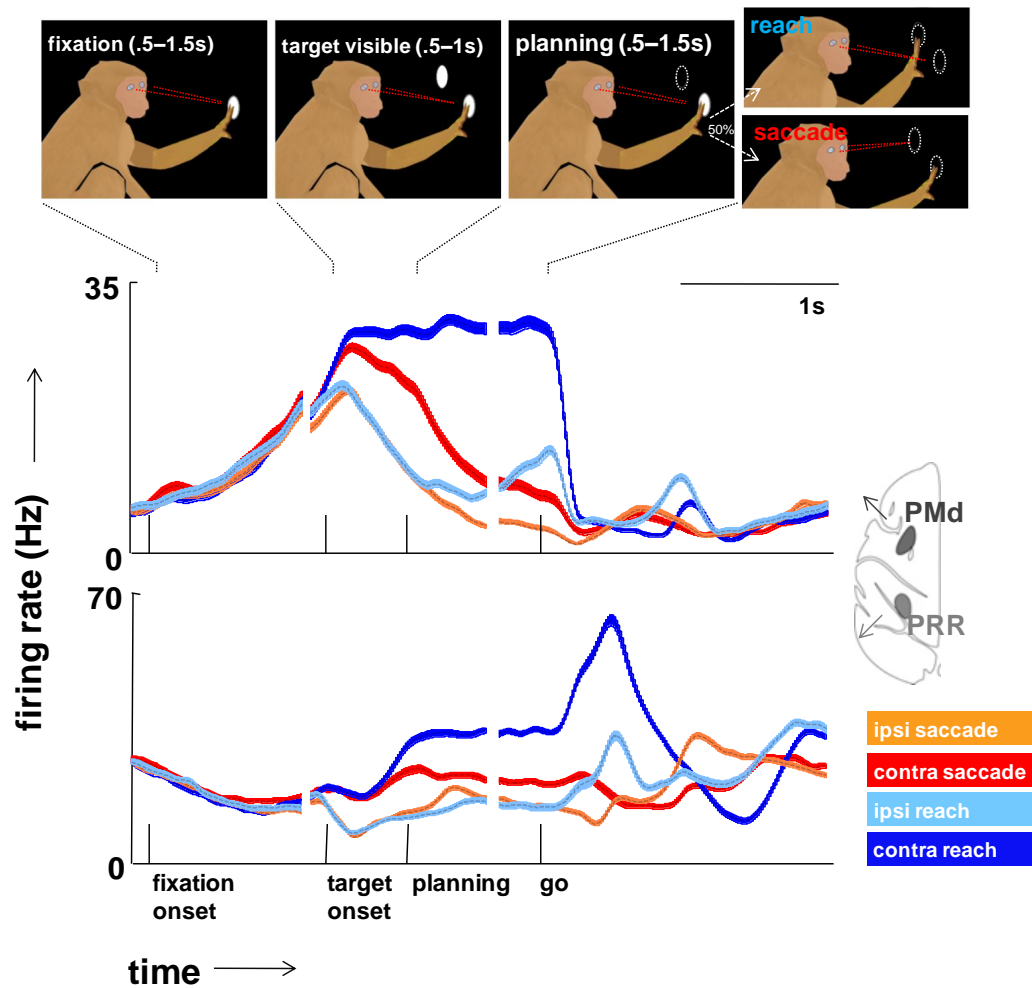


**Figure 1.5.5:** Reach-related example single cells from each region during the taskmonkey L. Spikes were convolved with a 20 ms gaussian and averaged across trials. Left column (from monkey "L") shows examples of instructed reach/saccade trials, where the intended effector is

apparent at target onset. Right column (monkey "R") shows choice trials from monkey "R" (we also recorded choice trials in monkey L; see Methods). Error bars are S.E.M. across trials. During the planning period, the mean firing rate in each cell differentiates between contra- and ipsilateral reaches and saccades. Insets represent recorded brain areas for each cell.

Figure 1.5.6 summarizes the formation of reach/saccade movement plans in these PRR and PMd recordings. PRR shows an overall bias toward reach movements in the contralateral visual space in both monkeys, as does the PMd in monkey L. The PMd activity in monkey R seemed to be highest for contralateral saccade movements. This may or may not be related to the fact that the monkey was using the ipsilateral (right) hand (see section 7). Overall, for monkey L, 57% of cells in PRR were effector/hemisphere tuned, in monkey L PMd 58% were tuned, in monkey R PRR, 27%, monkey R PMd, 63%. For each cell, the identity (ipsi/contra saccade/reach tuned) was assigned based on the highest average spike rate, as shown in figure 1.5.6. The relative weakness of effector/hemisphere tuning in monkey R is attributable to the use of only decision trials in that animal, with no instructed planning trials (the latter tend to have somewhat stronger decision-making activity). One can also analyze the difference in spatial tuning strength in these regions, given an effector plan (as in Quiñones-Díaz et al 2006 % of significant hemisphere tuning for saccades/reaches in PMd/PRR of animals L/R: 38%/41% PMd,L; 31%/53% PMd,R; 40%/43% PRR,L; 15%/20% PRR,R). The results of these various analyses are intended to show that all four brain regions contain cells which reveal the monkey's intended action, and that three of the four regions are biased toward contralateral reaches.

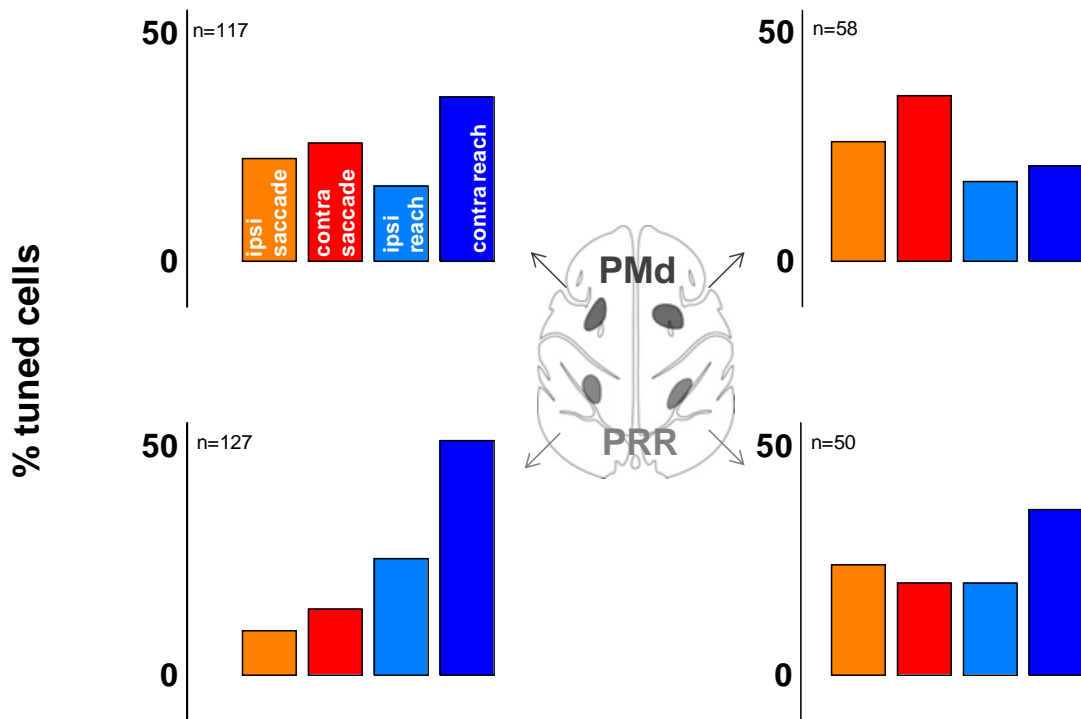


**Figure 1.5.6:** Summary of ensemble firing rates and tuning properties for each area. During the memory period, spiking rates were calculated in 50 ms bins, and then categorized by the action (ipsi-/contra-, reach/saccade) they preceded. An ANOVA was calculated across categories to determine cell tuning. Cells for which the distributions of spike rates across the four categories at any time were unlikely to arise from the chance distribution ( $p < .05$ , corrected) were classified tuned, and further categorized by the action following the maximal spike rate (for example, the two cells shown in Figure 1.5.5 are contralateral reach cells).

## **2 Evoked Responses**

### **2.1 Visually evoked responses**

Between brain regions known to be reciprocally connected but for which the precedence is unknown, an obvious question is “which fires first in response to a stimulus?”

Presumably, the brain area which responds first is likely to be upstream from the one responding second.

PRR and PMd are anatomically connected, and thought to interact during action planning. The popular view of the dorsal stream, outlined in fig. 1.1.1, predicts parietal areas to precede frontal in their representation of the visual stimulus. In contrast to this popular view, the following data show that PMd cells fire significantly in advance of PRR (fig. 2.1.1) when triggered by a visual stimulus.

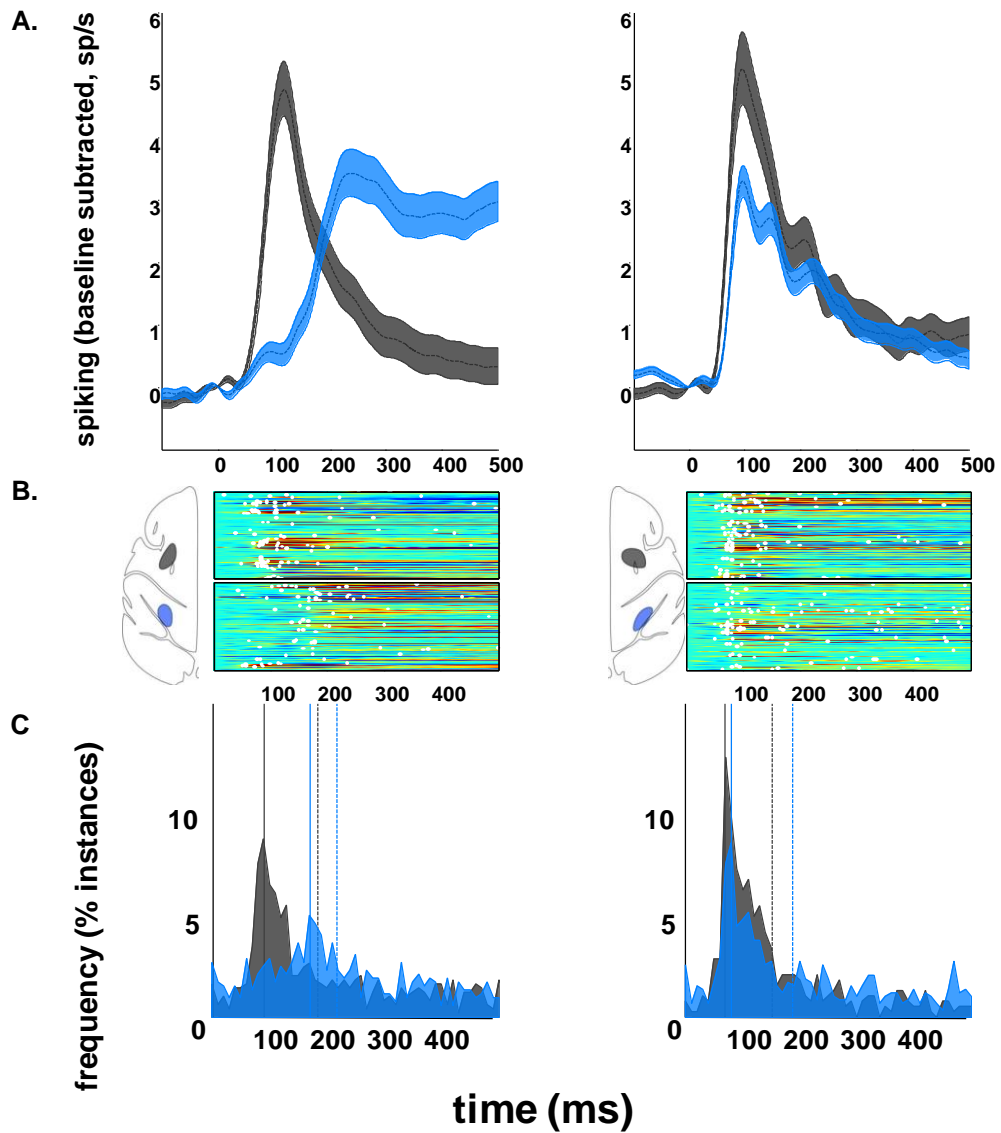


**Figure 2.1.1:** Onset-latency in response to a visual stimulus. **A.** Deviation in firing rate, averaged across cells and visual stimuli. For each cell, and for each visual stimulus direction, the baseline firing rate (determined just before the onset of the visual stimulus) was subtracted from the spike rate. The averaged absolute value produces this plot. Error bars are S.E.M. Individual spikes were convolved with a 20 ms gaussian to produce spike rates. **B.** Traces for individual directions and spikes, as described in A. For each, the first

derivative of the spike rate was calculated, and the first time it exceeded a chosen threshold (here,  $.4 \text{ sp/s}^2$ ), an "onset time" was assigned for that cell and direction (white dots). **C.** Histograms of onset times (as in B) calculated by measuring the deviation of the mean spike rate by one standard deviation from baseline after the appearance of a stimulus. Solid lines are peaks of the distributions (90/170 ms, F/P hemisphere L; 70/80 ms, F/P, hemisphere R), dotted lines are the peaks (185, 217, 152, 187 ms). PMd cells tend to respond earlier than PRR cells to the visual stimulus onset.

Note that in the case of the recordings from the left hemisphere, the visual response in parietal grows somewhat more slowly than in the right-hemisphere recordings. This could be due to somewhat more anterior recording locations used for this monkey. We believe this may indicate that the left hemisphere PRR is closer to Area 5 (more anterior along the IPS) than the traditional PRR location (more posterior, closer to the Genu of the IPS; see Snyder et al., [1997]). These cells therefore provide an even more dramatic example of the discrepancy between frontal and parietal timing.

The same timing difference seems to be true of the evoked potential. Following a visual stimulus, a visual transient appears in the LFP signal in both frontal and parietal cortices. The shape of the transient generally follows the pattern of a negative deflection in the LFP, which equates to a generalized positive deflection of the membrane potential, followed by a slower positive deflection. We measured the evoked potential in both regions, and found that the averaged shape of the evoked potential in PMd seems to qualitatively precede the evoked potential in PRR (fig. 2.1.2.A). A histogram of measurements of earliest-detectable deflections in individual examples of the LFP

likewise shows that evoked potentials occur tens of milliseconds earlier in PMd than PRR (fig. 2.1.2.B).

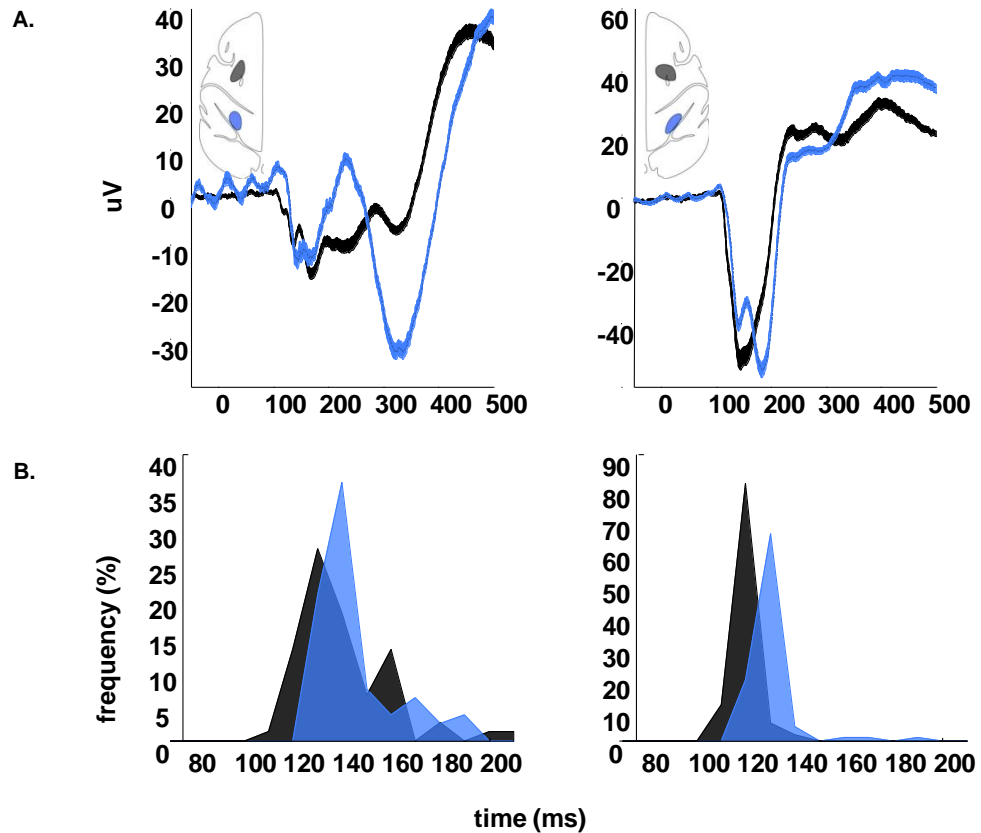


**Figure 2.1.2:** Onset latency of evoked potentials in response to a visual stimulus. **A.** Averaged evoked potentials. **B.** Earliest time of detected deflection, similar to fig. 2.1.1

These visual transients indicate that PMd responds earlier to visual stimuli than does PRR. These data seem to contradict the simple conception of parietal feeding forward to frontal, and suggest the existence of an auxiliary visual pathway feeding the frontal

cortex. While PMd receives extensive input from parietal regions [Tanne-Gariepy et al., 2002; Wise et al., 1997], these data do not support the idea that visual response in PMd are driven by inputs from PRR. It is possible that auxiliary visual pathways drive PMd, potentially through other parietal areas such as area 7m, Medial Dorsal Parietal, or Parieto-Occipital [Wise et al., 1997]. It is also possible that PMd receives input from heretofore unknown subcortical structures, as does FEF [Lynch et al., 1994].

## **2.2 Timing of responses to spatial and effector instructions**

These data show that frontal cells respond earlier to visual stimuli than parietal cells. However the processing of more abstract stimuli, such as an instruction about where or how to move, might occur on a different relative timescale in PRR and PMd. There is some controversy in the literature on the relative timing of non-trivial responses in the frontal and parietal lobe [Buschmann and Miller, 2007; Schall et al., 2007].

Figure 2.2.1 shows a summary of the detectability of the target through time, across cells. In both cases, the parietal lobe responds later than the frontal lobe, and with somewhat less discernability of the target. We performed a t-test across spike rates (50 ms bins) following an instruction to reach to the ipsi- or contralateral hemisphere. This produced a probability at each time point, for each cell. We then averaged these probabilities in the log domain over all cells in a given recording site, for comparison across recording sites. This is a perhaps an ad-hoc way of combining across probability measures, and is likely more conservative than necessary, but should allow for an honest comparison of timing between brain regions. Note that the component probabilities were probabilities calculated bin-by-bin, not cumulative probabilities.

Cumulative measures, or measures using greater time bins, would be useful for decoding, as would pre-selecting only tuned cells, which was also not done here. Decoding of target position and reach direction [Musallam et al., 2004] have been shown to be highly accurate in these regions. Figure 2.2.1 is not an ensemble decode. Rather, Figure 2.2.1 can be interpreted as something nearer to the probability of detecting the reach direction in a randomly chosen cell at a given 50 ms time bin.

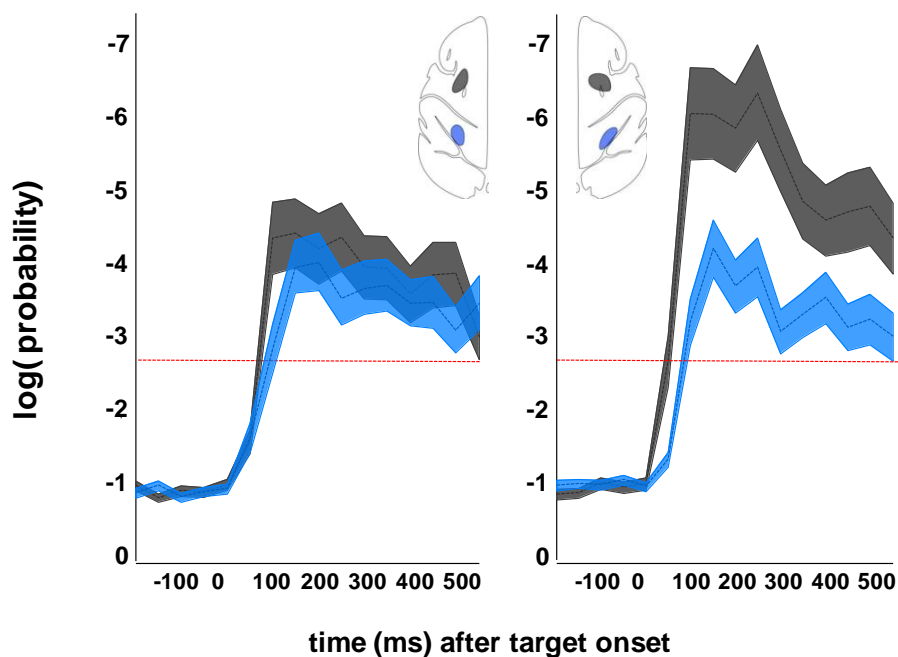


**Figure 2.2.1:** Timing of hemisphere differentiation in response to visual stimuli indicating movement direction. The y-axis represents the log of the joint probability across all cells recorded in either chamber. These data show that an average cell in PMd can be expected to respond earlier and more significantly to the identity of the target hemisphere than can a PRR cell.  $P=.05$  is shown in red. Error bars are S.E.M. in log space.

We further compared the timing with which we could detect the intended reach or saccade target after an instruction to reach or saccade. These instructions likewise appear to be processed earlier and more strongly in the parietal lobe than the frontal lobe (fig. 2.2.2).

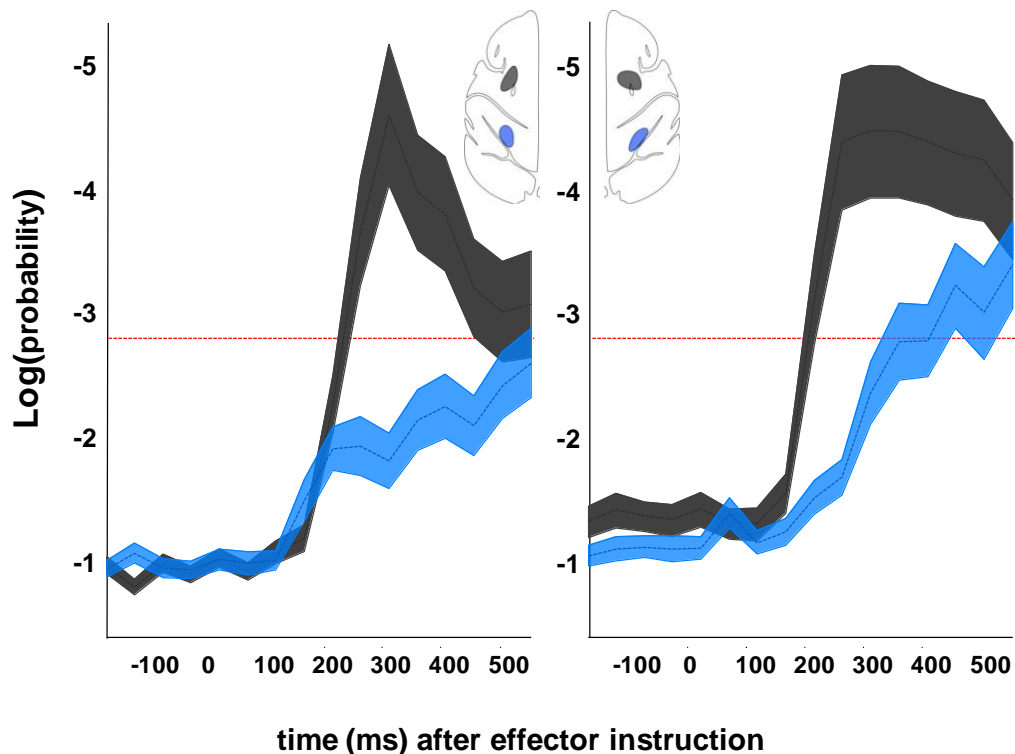


**Figure 2.2.2:** Timing of effector differentiation in response to visual stimuli indicating effector type. As in fig. 2.2.1, the y-axis represents the normalized log joint probability, or the expected log probability of a given cell's firing rates being identical between reaches and saccades. Over the course of a trial, following an instruction to make a reach or saccade to a previously known peripheral target, firing in these cells evinced a preference for reaches or saccades. It appears that data from the left hemisphere PRR recordings

do not quite reach significance at any time point, indicating the large number of cells with no discernable tuning. However, at least some cells do show very strong tuning in this region, as shown in the example cells in fig. 1.5.3. Note that while these results may appear to suggest weaker encoding of effectors in PRR than PMd, they are only intended for comparison of timing between the two regions, and not as an analysis of the relative decoding power from each. Considering only tuned cells would be expected to improve performance significantly, in line with previous work [Snyder et al., 1997; Cui and Andersen, 2007], as would considering accumulated evidence over time (fig. 1.5.6).

Again, these results do not represent the encoding of an upcoming reach or saccade in these regions. A central tenant of the idea of the population representation is that many units which encode a stimulus only weakly may be summed to encode it strongly. Assuming uncorrelated noise, the effector decode from an population of weakly encoding cells with the properties shown in 2.2.2 could rapidly approach low error. Decoding planned target location has been canvassed throughout the literature [Musallam et al., 2004; Mulliken et al., 2008], and for best results relies on an monkey's ability to adapt to the decode in turn. Decoding effector plans [Quiroga et al., 2006; Scherberger et al., 2005] is a less well-studied branch of the field, and beyond the scope of this manuscript. However, these data further support the notion that such information could be decoded from planning areas in parietal as well as frontal cortex, though with these particular parietal spots encoding the same data somewhat later than the frontal locations.

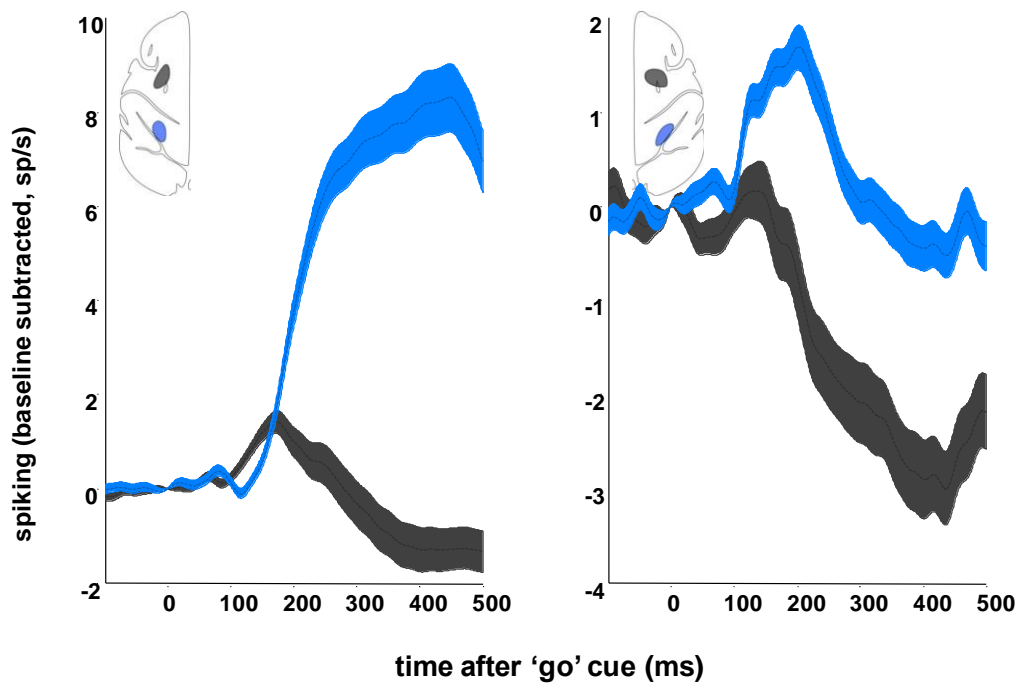


**Figure 2.2.3:** “Go”-centered firing rates. The average firing rates in PRR and PMd following the cue to move (baseline-subtracted, where baseline was determined at the time of the “go” cue). Error bars are S.E.M. The overall increase in strength in PRR firing, versus the decrease in PMd firing strength, is perhaps suggestive of a difference in the encoding of movement state.

Figures 2.2.1–2 show that PMd tends to respond sooner both to the appearance of visual targets, and the directional and effector instructions suggested by those targets. It is also worth inspecting the response of these cells to the cue to move (fig. 2.2.3). Here, another striking difference is still evident, with PRR responding on average more vigorously than PMd to the cue to move, as well as the ensuing movement. These are

gross analyses, and obscure much of the detail of the individual movement-related responses. However, they may indicate that PRR firing is more engaged in representing an ongoing movement than is PMd, even though they both have similar levels of planning activity (fig. 1.5.3).

When a movement plan has been instructed by an outside stimulus, the representation of the plan appears first in PMd, and second in PRR. These data seem to contradict the oft-held idea that posterior parietal feeds information about movement plans forward to PMd (fig. 1.1.1). Rather, their relative timing would suggest that PMd feeds PRR, at least when information comes from the outside, as in instances featuring a visual transient, or the response to explicit instructions. To add to these, we might also ask about the relationship between frontal and parietal areas when the signal does not enter from the outside. How much will the activity in PRR and PMd reflect upcoming movements if they are generated internally, that is, as the result of the monkey's decision?

### **3 Effector Decisions in Frontal and Parietal Cortices**

Section 2 showed that persistent activity in both parietal and frontal areas predicts an upcoming action, even in the absence of a stimulus which explicitly shows an instruction. However, persistent activity need not simply represent a delayed instruction. Recent data has shown that persistent cortical activity can represent a monkey's decision, even when the decision is completely freely made [Barraclough et al., 2004; Cui and Andersen, 2007; Curtis and Lee, 2010]. A freely made decision, in the absence of any explicit sensory instruction, or implicit instruction due to reward structure, is a good way to test the precedence of cortical structures, in that the activity can simply be said to represent storage or a recurrent stimulus response.

#### **3.1 Effector decisions during the planning period**

In the task described in fig. 1.5.2, we demonstrate PMd reports the monkey's movement with more strength than PRR. While the examples in fig. 3.1.1 show reasonably strong decision-making activity in both chambers, the average in PRR was somewhat weaker. This task featured the frequent appearance of visual stimuli, which instructed monkeys on a reach direction independent of their effector decision. However, we were concerned that in the context of a directional task, effector decision-making signals might become diluted by strong visual responses in these areas. To add to these data, we also explored decisions in the context of a task with no confounding visual stimulus.

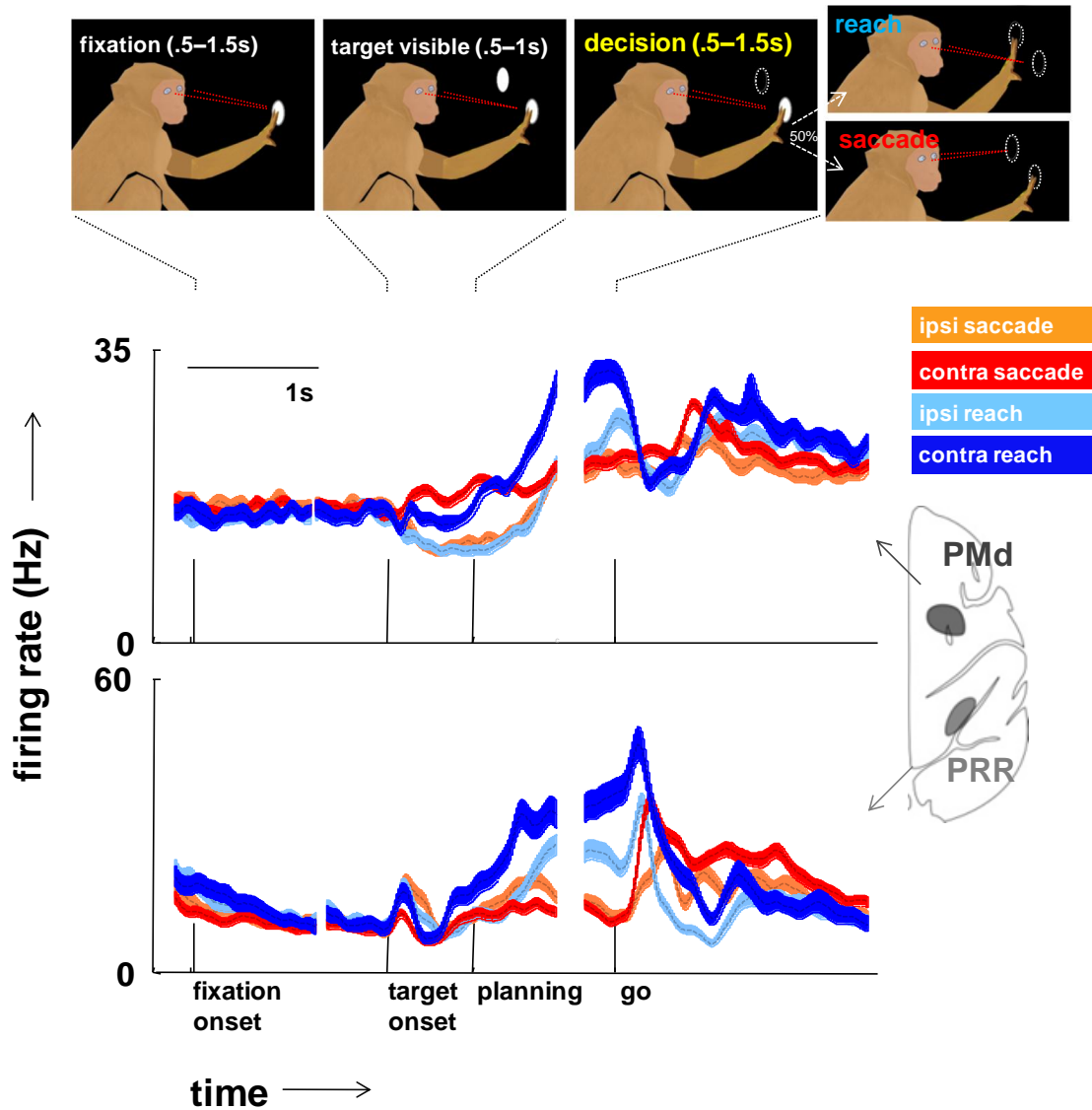


**Figure 3.1.1:** The examples above show decision-related activity in PMd and PRR during decision-making. In this example, the only data shown are free-choice data – the monkey freely chooses whether to reach or saccade. As in fig. 1.5.5, both parietal and frontal cells show effector-specificity, firing more in advance of reaches than saccades.

### **3.2 Effector decisions in PM and IPS during blind choice**

Please note that while most of this manuscript discusses a single data set recorded from PRR and PMd, the data in this section come from a slightly more rostral set of recording locations in both chambers (see fig. 3.2.1, inset). While we do make some generalizations of intraparietal and premotor function across these data sets in the conclusion, millimeters matter in cortex.

Heretofore, the tasks described have followed the general pattern of visual-response tasks. The general picture so far has been that, in response to visual stimuli, in representing stimulus position, and in representing chosen effectors, PMd precedes PRR. However, the presence of a visual stimulus may be a confounding factor to understanding the nature of persistent activity. In an effector-decision task, where a visual stimulus need not be provided or even implied, the visual stimulus may act as a powerful noise source. In its absence, we might be able to detect persistent activity predictive of a monkey's future actions earlier than expected.

The exact meaning of persistent activity has also been debated. Some have suggested this persistent activity in the IPS represents sensory accumulation [Gold JI and Shadlen MN, 2000], though it also grows with expectation [Janssen and Shadlen, 2005] and is modulated by expected value [Platt and Glimcher, 1999; Sugrue et al., 2004, Musallam et al. 2004]. Spatial attention tasks strongly engage these areas [Bisley JW and Goldberg ME, 2003]. However, persistent activity also predicts non-spatial aspects of movement, such as the effector (e.g. reach or saccade) to be used [Scherberger et al., 2005]. Emerging evidence suggests that persistent activity may represent an animal's internally generated decisions [Curtis and Lee, 2010]. It is not known whether decisions are reflected in action planning areas such as IPS and AS solely because of the

immediate value or expectancy of making an upcoming action, or whether spiking reflects an animal's intentions long before an output is ever expected. It would therefore be beneficial to know how early an upcoming decision is represented in spiking activity. In order to disambiguate the decision-making from the phenomenon of spatial attention, a decision between reaches and saccades may be employed [Cui and Andersen, 2007]. However no such task has yet monitored the onset of decision-making activity, due to the presence of visual instructions. In a non-spatial decision-making task in which an animal also expects a visual instruction, spiking activity reflecting the decision may become delayed until the visual instruction has been presented (as in Cui and Andersen [2007]). This is problematic for understanding the relationship between decision-making and persistent activity, because the expectation of a visual stimulus may obscure the earliest parts of the decision-making process. For the first time, this study investigates non-spatial aspects of premotor and parietal activity during non-spatial decision-making, in the complete absence of confounding spatial stimuli.

We recorded individual neurons in IPS and around AS in two animals (see inset icons, fig. 3.2.1.B). IPS recordings were made near the bottom of the sulcus, and AS recordings were centered on the posterior and medial side of the arcuate sulcus, anterior and lateral to the dorsal premotor cortex, but somewhat posterior and medial to the frontal eye fields. Some AS areas elicited eye or pinna movements in response to 20 uA stimulation, though not to the extent expected from frontal eye fields. Recordings were made using multielectrode drives, during a task in which the animals were required to make either a reach or saccade to a known target after holding a fixation spot for 1-2s, without any additional stimuli. The animals understood the target to be a single spatial location on one side of their body. The task discouraged the animals from creating a predictable sequence of choices by tracking the previous 5 choices, picking the most

probable choice following all previous such sequences, and rewarding the animals on a given trial only if they made the improbable choice (i.e. matching pennies; see Barraclough et al. [2004]). Our algorithm did not explicitly discourage strategies featuring interactions between actions and reward (e.g. win/stay, lose/switch). However, the data shown here were trial-filtered, so as to remove from the analysis any trials with predictable strategy-formation (2-back,  $p < .05$ ), as well as any trials in which the animals may have engaged in predictable sequential behavior despite the reward structure. Unlike previous experiments, we presented no visual target, so that we could inspect persistent activity continuously during the fixation period. After successful completion of a reach or saccade and an additional 200ms wait, the visual target finally appeared, preventing the animal's movements from drifting in space over the course of the task. We recorded in AS and IPS simultaneously, in order to compare activity in both regions under identical conditions.

Figure 3.2.1.B shows example cells, recorded from IPS and PM (insets; PM areas were verified to respond to 20 uA stimulation by eliciting eye movements and pinna responses). The first cell was recorded in IPS, and shows expectation-related activity characteristic of these regions [Janssen and Shadlen, 2005]. The second row shows a cell from AS with persistent activity that lasts throughout the fixation period. In this cell, spiking activity which predicts the decision actually begins before the trial starts, appearing just after the acquisition of the previous target.

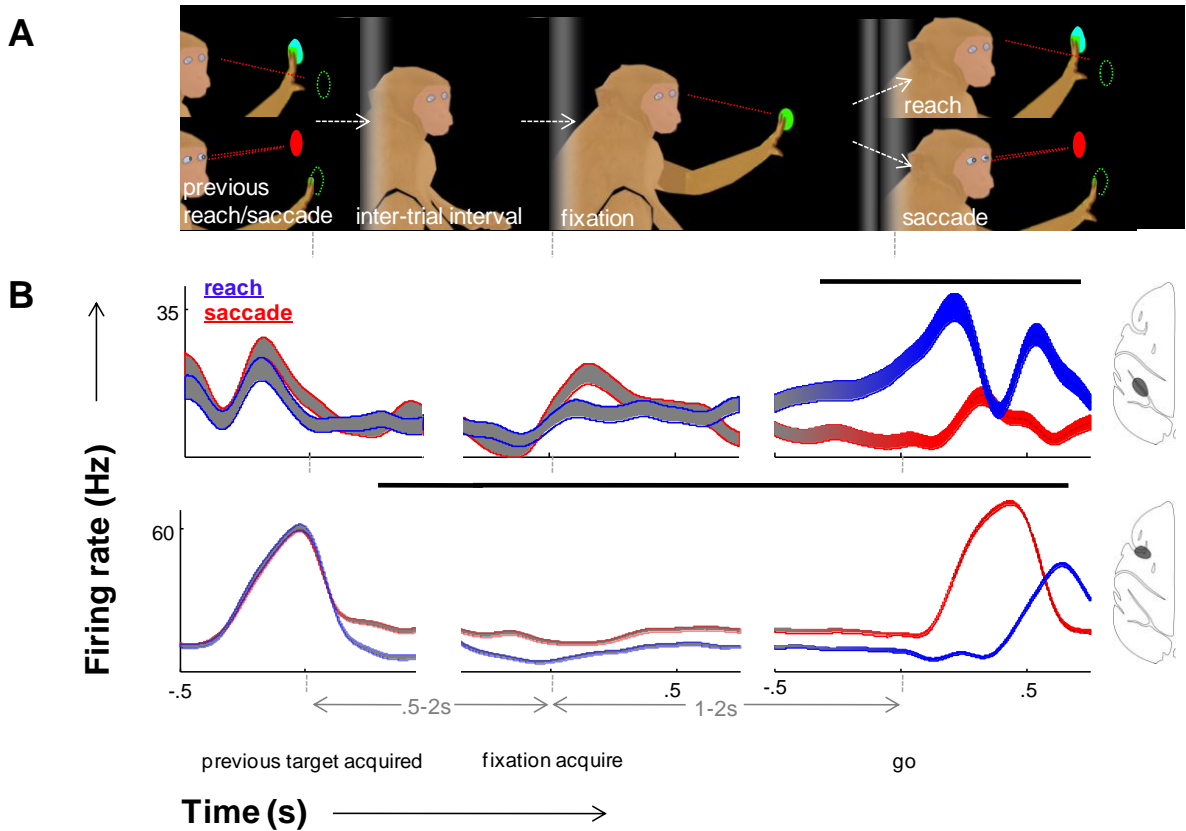


**Figure 3.2.1: A.** The monkey was required to maintain fixation with eye and hand for 1-2 seconds, after which the central fixation spot disappeared. This was the monkey's cue to either reach or saccade to a peripheral target. The monkey could choose whether to reach or saccade on a given trial, though he was discouraged from predictable choices across trials. After the target was acquired, and assuming the monkey was acting unpredictably, he received reward with 50% probability, and then reacquired fixation (during the inter-trial interval). **B.** Example cells from IPS (top row, inset) and PM (bottom row, inset), recorded during the same recording day. Each trace represents spiking activity (convolved with a 20 ms Gaussian and trial-averaged) preceding a decision to saccade (red) or reach (blue). Error bars are S.E.M. Black bars above the traces indicate time periods (evaluated at 20 ms

intervals) in which the traces are significantly different (unpaired t-test across trials, corrected for multiple comparisons). While the cell from IPS shows predictive activity as the "GO" cue becomes imminent, the PM cell's firing reflects the effector choice even before the fixation period begins.

Figure 3.2.2 summarizes the predictive activity in both recording areas in both monkeys. For each cell, in each 200ms bin, we calculated an un-paired t-test between the spiking activity in reach and saccade choice conditions. In both animals, a greater proportion of cells in AS correlate significantly with the upcoming movement, compared to IPS (animal L 35% AS vs. 19% IPS, animal R 9%/1%, by the time of the 'GO' cue). Overall predictive activity in animal R's IPS was very low, never reaching significance. Cells had already begun to report on the upcoming decision by the onset of fixation in both animals' AS (animal L 22%, animal R 10%) and in animal L's IPS (16%, <5% in animal R's IPS). The weakness of the data in animal R can partially be attributed to the far fewer units recorded in that animal (164, compared to 423 in animal L; we were forced to stop the experiment in animal R early due to an infection), and the fact that we recorded in cortex ipsilateral to the hand used. Thus, these plots are dominated by the results from animal L. However, in both animals the following was: at least 7% more cells in AS were significantly predictive of the effector decision compared to IPS, and more than 10% of AS cells significantly predicted the effector choice even before the animal acquired fixation.

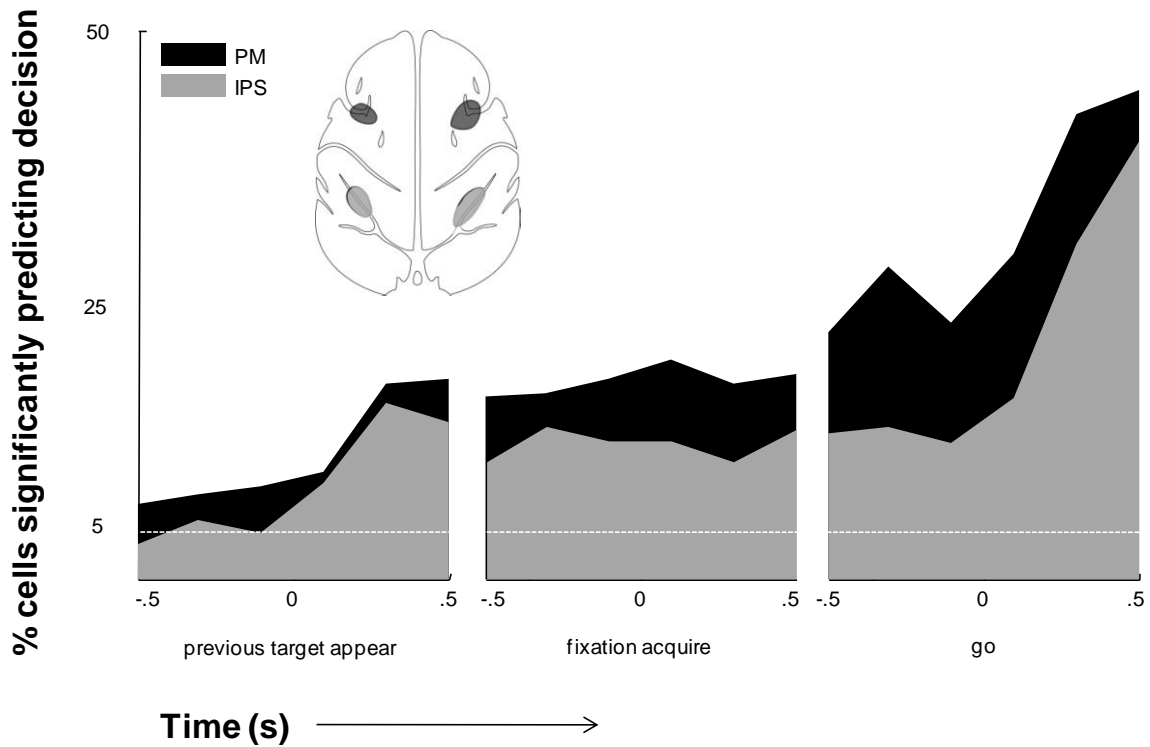


**Figure 3.2.2:** Aggregate data. Significant differences between spiking timecourses predicting effector decisions (unpaired t-test,  $p < .05$  corrected for multiple comparisons, 200 ms intervals) were binned across cells and monkeys. Both PM and IPS show evidence of effector decisions, with a greater percentage in PM. In both regions, a small but significant percentage ( $> 10\%$ ) of cells reflect the decision before the fixation period begins.

These cells' exact role in decision-making awaits further inquiry. In order to choose between two effectors, at least some kind of internal state variable is required to inhibit a saccade when a reach is planned, and vice-versa. During a speeded reaction-time task, it would make sense for such a variable to establish its state before the "GO" cue. Such

a state variable might show expectancy-related activity [Jannssen and Shadlen], since it would only be required near the end of the trial. While some cells (e.g. fig. 3.1.1.B, first row) show expectancy-related behavior, firing more as the expectancy of the “GO” cue increases, other cells (e.g., fig. 3.1.1.B, second row) begin differentiating between upcoming decisions before the trial even begins. The overall pattern in both brain areas seems to be that predictive activity begins to grow just after the acquisition of the previous target, which is when the monkey discovers whether he will be rewarded for his previous action. We filtered out trials which explicitly showed win/stay/lose/switch behavior, so we do not believe that the previous trial’s success or failure actually served as a cue for the monkey’s subsequent decision. However, it may be that the reward expectancy for each action could not be perfectly driven to 0, such that slight residuals in expected value based on the reward structure would bias the monkey’s decision. Therefore, small weight changes due to the previous reward could be amplified throughout the recursive network of the brain during the preparation for the next movement, and end up generating electrical activity corresponding to the monkey’s upcoming action.

The existence of predictive activity before the start of the trial suggests a high-level representation of decisions in both regions, independent of the behavioral context. Previous work has shown that sequences of behaviors may be simultaneously represented in IPS [Baldauf et al, 2008], though the present data constitute the first evidence that firing corresponding to a non-spatial decision can persist across a sequence of behavioral contexts. That predictive activity is somewhat greater in AS than IPS is consistent with the notion that decisions originate in the frontal lobe [Badre et al., 2009], nearer to sites which are directly innervated by dopamine [Thierry et al., 1973]. However, the strong representation of decision variables in the parietal lobe may

suggest that in a truly randomized task, decisions could be formed by a distributed network involving both areas. The growth of decision-related activity during the trial seems consistent with the subjective feeling of vacillating between choices or “mulling over” a decision, and these data may help explain how that feeling relates to electrical activity, particularly in the parietal lobe, which has been associated more with the awareness of intent rather than production of movement itself [Desmurget et al., 2009]. These results add to our understanding of the development of decisions in the brain’s electrical activity.

## **4 Oscillatory Properties of Frontal and Parietal Cortices**

Section 2 showed the relative similarities in the spatial and effector-specific properties of parietal and frontal neurons during planning. Yet, section 3 shows that despite their similarities in coding properties during planning, premotor neurons represent behaviorally relevant information more quickly and vigorously than parietal neurons. With respect to transient events, PMd precedes PRR. However, as we will see in the following section, PRR exhibits significantly stronger oscillations than PMd during planning.

### **4.1 Oscillatory Spectra**

Whereas PMd LFPs show fairly typical  $1/f^n$  spectra, LFP spectra in PRR show a significant peak in beta-band activity (fig. 4.1.1).

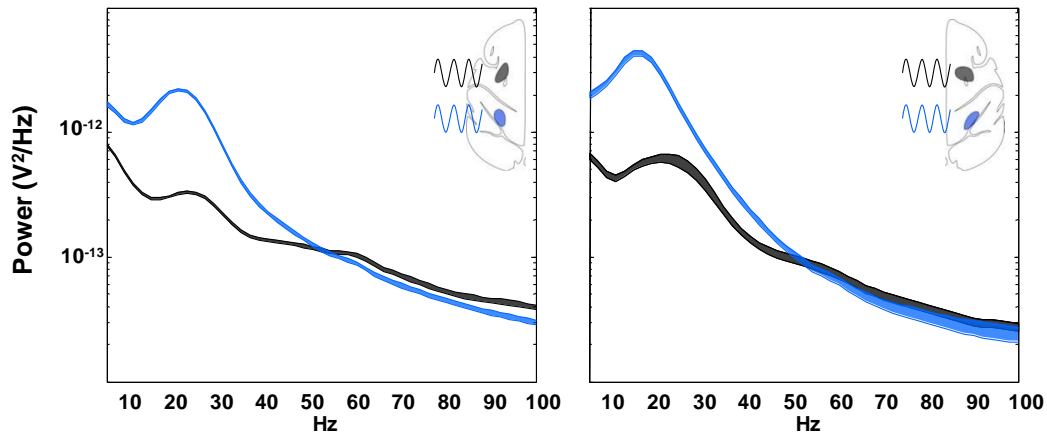


**Figure 4.1.1:** LFP 20 Hz spectrum in PRR and PMd. PRR LFPs have more power across the frequency spectrum from 1-100Hz. PRR also shows a marked peak in LFP power around the beta (15-25Hz) band. Estimates were made using consecutive windows of 200 ms each, during the planning period, with each estimate averaged over 200 such windows (see Methods). Error bars are S.E.M. Spiking spectra mirror the asymmetric LFP spectra (fig. 4.1.2). There is more beta-band (15-25Hz) activity in PRR cells than in PMd cells, which is evident not just in local field potentials, but in the cells' raw spectra. Therefore, we add an additional axis along which these two areas differ: PRR cells respond more regularly during steady state, exhibiting fine timing around the beta-band rhythm which is not present in PMd cells.

Likewise, the raw spiking spectra show strong beta-band activity in PRR, but not PMd (4.1.2). These data hint at a striking oscillatory difference between these regions, which may have functional implications.

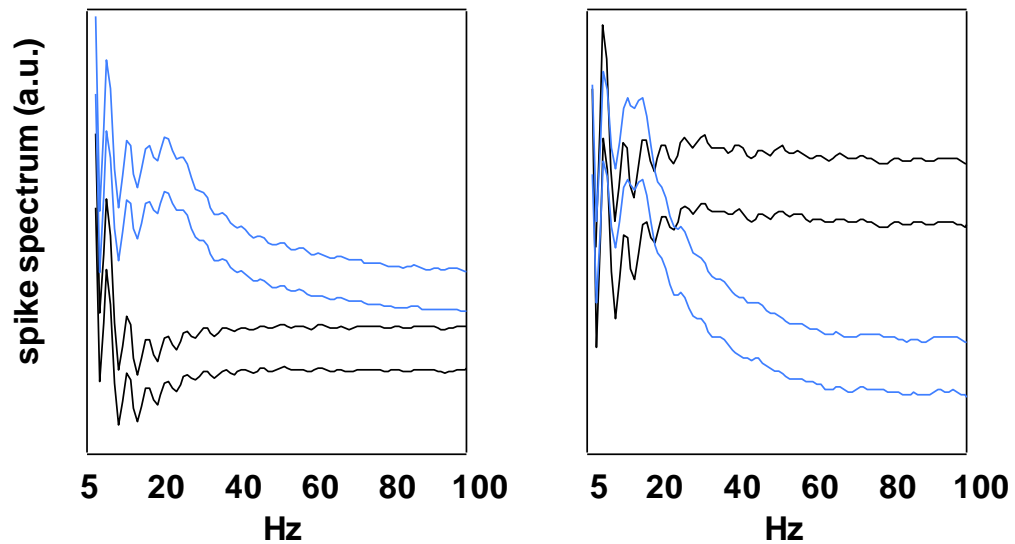


**Figure 4.1.2:** Spiking spectra likewise show different oscillatory properties. These are averaged (in log domain) direct estimations of individual spiking spectra (a.u.= arbitrary units, see Methods). Despite the difficulty in interpreting such spectra from individual spikes [Jarvis and Mitra, 2001], a peak in beta-band activity is evident in spiking spectra from both monkeys' PRR which is not evident in the PMd spiking spectra. Error bars are S.E.M.

## 4.2 Development of LFP over the course of a task

Growing evidence has shown the LFP to exhibit strong behavioral correlations [Pesaran et al., 2002; Scherberger and Andersen, 2006; Hwang and Andersen, 2009]. The LFP frequency profile and overall power are qualitatively different between PRR and PMd during the planning period (fig. 4.1.1). How do they compare over the course of the task?

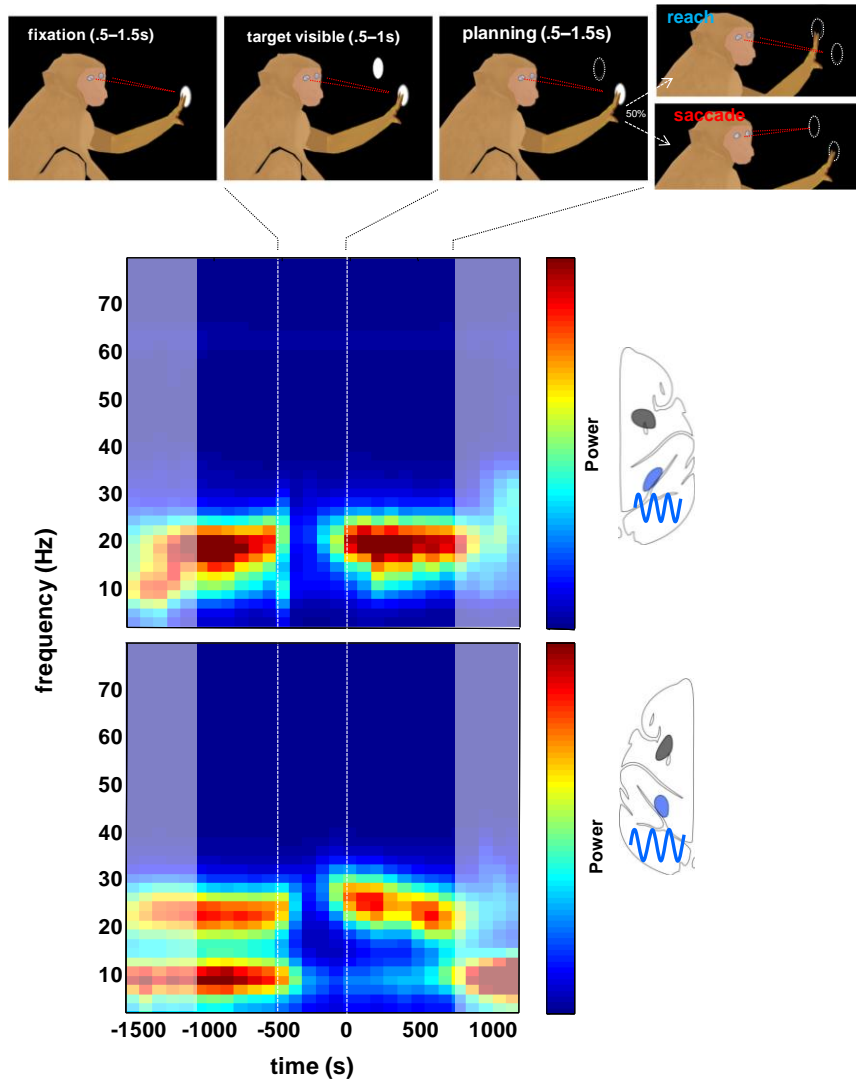


**Figure 4.2.1:** PRR LFP spectrum development over the course of the trial. Target presentation extinguishes beta-band LFP activity, but it resurges during the planning period. These data were taken from segments of monkey R and L's data featuring targets visible for .5 seconds. Power scale was chosen to highlight relevant activity in the alpha and beta-band (see fig. 4.1.1). 200 ms windows and a single taper were used. Notable also is the additional alpha activity in monkey L during fixation, which is completely absent during planning. The body and sensory state during fixation and planning are identical, LFP power

reveals a difference in the brain state. Grayed areas are those which include a mixture of states (fixation and target, or planning and movement, due to variability in fixation and planning times).

Consistent with earlier reports on parietal LFPs [Pesaran et al., 2002], the PRR LFP is strongly related to the monkey's brain state. It is remarkable to note the extent to which a visual target extinguishes beta-band activity. We asked whether extending the period during which the target was presented to 1 second would continue to suppress beta-band activity, or allow it to return. Figure 4.2.2 shows the results.

These data suggest that beta-band activity does return in the ensuing time after the appearance of a target, even if the target remains on. However, beta-band activity in this case is still greater during the memory period, reaching a value significantly above its peak value during the target presentation. These data seem to suggest that beta-band activity is high during any kind of continuous brain state in the fixating monkey. However, periods of preparation, such as fixation and planning, cause particularly high values of the beta-band power.

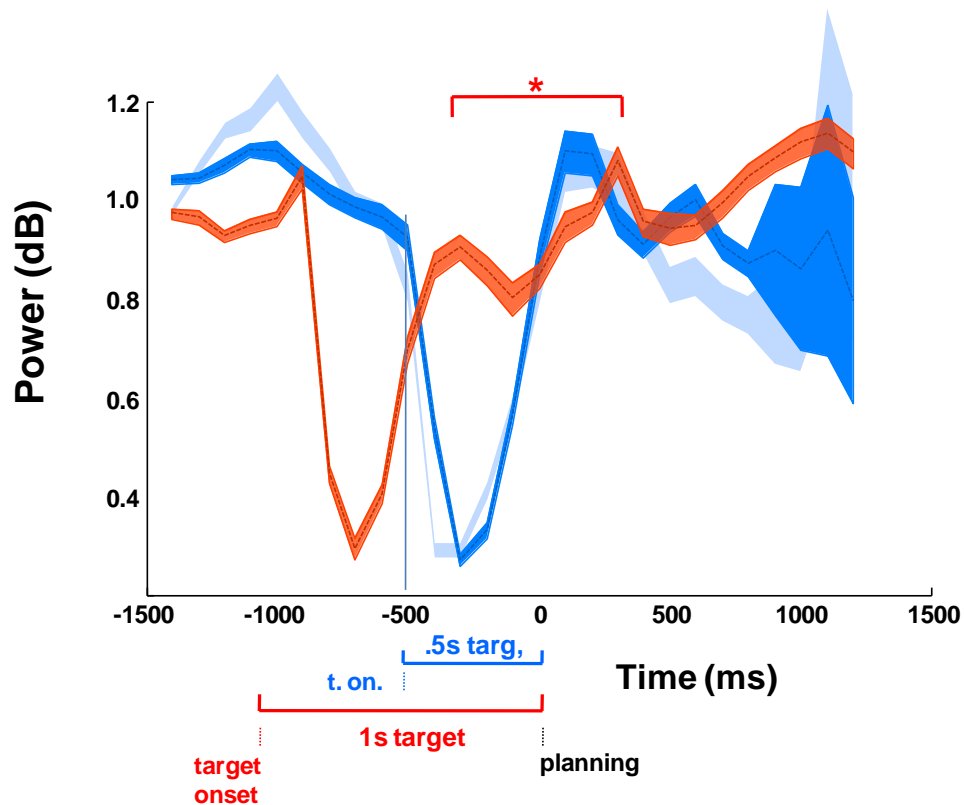


**Figure 4.2.2:** PRR LFP spectrum by length of planning period. Power at the primary frequency band (23 Hz, monkey L; 17 Hz, R) is calculated with respect to the average power during fixation. Blue curves represent target onset periods of .5 seconds (dark blue = monkey L, light blue = monkey R). Red represents additional recordings taken with targets of 1 s. Abolishment of beta-band activity by target onset (dotted lines) is evident. For the 1 s target, beta-band power reappears after a brief interlude of several hundred milliseconds, while the target is still on. However, b-band power is yet greater during the planning period (t-test, \* =  $p < 1e-30$ ).

Does the LFP also correlate with the identity of the upcoming movement plan? Figure 4.2.2 shows a comparison of LFP activity between reaches and saccades in PRR. Data from this manuscript are compared to previously reported data from Scherberger et al. [2005]. In the latter case, and in the case of our left-hemisphere data, reaches were preceded by increased power in the beta (20 – 30Hz) band, as well as somewhat decreased power in the lower frequency bands (0 – 15z). Data recorded in monkey R show a much smaller difference between reaches and saccades. This could be due to the use of the right arm, or the lack of instructed-effector trials in these data, which could weaken the overall effector-related planning activity. Similar to previous reports [Scherberger et al., 2006; Pesaran et al., 2002], with from 1 – 3dB higher activity in the 20 – 30 Hz band for movements contralateral hemisphere in both monkeys, and a concomitant decrease of around the same amount in the lower frequencies (0 – 20Hz). Many LFPs show evidence of tuning. On an LFP-by-LFP basis, at least 70%/37% (monkey R/L) of LFP recordings showed weak tuning in at least one frequency band. A more complete review of tuning in PRR LFPs can be found in Hwang and Andersen [2011],[SOM].

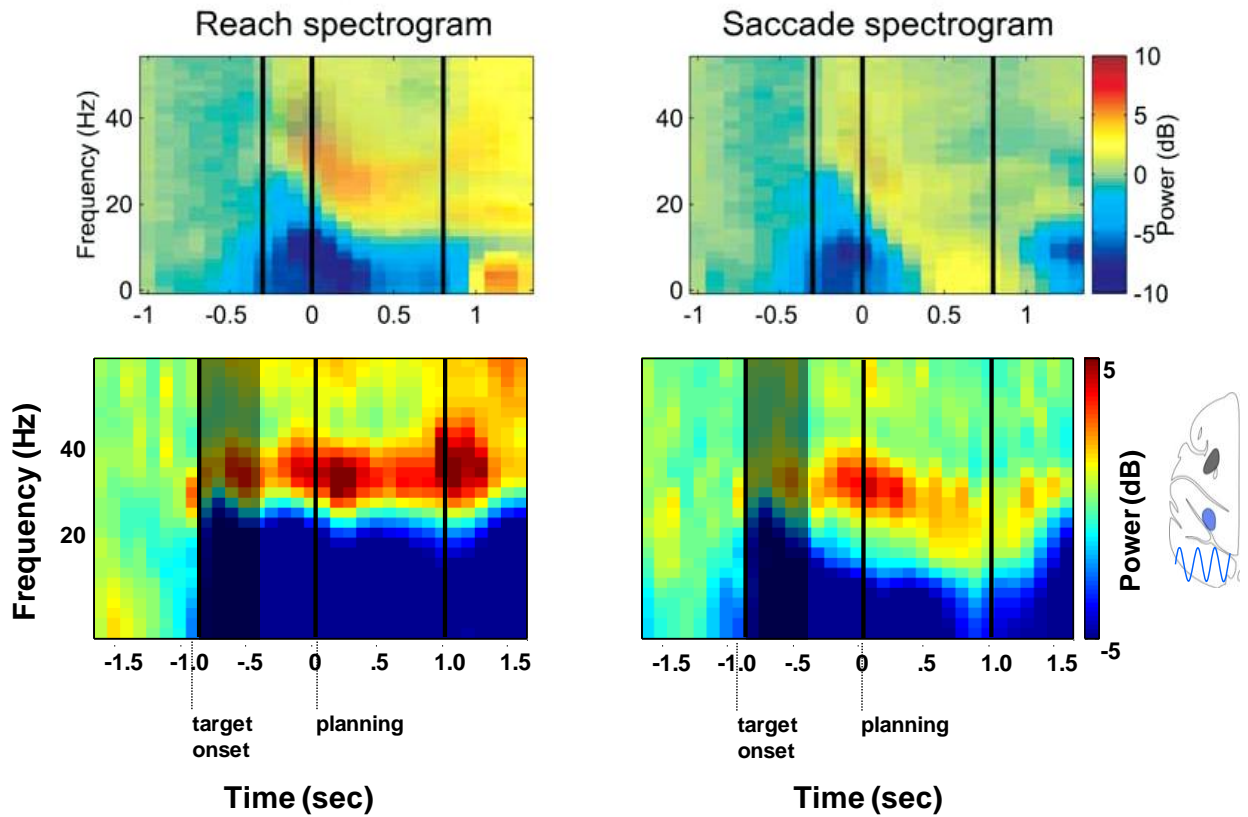


**Figure 4.2.3:** Comparison of LFP spectra based on effector choice. Top row adapted from Scherberger et al. [2005]. Preferred and anti-preferred directions are combined. Spectral estimates at each frequency are normalized to the baseline value at that frequency, calculated during fixation. Bottom row shows data from PRR in monkey/hemisphere L. Reaches have somewhat greater 25 – 35Hz power over the course of the planning period, as well as a significant drop in lower-frequency (1 – 20) Hz power. First .5 s of target presentation is grayed, since 1 s and .5 s target experiments were combined for these plots.

The data above show PRR LFPs to vary with the brain state as time progresses throughout the trial, as well as varying with the upcoming effector movement plan, and

hemisphere plan. Do frontal LFPs, which are somewhat weaker (fig. 4.2.1) carry similar behavioral information? Figure 4.2.4 shows the progression of frontal LFP power over the course of the task. Beta-band activity does exist, particularly in the fixation period for monkey R. However, it is largely overshadowed by much lower alpha-related activity. One common point to both monkeys/hemispheres is the presence of a short transient in the alpha activity immediately following the presentation of a target.

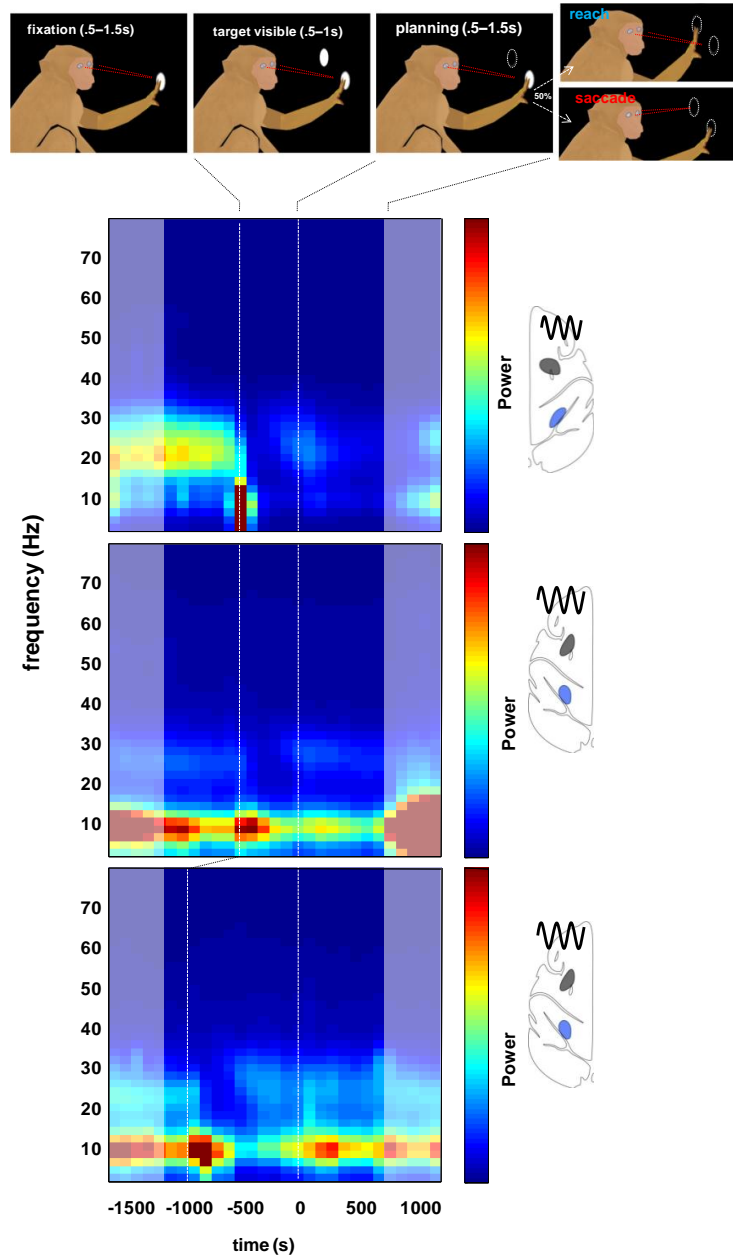


**Figure 4.2.4:** Progression of LFP power over the course of the trial. Settings are as in fig. 4.2.2, though we have also included the 1-s target trials (as in fig. 4.2.3). Faint beta-band activity is visible, and does seem to follow a similar pattern to PRR beta-band activity, turning on during fixation, extinguishing at the presentation of a target, and reappearing

during the planning period. However, this activity is largely overshadowed by much lower 8–10Hz alpha activity. Among its other features, this alpha activity exhibits a short transient following the presentation of a visual stimulus.

This section has shown that LFP power correlates strongly with brain state, and also with movement plan. The way in which beta-band power correlates with upcoming movements is not identical between monkeys. Classically, both spikes and LFPs predict planned movements, whereas individual LFP recordings are more accurate than spikes at reporting the monkey's brain state [Pesaran et al., 2002]. These LFP recordings seem to have a particularly strong relationship to preparation and planning brain states. Significant power exists in both the alpha (8–10Hz) and beta (15–30Hz) bands of the LFP in both brain regions. How will spikes recorded in the same brain interact with LFPs, and will these patterns persist over long-range interactions?

### **4.3 Spike-LFP coherence within PRR and PMd**

Spike-LFP coherence within a brain area has long been shown not only to be greater than chance, but also to correlate with behavioral variables, such as perception [Gray and Singer, 1989; Fries et al., 2001] and action plans [Pesaran et al., 2002]. In order to understand cross-cortical interactions using a measure like spike-LFP coherence, we should first understand the measure within a single cortical area. The analyses shown in this section indicate synchronization between spikes and LFPs at the beta, and to a lesser extent alpha, frequencies during fixation and planning.

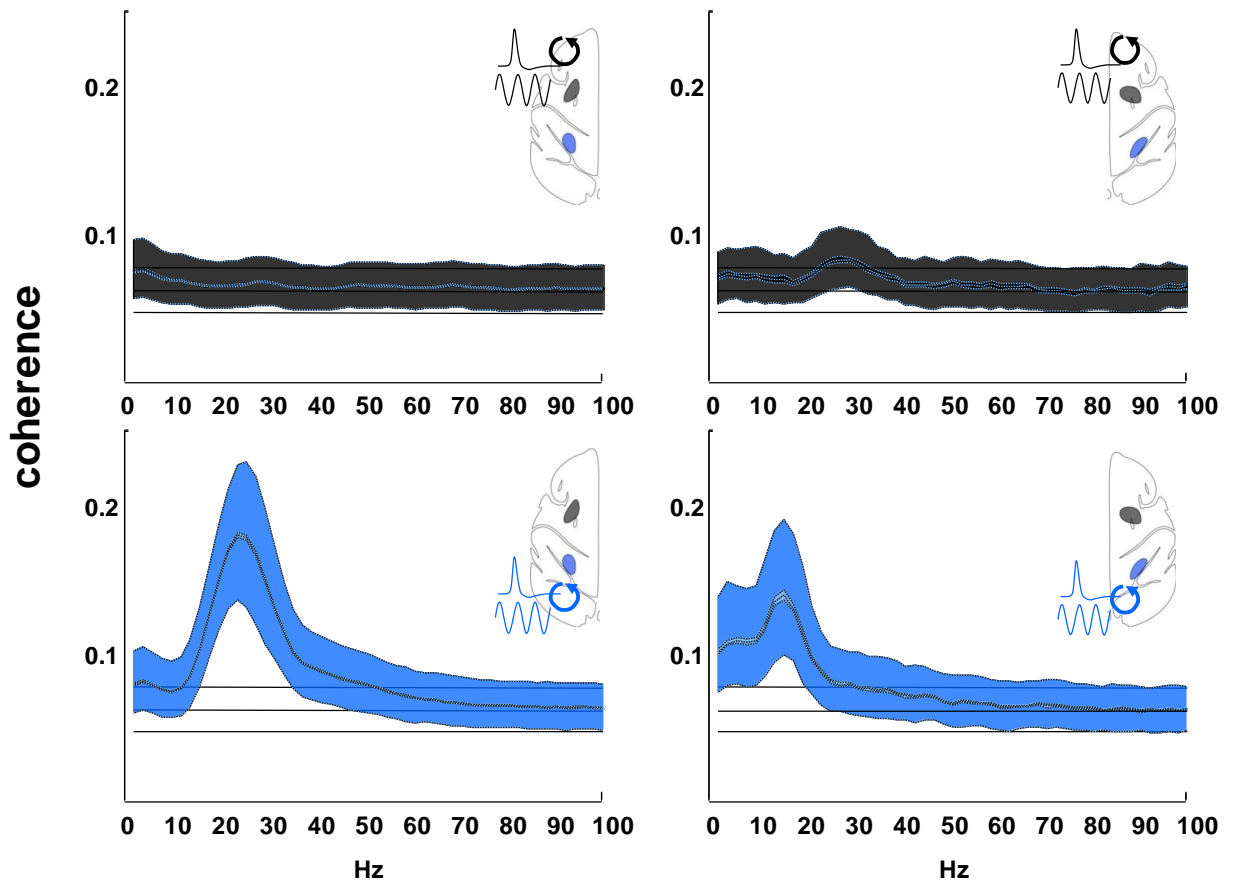


**Figure 4.3.1:** Spike-LFP coherence in PRR and PMd. As with the overall LFP power (fig. 4.1.1), coherence between spikes and LFPs in each region is significantly different during the planning period. Top row shows within-PMd spike-LFP coherence. Bottom row, within-PRR spike-LFP coherence. Coherence was estimated with stacks of 200 200-ms windows, using only spikes and LFPs from different electrodes (see Methods). Horizontal lines indicate values above which 66%, 50%, and 30% of the chance distribution lie, and outside and center lines indicate the same for the measured distribution.

Figure 4.3.1 shows significant spike-LFP coherence in both PMd and PRR in a swath of frequencies, however PRR is by far the more significant. Moreover, like PRR LFP power, PRR spike-LFP coherence shows a prominent peak at a specific point in the beta band (17 Hz, monkey R; 23 Hz, monkey L). Figure 4.3.2 shows beta-band spike-LFP coherence in PRR appears during fixation, is extinguished by target onset, reappears during planning, and is once again extinguished by movement onset. In this way, PRR spike-LFP coherence seems to follow the general trend of PRR LFP power (fig. 4.2.1–2).

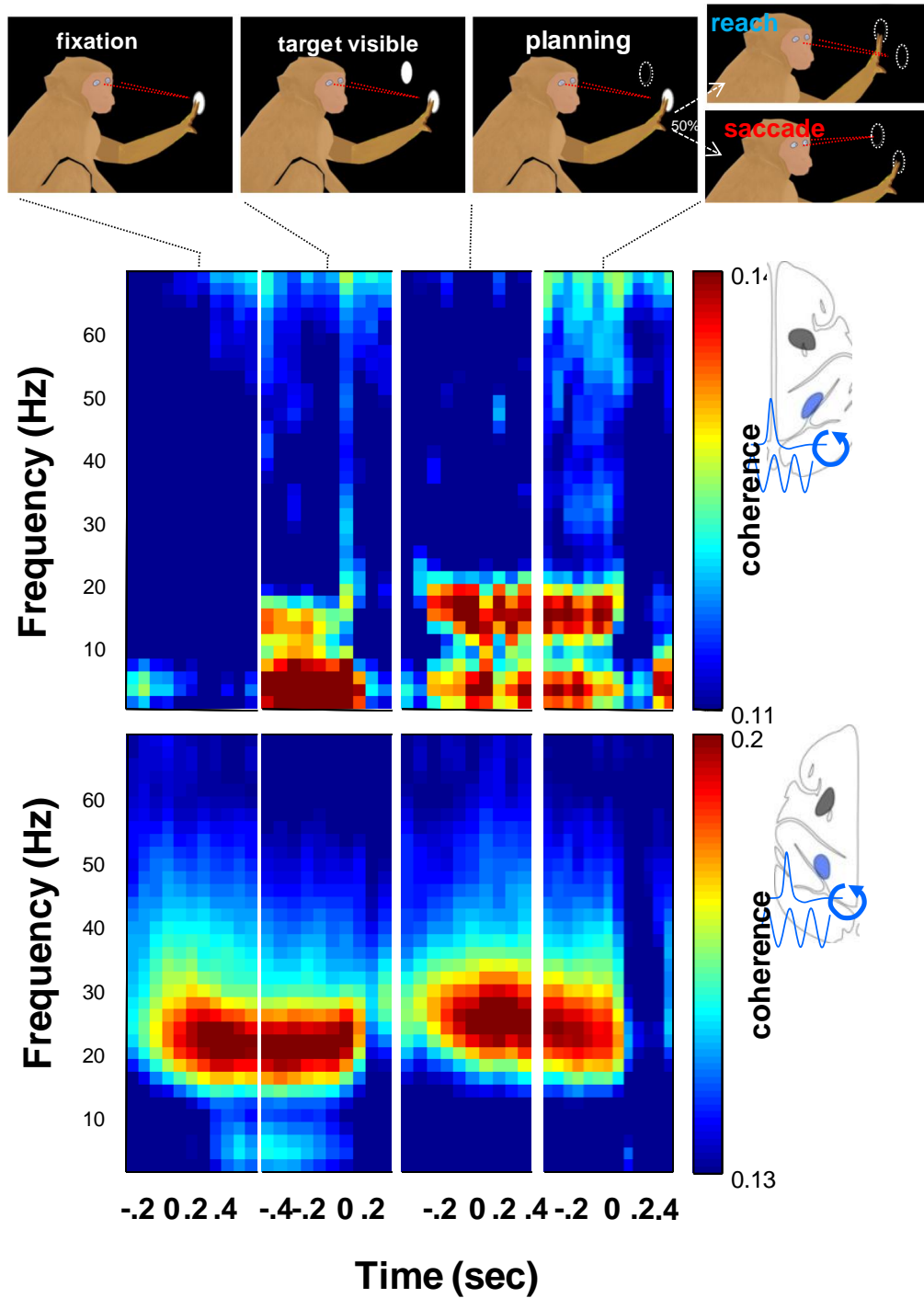


**Fig. 4.3.2:** Task-development of PRR-PRR coherence. Coherence was calculated over windows centered at particular time points in the task (otherwise, same parameters as fig. 4.3.1, see Methods). Each sub-window is centered at a specific phase of the task – fixation, target

onset, planning, and movement. Center row is hemisphere R, bottom row is hemisphere L. Both animals show pronounced beta-band spike-LFP coherence during the planning period, and the fixation period (to a lesser extent in R, which also shows pronounced low-frequency coherence).

Also, like PRR LFP power, PRR spike-LFP coherence in hemisphere L exhibits a relationship between planned effector and beta-band activity. Here, lower-frequency beta-band activity differentiates between saccades and reaches. Another view of the same phenomenon shows that the peak frequency for reaches is higher than for saccades (see fig. 4.3.3 caption). As with LFP power, hemisphere R did not show an overall bias toward any combination of effector and direction plan. This lack of overall bias caused us to ask whether there were indeed any relationship between PRR spike-LFP coherence and behavior plan in hemisphere R, as we would expect from previous data [Hwang and Andersen; 2009]. We performed a test of equal phase and angle on a the frequency-domain version of a spike-triggered LFP window (section 1.5, eq. 4), for spikes preceding each of the four movement types (ipsi- and contralateral saccades and reaches). The test can be thought of as a circular ANOVA on both phase and concentration of a quantity on a circle (here, the spike-triggered phase of the LFP frequency). This test was performed on each spike-LFP pair, and then averaged in the log domain over all spikes. The resulting p-value, akin to a joint probability corrected for multiple comparisons, showed the probability that spikes in the entire population tend to cohere with LFPs at the same phase and frequency depending on the upcoming action plan. The result, at the time of peak coherence, was negative ( $p < .01$ , hemisphere R;  $p < .05$  hemisphere L), suggesting that the distributions are different, even if there was no

visible overall bias. Therefore we propose that spike-LFP coherence is slightly different in phase and magnitude depending on the upcoming action, but weakly so. An overall bias toward stronger coherence preceding saccades is visible in data from hemisphere L, though this coherence is also at a significantly lower frequency.

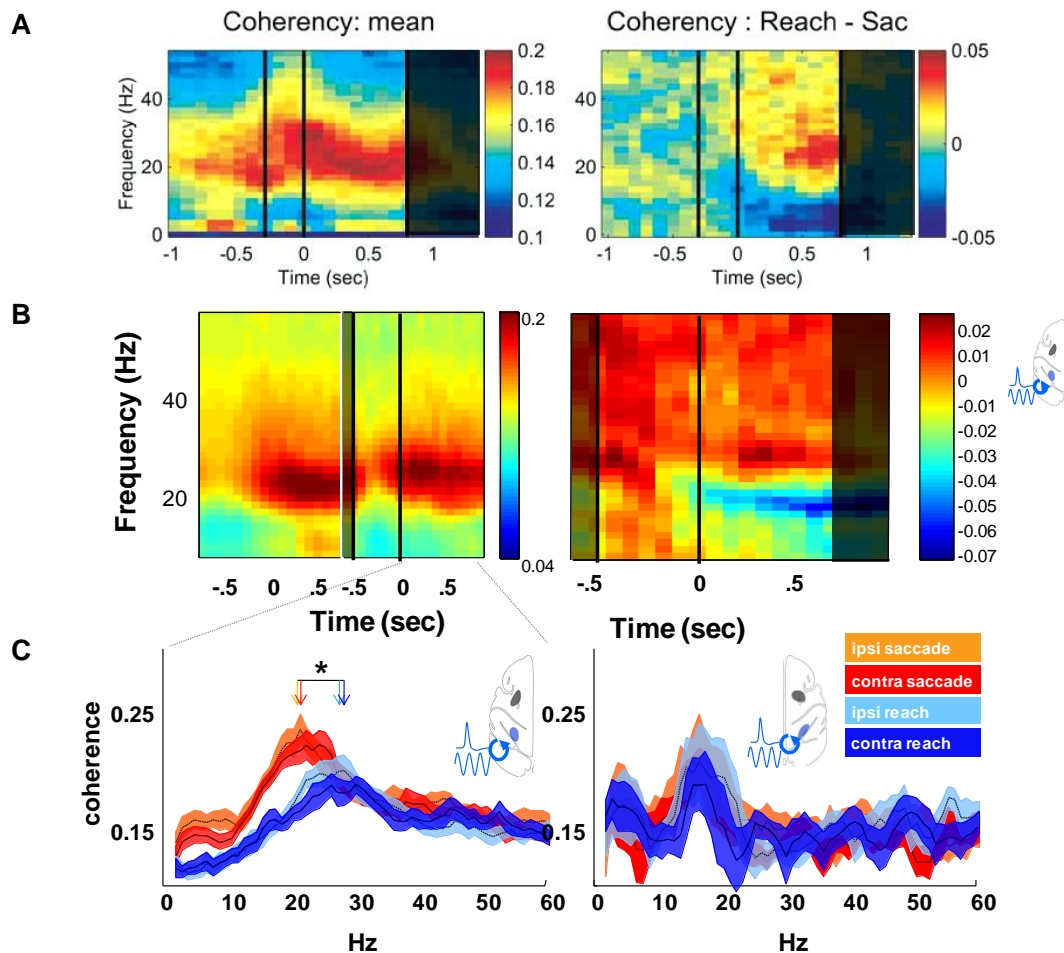


**Figure 4.3.3:** Effector-specificity of PRR-PRR spike-LFP coherence during the planning period. **A.** Adapted from Scherberger et al. [2005] showing the mean within-PRR spike-LFP coherence. **B.** Analysis for similar conditions, calculated from this manuscript's data (grayed areas are potentially non-overlapping segments between A and B).

Somewhat clearer B is the phenomenon of target presentation extinguishing the coherence, possibly because of windowing differences in calculation. Also, while both data sets show the drop in lower-frequency (10–20Hz) beta-band activity in common (ttest, 17 Hz coherence for all reaches vs. saccades,  $p < 1e-3$ ), the increase in higher-frequency beta is much subtler in these coherence data than in the LFP power estimates (fig. 4.2.3). **C.** Coherence, calculated with consecutive windows for each effector movement. Lines are as in fig. 4.2.1. Here, spike-LFP coherence was calculated only on the same electrode, for comparison to the figure from Scherberger et al., which accounts for the higher-than-normal baseline coherence. Lower-frequency increase in beta-band coherence is evident for saccades vs. reaches in hemisphere L. Possibly more informative is the suggestion that the peak frequency changes (mean 22 Hz/saccades vs 29 Hz/reaches, ttest  $p < 1e-3$ ; hemisphere R,  $p < .5$ ) based on upcoming effector movements.

Despite the weakness of the PMd spike-LFP coherence during the planning period, we also plot this quantity over the course of the trial. We find significant spike-LFP coherence between PMd spikes and PMd LFPs, but only just after the appearance of the target, and at a significantly lower frequency. Data may be consistent with the coherence profile shown in earlier cross-cortical coherence data from our lab [Pesaran et al., 2008], though they do not extend to the planning period. Hemisphere R also shows significant beta-band coherence during the fixation period. These data suggest that while beta-band coherence is not absent in PMd altogether, spikes there do not strongly phase lock at the beta frequency during the planning period.

Significant coherence within the PRR may be predictive of cross-cortical coherence, though it is not clear exactly what should be expected. On one hand, if the LFP in the beta band represents a signal broadcast over multiple brain regions, we would expect parietal spikes to cohere with it whether the LFP is recorded in PRR or PMd. On the other hand, the increased strength, and therefore fidelity, of the LFP in PRR may reveal coherence between PMd spikes and PRR LFPs that is not available in PMd alone.

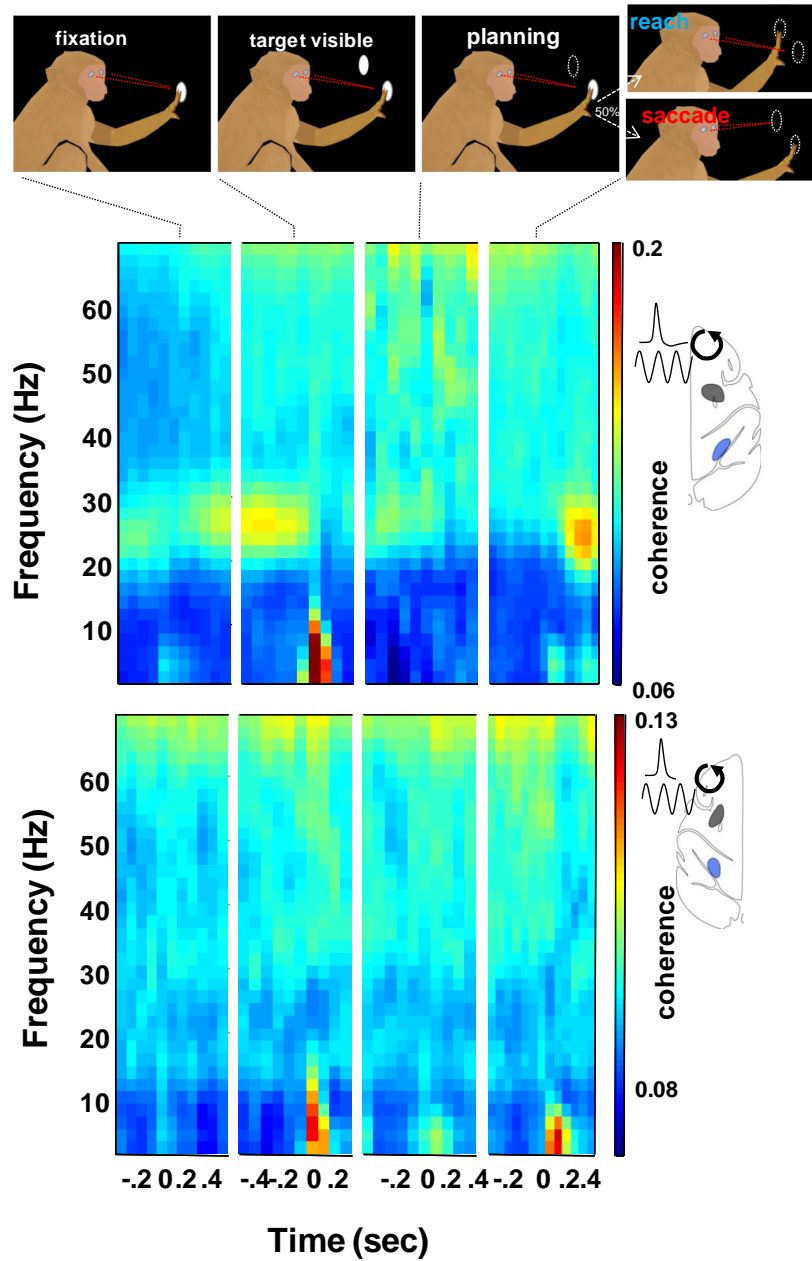


**Figure 4.3.4:** Task development of PMd-PMd spike-LFP coherence. Parameters are similar to fig. 4.3.2, but calculated within PMd. A small amount of beta-band activity is visible in hemisphere R during fixation, and a large and low-frequency event follows target presentation, but PMd spike-LFP coherence is weak or absent during planning.

## 5 Interaction of Signals Across Cortex

The primary focus of this manuscript is to determine whether there are significant interactions between small-scale signals across functionally similar but anatomically distinct cortical regions. Section 2 showed planning activity which is highly similar between cells recorded in PRR and PMd. However, section 3 showed that PMd tends to respond sooner to visual targets and movement instructions. The latter would seem to suggest that PMd is upstream of PRR in response to a visual stimulus. But, does PMd drive PRR during steady-state, or visa-versa? Can we answer this question using interaction between neural signals recorded in the two areas?

### 5.1 Spike-spike interactions

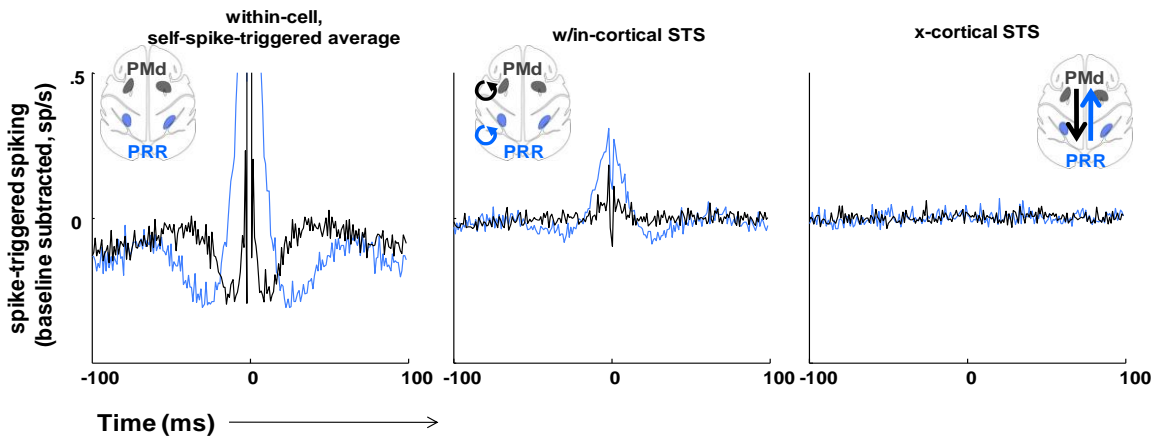


**Figure 5.1.1:** Within- and across-cortex spike-spike relations during planning. **A.** Individual cells autocorrelate, showing some periodicity. **B.** Spike-triggered-averaging of independent cells within the same brain region. STA of parietal spikes with each other shows periodicity in the 15 - 25Hz range. STA of frontal spikes is less periodic. **C.** Spike-

triggered averaging of spikes in one brain region with spikes in another shows no significant interaction.

An obvious first question to ask is whether spikes in one brain region show a significant timing relationship to spikes in a second, though conventional wisdom suggests this is unlikely. Indeed, our data suggest no significant relationship on average. Spike-spike cross-correlations, or spike-triggered-averages of other spikes, show no apparent activity across cortex. Local field potentials (LFPs), which may represent a different facet of local processing in the brain, and represent cortical information on a larger scale, may give a hint of these regions' interactions. First, we will ask whether LFPs synchronize cross-cortically (section 5.2), which should give a good overview of the interaction between these areas. More specifically, though, the spike-LFP coherence has been proposed to have specific, directional meaning for communication between brain regions. Section 5.3 will answer for the first time whether cross-cortical spike-LFP coherence occurs during action planning.

## **5.2 LFP-LFP coherence**

Current thinking on the local field potential suggests that it is a highly localized signal, with functional properties that extend over tens but not more than hundreds of microns [Katzner, 2009]. These make LFPs an attractive candidate for use in assessing long-range communication, and significant recent effort has gone into interpreting cross-cortical LFP-LFP interactions [Buschmann and Miller, 2007; Gregoriou et al., 2009]. The primary measure of interaction will be the coherence.

Nearly any interpretation of functional coupling via synchrony suggests that a change in cross-cortical spike-LFP coherence will result in a change in communication efficacy from the spiking region to the LFP location. With the intent of revealing such changes in communication efficacy, recent studies have shown significant cross-cortical interactions between local field potentials [Buschmann and Miller, 2008], and between multi- and single-unit spikes and LFPs [Pesaran, Nelson and Andersen, 2008; Gregoriou et al, 2009; Verhoef et al, 2011], across widely disparate parts of cortical territory during tasks involving both areas.

Since LFP-LFP coherence is subject to external noise (such as mechanical vibrations in the equipment and 60 Hz line noise, neither of which affect action potentials nor spike-LFP coherence), it should be interpreted with caution.

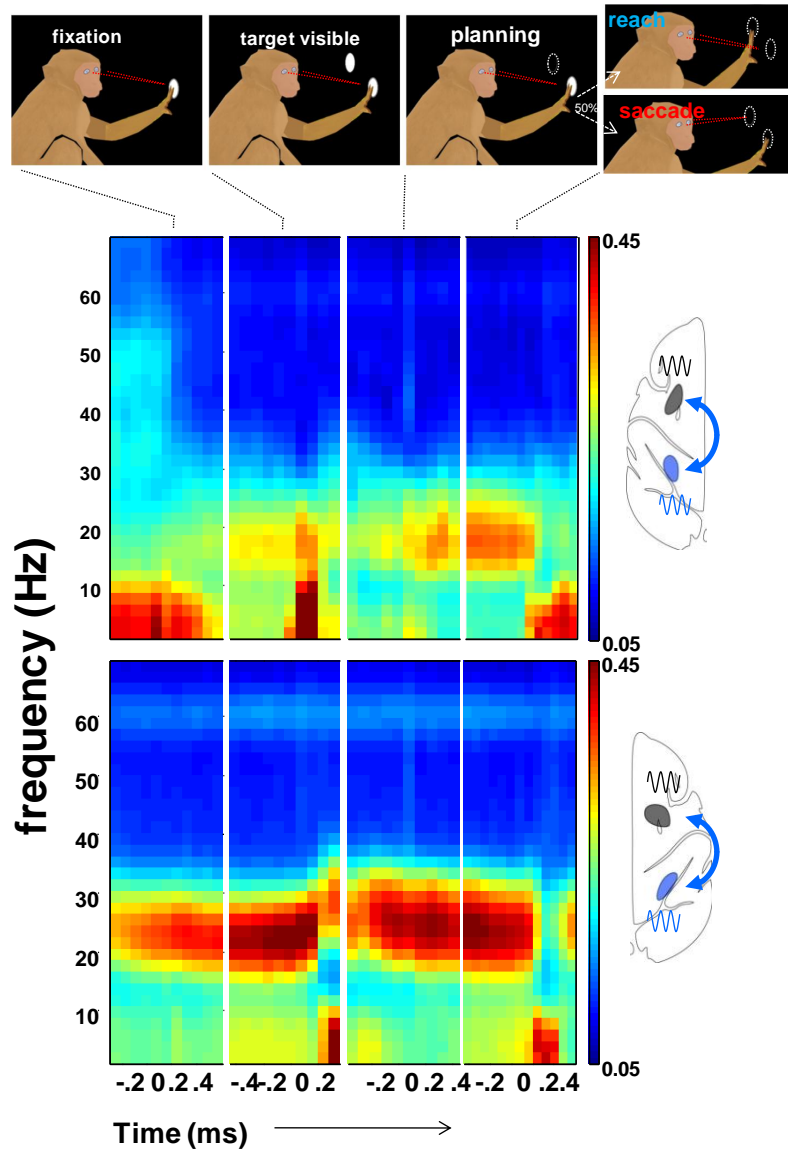


**Figure 5.2.1:** LFP-LFP coherence is highly significant (chance level is .12), and shows similar features to the PRR and PMd within-cortex spike-LFP coherence (figs 4.3.2-4), as well as the raw LFP power in each area (fig. 4.2.2). Generally, LFP-LFP coherence is strong during the planning period at the beta frequency band, and much weaker at other frequencies, especially above 60 Hz. Horizontal line noise is visible at 60 Hz in the lower plot for hemisphere R, which conveniently gives an idea of the scale of the frequency spread imposed by the

single taper. Fixation-period coherence is significantly different between the two hemispheres, but the target-onset related event, and the planning period coherence are qualitatively similar.

Figure 5.2.1 shows evidence of cross-cortical LFP-LFP coherence, which varies over the course of the task. Figure 5.2.2 shows the same quantity during the planning period only, where it is subdivided by planned effector. As with earlier data, behavioral variations in frequency are evident in hemisphere L.

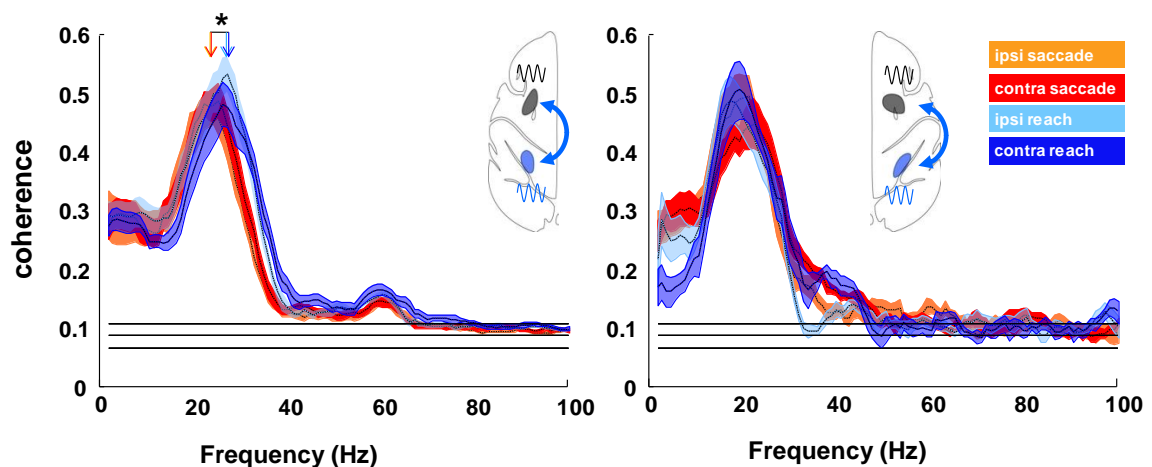


**Figure 5.2.2:** Average LFP-LFP coherence by effector and spatial location. As with fig. 4.3.3, windows are broken down by planned action (ipsi-, contra-lateral saccades and reaches), and the coherence (here, LFP-LFP) is compared across conditions. Also, similar to the within-PRR spike-LFP coherence in hemisphere L shown in fig. 4.3.3, the cross-cortical LFP-LFP coherence is significantly higher in frequency in advance of reaches compared to saccades (\* =  $p < 1e-5$ ).

The frequency shift shown in fig. 5.1.5, left hemisphere, matches the shift in within-PRR spike-LFP coherence, described in fig. 4.3.3. The general trend seems to be that reach plans are accompanied by more power in high-frequency bands, and less power in low-frequency bands. While the picture from earlier results in PRR alone may suggest increased high-frequency activity from 20–80 Hz, this manuscript's data suggest that only frequencies of 20–40 Hz are increased in advance of reaches, and shared across cortex. In this light, it seems that reach plans actually shift the underlying beta *frequency* upward, which potentially constitutes new evidence of frequency coding [Akam and Kullman; 2010] in cross-cortical interaction. Additionally, and perhaps not inconsistently, saccade plans seem to be accompanied by an overall increase in oscillatory power and coherence at in the lower half of the beta-band (10–23Hz, monkey L). Considering that beta-band activity may actually suppress movements [Zhang et al., 2008], smaller overall beta-band activity may actually disinhibit an upcoming reach. Note that while there is no overall bias for saccades in frequency or magnitude of LFP-LFP coherence in monkey R (except perhaps at < 10 Hz), we have already shown that within-PRR coherence codes weakly for the upcoming plan on a unit-by-unit basis.

The bias of cross-cortical LFP-LFP coherence with the upcoming behavior is significant (in hemisphere L), but weak (fig. 5.1.5). While coherence is thought to subserve communication, it is not clear whether communication should occur more in advance of a particular kind of action, or simply during the phase of the task in which the action is being planned. In fact, coherence may simply act as a channel along which signals already encoded in spikes can pass during a phase of a task requiring communication. Under this theory, one would expect little variation in coherence depending on the

upcoming action. However, a functional channel can only exist over an existing anatomical one, and so one should expect anatomical variation in coherence strength. PRR and PMd are known to be connected [Tanne-Gariepy et al., 2002]. However, to our knowledge no evidence exists for a connection between PRR and saccade-related areas in the arcuate sulcus, such as the FEF. We therefore repeated our experiment, but varying the frontal recording location along an anterior and lateral vector secant to the arcuate sulcus (fig. 5.1.4). The LFP-LFP coherence did indeed vary with anatomy, decreasing as the frontal electrode diverged further from the site of known connection with PRR. These are not the first LFP-LFP results to vary with anatomy — Verhoef et al. [2011], showed LFPs in anterior intraparietal areas to cohere more with connected, as compared to unconnected, regions in temporal lobe.

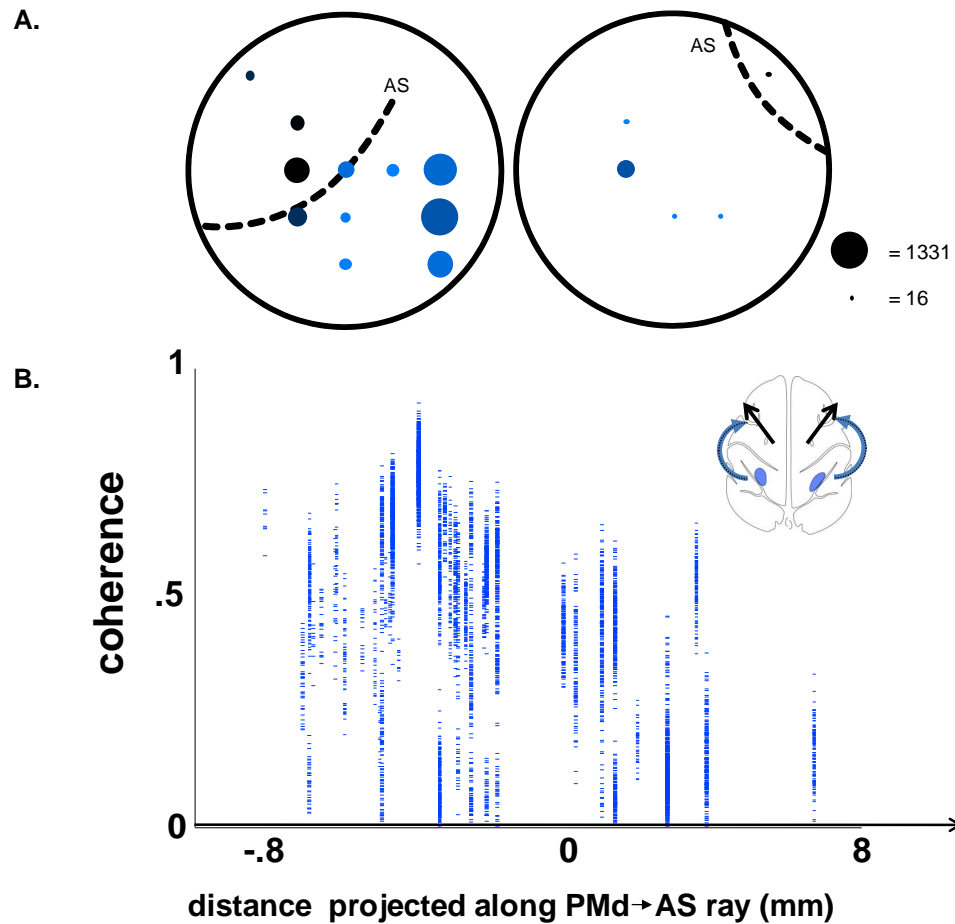


**Figure 5.2.3:** PRR-frontal coherence variation with frontal cortical anatomy. **A.** coherence of PRR LFPs with LFPs recorded over different parts of the frontal chambers. Color intensity represents % significant coherence. Dot area represents the number of recordings in that location (smallest = 10, largest = 500, same scale in A and B). PRR spikes are from the locations shown in fig. 1.5.1. Blue circles represent approximate estimated injection sites of retrograde tracers from PMd indicating a medial parietal area including PRR, as reported in Tanne-Gariepy et al. [2002]. **B.** % significant coherence, projected onto a line from the primary PMd recording spot, through the arcuate sulcus (same dot scale). Correlation between PRR-PMd spike-LFP

coherence and distance along PMd  $\rightarrow$  AS ray:  $r = -.54$ ,  $p < 0$ . This specificity may constitute evidence that coherence acts along anatomical connections, perhaps signifying a flexible communications channel. Behavioral variation in the coherence could be interpreted as the opening and closing of such a channel.

A related measure to LFP-LFP coherence is Granger causality. Granger causality in the frequency-domain has been applied to EEG signals [Baccala and Sameshima, 2002] in order to determine directionality of influence across the cortex. LFPs are orders of magnitude more spatially localized than EEG (see section 1.5, and Poulet and Petersen, 2008). We therefore analyze data from individual recording days in each hemisphere featuring strong LFP-LFP coherence, to look for a directional influence (fig. 5.1.4).

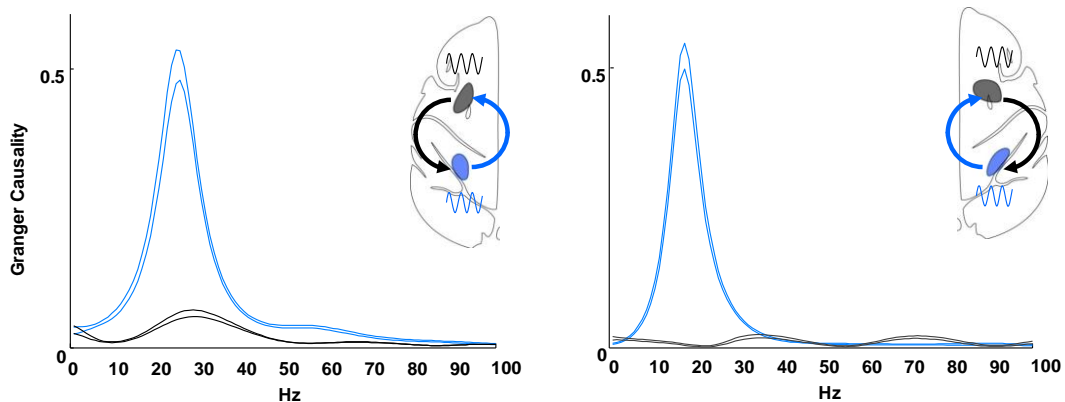


**Figure 5.2.4:** Granger causality calculated between LFPs in PRR and PMd data during the planning period. Blue traces are parieto-frontal causality, black are fronto-parietal. Errors are SEM.

Granger causality describes the extent to which one signal can be modeled on another's previous values, over and above the power it has in modeling itself. A signal Granger-causes another in the frequency domain when variations in that frequency's amplitude or phase in one area predict similar variations in the second area. The analysis in fig. 5.2.4 indicates significant and asymmetric Granger causality in the parieto-frontal direction.

Consistent with other reports [Brovelli et al., 2004], these results may constitute preliminary evidence that PRR drives PMd in the beta-band. Do individual spikes indicate the same?

### 5.3 Spike-LFP coherence across cortex

Section 5.2 showed that PRR and PMd strongly interact in the beta-band during planning. However, the LFP-LFP coherence is subject to limited interpretation. While LFPs may represent synaptic activity from afferent inputs to a brain region [Mitzdorf, 1985], they doubtless also contain information about local processing. Spikes unambiguously represent the output of a given brain region, and while they do not interact strongly with each other across cortex (Section 5.1), they may interact with cross-cortical LFPs, providing a narrower interpretation than the one available from LFP-LFP coherence alone. In engineering applications, coherence is a measure of the effect of an input on an output at a particular frequency [Bendat and Piersol, 2000]. As such, coherence between spikes in one brain region and LFPs in another may indicate that spikes, the outputs of one brain region, are directly or indirectly driving LFPs, the inputs to another [Mitzdorf, 1985]. Additional interpretations for the coherence exist within neuroscience. For example, phase-locking between spikes and oscillatory potentials within and across brain areas could represent increased efficacy of communication, whereby spikes arrive at an advantageous time with respect to the sub-threshold membrane potential [Fries, 2005], or by adopting a frequency for which downstream targets are tuned [Akam and Kullman, 2010]. Nearly any interpretation of functional coupling via synchrony suggests that a change in cross-cortical spike-LFP coherence will result in a change in communication efficacy from the spiking region to the LFP location. With the intent of revealing such changes in communication efficacy, recent studies have shown significant cross-cortical interactions between local field potentials [Buschmann and Miller, 2008], and between multi- and single-unit spikes and LFPs [Pesaran, Nelson and Andersen, 2008; Gregoriou et al, 2009; Verhoef et al, 2011],

across widely disparate parts of cortical territory during tasks involving both areas. We therefore undertook to test for the significance of cross-cortical PRR-PMd and PMd-PRR spike-LFP coherence.

We find no significant coherence between spikes in PMd and LFPs in PRR (fig. 5.3.1.A). In contrast, spikes cohere significantly in the other direction. PRR spikes cohere significantly with LFPs measured in PMd (fig. 5.3.1.B). 45% / 42% (hemispheres L/R) of cells recorded in PRR cohered significantly with PMd LFPs in the beta-band. While this cross-cortical coherence is weaker than the beta-band spike-LFP coherence within PRR (80%/63%R of cells cohere significantly with LFPs within PRR alone, see section 3.3), this cross-cortical spike-LFP coherence nevertheless represents a significant deviation from chance (fig. 5.3.1.B). Previous reports of cross-cortical spike-LFP coherence [Pesaran et al, 2008; Gregoriou et al, 2009] feature symmetric interactions, though these studies did not involve a planning period. Note that even though parietal LFPs are stronger than PMd LFPs in the beta-band, it is PRR spikes that cohere with PMd LFPs, not vice-versa.

Intra-cortical parietal spike-LFP coherence is high in the beta range (section 3), as is cross-cortical LFP-LFP coherence. These two factors combined might be sufficient to explain the existence of cross-cortical spike-LFP. In other words, spikes in PRR might simply synchronize with LFPs in PMd as a side effect of their synchrony with nearby PRR LFPs, and PRR LFPs synchronizing with PMd. On the other hand, it could be that PRR spikes have special information about PMd LFPs, which is not shared by LFPs found in PRR. These possibilities could be distinguished via an additional, partial spike-LFP analysis [Bendat and Piersol, 2000; Albo et al, 2004; Pesaran et al, 2008]. The partial coherence reveals the portion of PRR-PMd spike-LFP coherence that is not

explained by the product of PRR-PRR spike-LFP and PRR-PMd LFP-LFP coherences. The PRR-PMd spike-LFP coherence survives the partial coherence treatment (fig. 5.3.1.C), indicating that PRR spikes contain phase and amplitude timing information about distant PMd LFPs which is not available in PRR LFPs. Whatever the exact interpretation of the meaning of the cross-cortical spike-LFP coherence, therefore, it should be examined in its own right, without assuming it represents the same as the within-parietal spike-LFP coherence or the parieto-frontal field-field coherence.

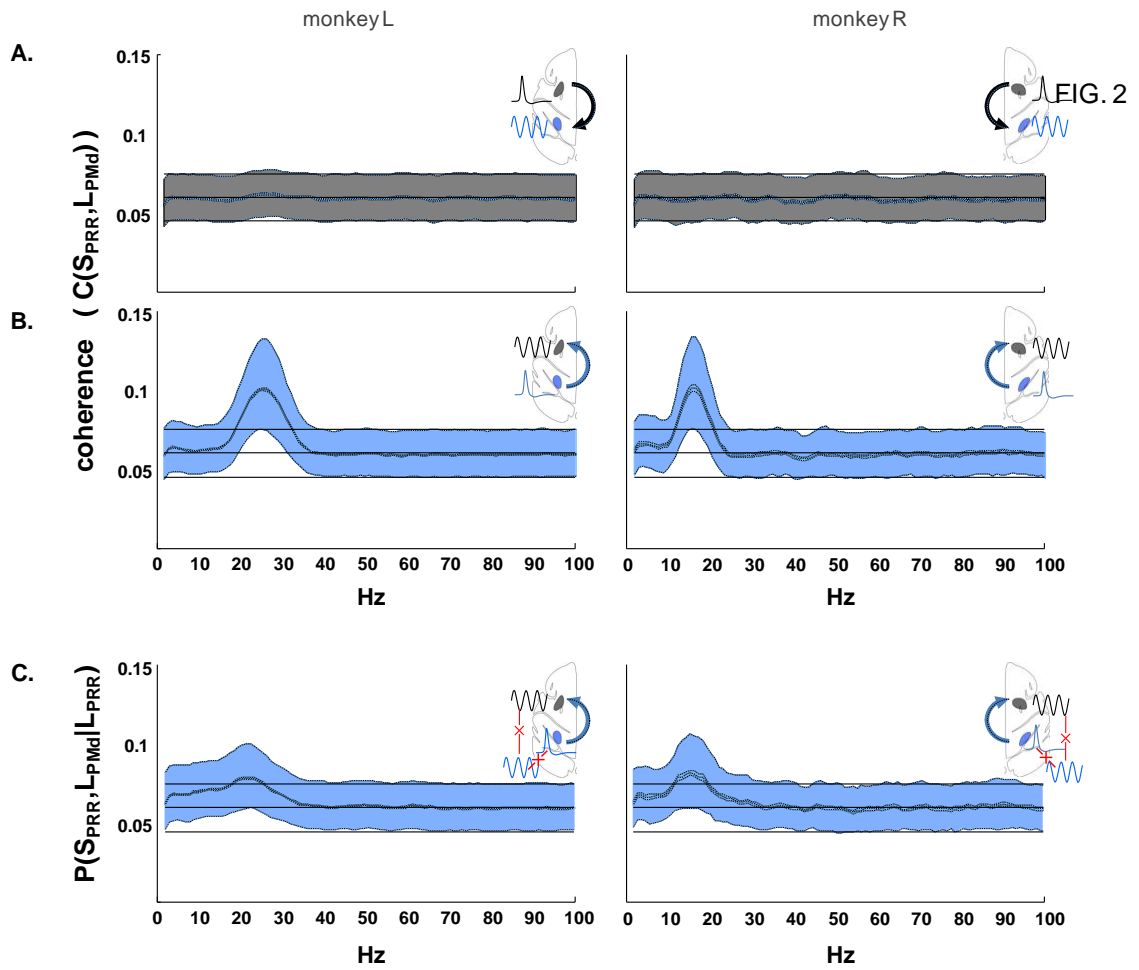


**Figure 5.3.1:** Cross-cortical spike-LFP coherence during the memory period. **A.** Coherence between PMd single-unit spikes and PRR LFPs. Center lines are surrounded by 5% distribution lines, describing coherence values 2.5% below and above the median. Outside lines represent 60% of the distribution. Center and outside black lines represent median and 60% distribution lines for the chance distribution. **B.** Coherence between PRR single-unit spikes and PMd LFPs. **C.** Partial coherence between parietal spikes and frontal LFPs, with respect to parietal LFPs

The conventional coherence measure (section 1.3) conflates amplitude and phase relationships. To understand whether phase-locking alone was sufficient to explain these results, the analyses from figure 5.3.1 were repeated using a measure of phase locking between spikes and LFPs (section 1.3, eq. 3). This method, while unconventional, does not suffer from mixing of phase and amplitude correlations (Gregoriou et al, 2009). The results were as follows: chance-level PMd-PRR spike-LFP coherence was detected, significant PRR-PMd spike-LFP coherence was detected at 17 Hz/23 Hz (for animal R/L), with > 35% of cells showing significant coherence for both animals, and > 20% of cells showing significant partial phase-locking with respect to parietal LFPs. Therefore, a large component of the coherence reported here is attributable to phase locking rather than amplitude correlation. The below concentrate on the conventional coherence to leave open the possibility for amplitude correlation, which is important for some interpretations of interactions between regions. However, phase-locking alone will be important for the following series of results, where the PRR-PMd spike-LFP coherence is further characterized across phases of the task and trial types.

Figure 5.3.2.A shows the planning period coherence in an example cell, broken down by the action being planned, with coherence averaged over trials and PMd LFPs. This is the same PRR example cell as shown in fig. 1.5.5, second row. Note that while this cell fires most for contralateral reaches, its highest coherence magnitude is for ipsilateral reaches (though, its highest cross-cortical coherence *frequency* is for contralateral reaches).

Figure 5.3.2B shows the development of the average PRR-PMd spike-LFP coherence over the course of the trial. Cross-cortical coherence appears during fixation, disappears at target onset, and reappears during the planning period. The averaged coherenceogram in fig. 5.3.B averages over some differences between monkeys/hemispheres. Namely, in hemisphere L, where recordings were taken from the contralateral hemisphere to the

movement, coherence was equally high in magnitude during fixation and memory period ( $p < .5$ , t-test), but higher in frequency during the memory period ( $p < 1e-10$ , t-test). In hemisphere R (ipsilateral hemisphere to the arm used) coherence was significantly higher in magnitude ( $p < 1e-10$ , t-test) and frequency ( $p < .05$ , t-test) during the fixation period. The difference in these results (frequency change in one animal, magnitude change in the other) may be attributable to the hemisphere difference. However, both an increase in phase-locking [Womelsdorf et al, 2007] and an increase in frequency [Akam and Kullman, 2010] could be consistent with an increase in functional communication during the memory period.

Perhaps the most striking differences are between the target presentation period and memory period. During the presentation of visual targets, PRR–PMd spike-LFP coherence is lower than the memory period ( $p < 1e-3$  L,  $p < 1e-10$  R), as is the frequency in animal L ( $p < 1e-3$ ,  $p = .28$  in animal R). Both PRR and PMd are responsive to visual stimuli, and yet they cohere much less in the beta band when stimuli are present. In some cells there is a significant, transient, fronto-parietal and parieto-frontal increase in spike-LFP coherence between 5–15Hz, just after target presentation. Because of its transience, this visual-onset effect may not be well-described by the coherence measure, which is designed for linear, time-independent systems. However, it should be noted that the latter effect is qualitatively similar to the cross-cortically symmetric, transient effects seen in Pesaran et al, 2008, and is also shared by PMd-PRR spike-LFP coherence. Also, similar to Pesaran., 2008, the visual response to a target occurred 15-20ms sooner in PMd than in PRR, which is surprising given the traditional assignment of the intraparietal sulcus upstream from PMd in the dorsal visual stream [Goodale and Milner, 1992]. However, this report focuses on sustained effects,

not stimulus onset-related effects. The sustained coherence in the 15-25Hz band is much higher after the targets have disappeared than when they are present.

While the cross-cortical coherence magnitude does not necessarily follow the rate coding profile of the spike in question, coherence may have a significant relationship to the particular action being planned independent of the spike-rate profile. To explore this possibility, we applied a test of the equivalence of the distributions of spike-triggered LFP phases across different planned actions in the four cases. For each spike-LFP pair, this test produced a p-value (the probability that the distributions were identical) at each frequency and time point, the log of which was then averaged across cells [Fisher, 1993]. The results (fig. 5.3.2.C) suggest that for many cells, spike-LFP coherence significantly codes for the action being planned around the time of the peak coherence magnitude in the beta band. Across cells, monkey R showed no average pattern in coherence amplitude or frequency according to the planned action, with different spike-LFP pairs coding for these variables in different ways. However, an average of all spike-LFP pairs coding for these variables in different ways. However, an average of all spike-LFP pairs in monkey L shows that spike-LFP coherence is significantly higher frequency in advance of reaches than saccades ( $p < 1e-2$ ), and higher frequency for contralateral reaches than ipsilateral reaches ( $p < 1e-3$ ). The low-frequency spike-LFP interaction which follows visual onset also carries significant predictive power for the visual target (fig. 5.3.2.B).

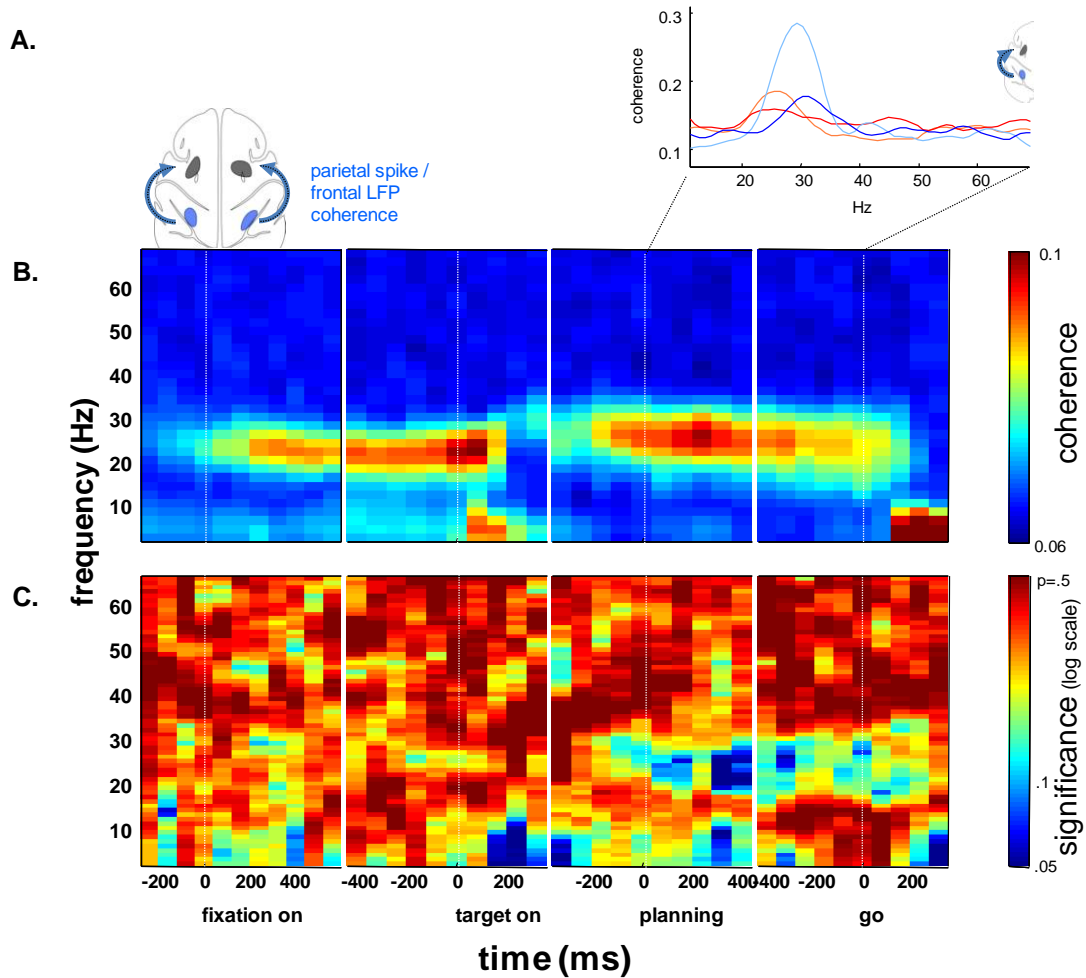


**Figure 5.3.2:** Task-related variation in PRR-PMd spike-LFP coherence.

**A.** Spike-LFP coherence from example parietal cell from fig. 1B with frontal LFPs. Each trace represents the average cross-cortical coherence in advance of a particular action (ipsi-/contra-, saccade/reach). **B.** Cohereogram of PRR spikes (single-unit and MUA) and PMd LFPs in both monkeys, calculated in 200 ms windows, and centered on different phases of the task, averaged over all parietal spikes, frontal LFPs, and trial types. Coherence appears during the fixation period, disappears during the target onset, and reappears at a slightly higher frequency and magnitude during the planning period. **C.**

Significance of phase-locking between PRR-spikes and PMd LFPs according to the action being planned. Phase-locking of PRR spikes to PMd LFPs was tested for variation with the planned action (reaches or saccades to the ipsi- or contralateral hemispace). The phase and magnitude of each spike with respect to the PMd LFP was compared across the four possible actions being planned. The results across all cells were averaged in the log domain. A low probability (blue) indicates that the distributions are unlikely to be identical. At most times and frequencies, phase-locking between PRR spikes and PMd LFPs is invariant with the action being planned. However, around the time and frequency of the peak coherence, (200-400 ms into the planning period), they are unlikely to come from the same distribution, indicating that spikes synchronize at a different frequency or phase according to the upcoming planned action. The low-frequency event corresponding to visual onset also results in a significant difference in the distributions. The latter may be the same kind of target-elicited event that was measured in Pesaran et al. [2008].

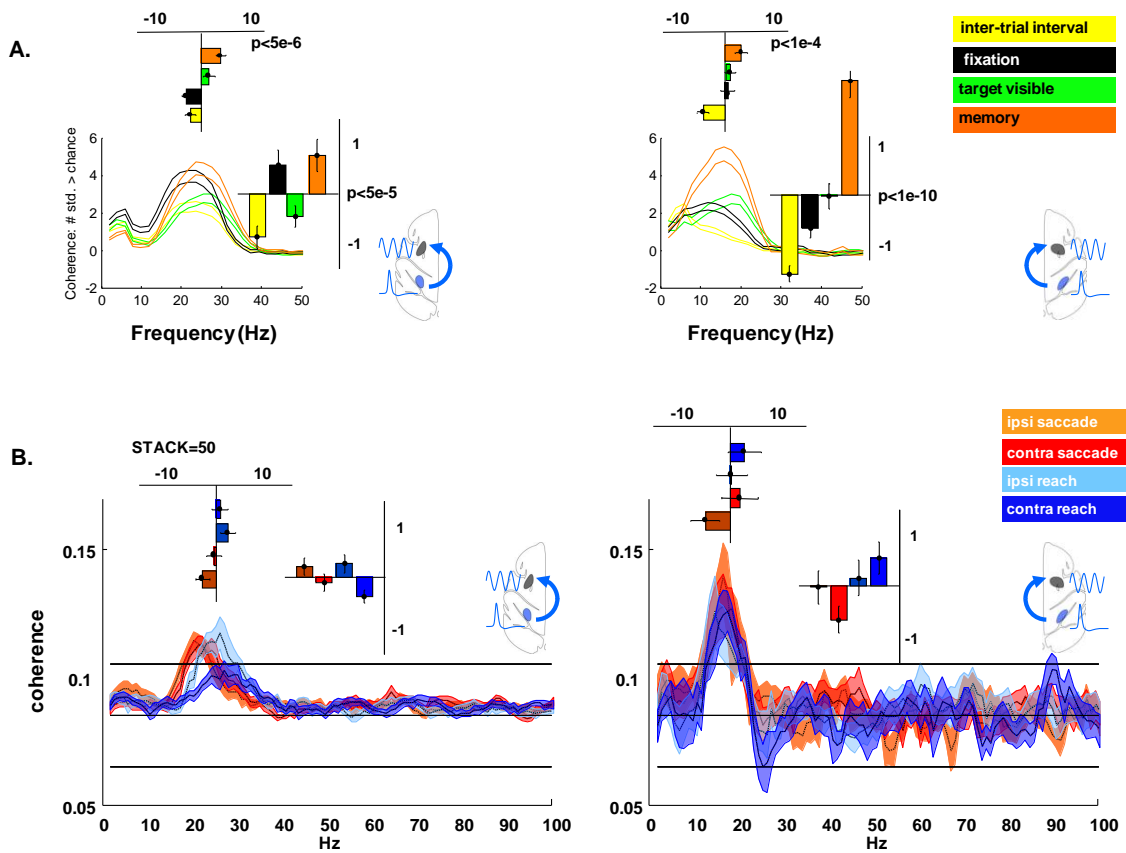


**Figure 5.3.3:** A more detailed treatment of ask-dependence of PRR spike / PMd LFP coherence. **A.** PRR / PMd spike-LFP coherence by brain state. Y-axis represents the number of standard deviations by which the coherence exceeds the mean (see z-transform, Methods). Error bars are S.E.M. Bar plots are expanded views of each axis. Top bar plot, peak coherence frequency for each cell was collected for each brain state, and the means and standard errors are plotted on the bar graph. The probability that all brain states have the same coherence frequency is  $< 5e-6, 1e-4$  (for monkeys L/R, anova). The probability that the planning period coherence is higher in frequency than the fixation period is  $p < 1e-6, .05$  (L/R, t-test). Bar plots to the right are the same, but for the peak coherence magnitude. Only in monkey R was the coherence significantly higher during planning than fixation ( $p = 0$ , t-test). **B.**

PRR / PMd spike-LFP coherence by planned action. Format is the same as in B. Here, we only consider coherence during the planning period, and only cells with significant coherence during the planning period were considered. The planning period was subdivided into trials according to the upcoming action (ipsi- and contra- reach and saccade), and stacks of 100 windows were used (rather than 200).

If the coherence represents a functional channel between brain regions, such a channel would operate only over existing anatomical links. Therefore, we would not expect to find significant coherence between PRR and frontal areas to which it is not known to project. Still recording spikes in PRR, we now varied the location of the other recording site over the extent of the frontal chamber (fig. 5.3.4), into and beyond the arcuate sulcus, the seat of the frontal eye fields (FEF). In contrast to the PMd, and to the best of our knowledge, there are no reports of monosynaptic anatomical connections between PRR and FEF. We found that the coherence was smaller between PRR and the regions around and beyond the arcuate sulcus. This is consistent with the idea that coherence represents a functional connection within existing anatomical networks.

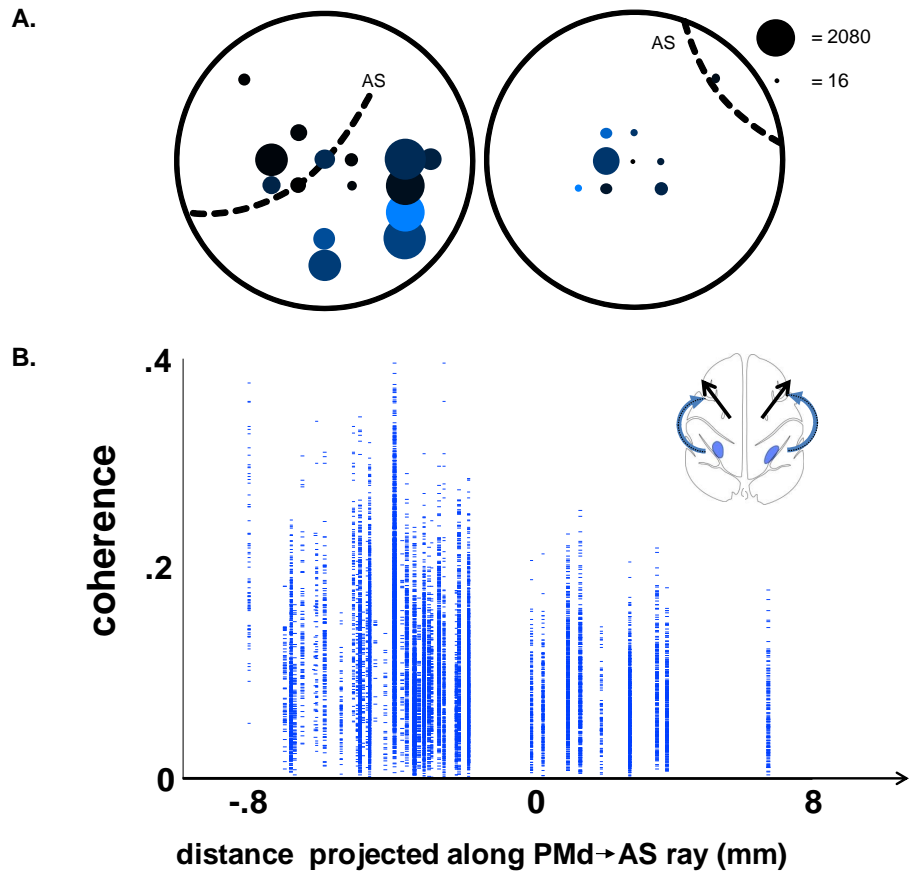


**Figure 5.3.4:** Anatomical variation in beta-band x-cortical spike-LFP coherence. **A.** coherence of PRR spikes (single-unit and MUA) with LFPs recorded over different parts of the frontal chambers. Color intensity represents % significant coherence. Dot area represents the number of estimates made in that location. Each estimate represents 200 windows, so a single spike-LFP pair can give rise to multiple estimates. PRR spikes are from the locations shown in fig. 1.5.1. **B.** Individual spike-LFP coherence estimates (horizontal jots), projected onto a line from the primary PMd recording spot, through the arcuate sulcus in both monkeys. Coherence between PRR spikes and LFPs in frontal areas is negatively correlated with distance of the frontal recording location along the PMd-AS ray ( $R = -.26$ ,  $p < 1e-10$ ).

## 5.4 Discussion of asymmetric cross-cortical coherence

We have discovered significant coherence between single-unit action potentials in PRR and LFPs measured in PMd (fig. 5.3.2). This coherence, which is not explained exclusively by the interaction of within-PRR spike-LFP coherence and PRR-PMd LFP-LFP coherence (fig. 5.3.2.C), is well-isolated in frequency space, peaking in the beta-band (15–25 Hz). It is modulated by brain state, persisting in the absence of visual stimulation, and attaining its highest frequency and/or magnitude during the planning period as the monkey prepares a saccade or reach to a remembered target. It is likewise modulated by the direction or effector planned for an upcoming movement, though more weakly. More dramatic was the anatomical relationship between PRR spikes and LFPs in the traditionally reach-related PMd, as opposed to LFPs within and beyond the arcuate sulcus.

These data may point to a more general beta-band phenomenon. The overall pattern of the PRR-PMd coherence is similar to the oscillatory activity within the parietal lobe alone. For example, medium- to high-frequency (20–40Hz) parietal LFPs occur during periods of steady state, and are interrupted by brief low-frequency events just after visual stimuli or movement onset [Scherberger et al., 2005; Hwang and Andersen, 2009]. PRR LFPs therefore seem to report with high accuracy on the brain state [Hwang and Andersen, 2009]. The cross-cortical results shown here are consistent with this general pattern (fig. 5.3.2.B), showing highly significant differences between brain states, particularly target presentation vs. planning. Beta-band PRR LFP power, within-PRR spike-LFP coherence, and PRR-PMd cross-cortical spike-LFP coherence may all be part of one larger phenomenon across multiple brain areas, interacting particularly strongly with or sourced from the medial bank of the intraparietal sulcus.

This beta-band phenomenon may also include other parts of the parietal lobe, as well as other connected cortical regions. The results shown here are qualitatively similar to recent results from Verhoef et al. [2011], who recorded from anterior intraparietal sulcus and inferotemporal sulcus. While the main task in this manuscript was 3–d rotation, only neurons recorded in their parietal region showed long-range coherence, and it was strongest in the beta-band and during fixation, and during the presentation of an all-black visual stimulus on a white background, which bears some similarity to the planning period described in this manuscript. These results may indicate that spikes in the parietal lobe cohere with a widespread beta-band phenomenon which interacts with frontal and temporal lobes. Note also that Verhoef et al. found anatomical differences in LFP-LFP coherence between AIP and different parts of the infero-temporal sulcus, which show the same coherence-by-anatomy relationship as our results (fig. 5.3.4), though the results shown here are more specific, in that they localize the anatomical variation to spike-LFP coherence. Verhoef et al. employed a spectral Granger causality measure on MUA-LFP interactions. Brovelli et al. also used spectral Granger causality measure on subdural EEG potentials recorded during a movement task, and found that MIP/AIP signals “cause” premotor beta-band oscillations [Brovelli, 2004]. These results bear some similarity to the suggestion in fig. 6.1.1., that the intraparietal sulcus could be sourcing the beta-band activity.

The network of beta-related cortical populations is likely to extend beyond the intraparietal sulcus and premotor areas. Among other possible structures involved, the basal ganglia stands out as a candidate due to its association with beta-band activity. Though beta activity may be amplified by the basal ganglia [McCarthy et al., 2011], beta-band activity is thought to be sourced in the cortex [Hutchison et al., 2004]. The intraparietal sulcus may be one of the primary cortical drivers. The basal ganglia have

also been shown to modulate motor activity and select for actions. It may be that beta-band activity entrains a large number of areas including the IPS, premotor cortex, thalamus and basal ganglia for the purpose of action planning and decision-making.

Where is the source of this beta-band activity? Section 6.2 will explore whether it is possible for asymmetric spike-LFP coherence from PRR to PMd to arise from direct PRR drive, but it is impossible to rule out a common driver to both regions.

Nevertheless, several results weigh against the common-driver hypothesis. First, the special knowledge of PRR spikes about PMd LFPs, indicated by the partial spike-LFP coherence [Bendat and Piersol, 2000; Albo et al., 2004; Pesaran et al., 2008], suggest that PMd LFPs, which may in part represent inputs to PMd from other areas, are apprised of timing information from PRR spikes which could be washed out in PRR LFPs by noise from still other regions. Second, the variation of spike-LFP coherence over cortical anatomy can be simply understood by beta-drive of PMd directly by PRR, to which PMd is known to be anatomically connected. In order for a third area to be responsible for beta-band activity in PRR and PMd, it would also have to avoid driving non-connected regions in the arcuate sulcus. Simplicity therefore argues that at least some of the beta-band activity in PMd should come directly from PRR, rather than an unknown common source.

If beta-band LFP power in the parietal lobe is stronger than in the frontal, why is it that frontal spikes do not cohere with parietal LFPs, rather than vice versa? This asymmetry may be simply explained by the nature of the spike and LFP signals. If spikes represent a noisy version of fluctuations in the subthreshold membrane potential, and if a large component of the LFP is an average over the membrane potentials of many cells with the same beta input, LFPs can more accurately represent that beta-band input than

individual spikes. Even if the LFP power is low in the beta band, as it is in the frontal lobe, an averaged version of a beta-band signal available to all frontal cells can represent the timing properties of that beta-band signal with high accuracy. In other words, a signal common to the membrane potentials of all cells in a region will always be better represented by LFPs than individual spikes.

No matter the exact mechanism, if beta-band LFP power and coherence effects could be traced to a single source or oscillatory network, it would significantly reduce the complexity of understanding oscillatory dynamics within and between these areas. Identifying beta-band power and coherence values as coming from a single source could also serve as a fruitful way to reduce the massive dimensionality of spiking and LFP data for parietal- and premotor-based cortical prosthetics. Marginalizing a single beta-band source from hundreds of signals recorded from an electrode array would significantly simplify spectral analysis, while simultaneously improving signal-to-noise by de-mixing the beta-band source from unrelated biophysical events.

Some of these results are different between monkeys, which may be attributable to experimental differences. The phase of PRR-PMd spike-LFP coherence is different between the two animals: 0 degrees of phase lag of spikes behind LFPs in monkey L, 70 degrees in monkey R. The implied time lag from spike to LFP peak in the latter case (~ 40 ms) is much longer than expected propagation time (~ 1 – 10ms) of spikes originating in PRR to PMd. While monkey R's recording chambers were placed in the right hemisphere, he also used his right (preferred) hand. It should be noted that coherence could also result in a decrease in communication efficacy, where spikes adopt a disadvantageous phase [Womelsdorf et al., 2008], and that the adoption of a 70-degree-lagged phase in the ipsilateral hemisphere to the arm being used throughout

the task could actually favor the contralateral, controlling hemisphere. Also, PRR-PMd spike-LFP coherence seems to be stronger compared to the other task phases in monkey R than monkey L, whereas the frequency differences between fixation and planning are more apparent in monkey L.

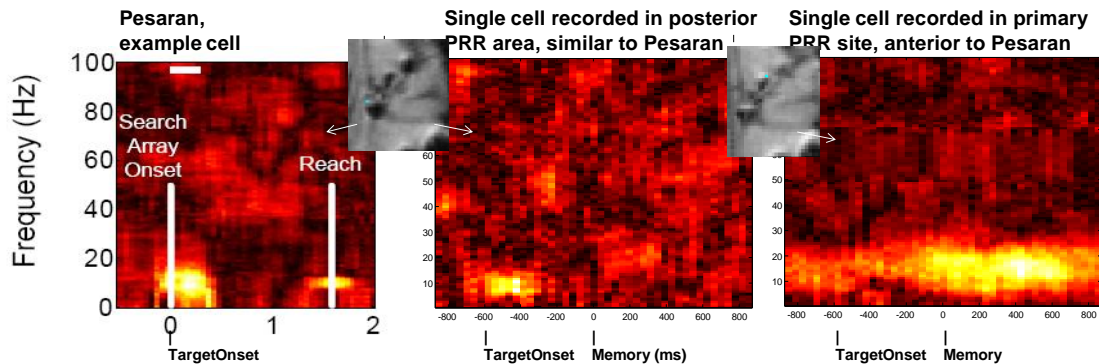


**Figure 5.3.5:** Comparison between data from different PRR-PMd experiments. Left plot: reproduced from Pesaran et al. [2008]. Center plot: data recorded from the same animal, for effector planning experiments, believed to be in the same cortical location. Visual stimulus induces transient, low-frequency coherence event (left and center). Right plot: persistent coherence appears in spikes recorded in a more anterior location.

Our results are also qualitatively different from an earlier report by Pesaran [2009] (fig. 5.3.5). Data from that report were collected during a task with no memory period. PRR recordings from that report were also more posterior to those described here. These methodological and anatomical differences may account for the difference between their 10-15 Hz, cross-cortically symmetric, transient effect which is also partially visible in

these data and the 15–25 Hz, asymmetric, sustained coherence during planning, which is not apparent in the Pesaran report.

These data show that PRR-PMd spike-LFP coherence is at its strongest or highest frequency during the memory period. Nevertheless, the cross-cortical coherence is also strong during fixation in animal L, in the contralateral hemisphere to the arm being used. Therefore, we might expect that there are other factors contributing to the coherence than simply working memory. Both periods of high coherence occur while the animal is maintaining a fixed arm position, and both involve the expectation of a behaviorally relevant signal [Janssen and Shadlen, 2005; Verhoef et al., 2011]. Disambiguating any postural and expectation-related components of the coherence from those related to movement planning awaits further study.

Spike-LFP coherence strength in the gamma band [Gregoriou et al, 2009; Womelsdorf et al., 2008; Fries et al., 2001] has been reported to code for the attended part of visual space or intended movement. Spatial attention cannot explain those components of beta-band PRR-PMd spike-LFP coherence which are effector-related (such as the variation of coherence frequency with planned effector, especially in animal L), nor does it seem consistent with the fact that this coherence is maximal when the spatial target is absent.

Also, different from gamma oscillations reported previously, which occur over a wide range of frequencies [Gregoriou et al, 2009], the beta-band LFP spectrum in these data is narrowly constrained to the 15–25Hz band (see section IV), and this peak becomes much sharper in the coherence spectrum, both within and across cortex (compare fig. 4.1.1, 5.1.5, and 5.3.3). This isolation of a particular frequency, combined with the large phase-locking component, is consistent with the idea that coherence supports phase-

locking at a given frequency [Womelsdorf et al., 2008]. In contrast, the effector-specificity of the coherence frequency in the contralateral-hemisphere recordings (animal L) may indicate a frequency-based tuning component to the coherence [Akam and Kullman, 2010].

Compared to other reports of cross-cortical coherence [Gregoriou et al., 2009; Pesaran et al., 2008], the variation of planning-period beta-band coherence amplitude, phase and frequency to the upcoming action is weak, only barely crossing the  $p < .05$  significance threshold in the beta band at the peak of the coherence. Admittedly, the cross-cortical coherence itself is very near chance level (fig. 5.3.1), so our measurement resolution may not be sufficient to detect significant behavioral coding in the coherence. However, another interpretation of the meaning of coherence is that, rather than explicitly coding for sensory or movement variables, it represents the formation of a channel for communication. Under the latter interpretation, spikes either communicate via adopting a preferred phase [Womesldorf et al., 2007] or preferred frequency [Akam and Kullman, 2010] with respect to LFPs in their target region. Information in the spike rate would be communicated by the functional channel, though the channel itself would remain open no matter what information passed along it. It is possible that both the coherence-for-coding and coherence-as-channel mechanisms can exist in the cortex. Without ruling out the former, these data seem more in line with the latter hypothesis. Reach plans encoded in the rate of cell firing might be transmitted via the channel of their coherence with distant LFPs, though the channel itself remains open independent of the identity of the plan. This channel only acts over existing anatomical connections (fig. 5.3.4), in this case linking reach-related areas. When communication is required (as in the memory period), parietal spikes may adopt the right phase/frequency with respect to distant LFPs. However, during task phases requiring no communication (inter-trial interval,

target-presentation), spikes in PRR are less likely to synchronize with their distant PMd targets.

## **6 Comments on recurrent networks**

### **6.1 Consequences of a single $\beta$ -band input into a recurrent network**

The coherence asymmetry and anatomical selectivity of PRR-frontal coherence, suggested to us a simple model. Differing oscillatory properties among anatomically connected regions may naturally cause asymmetric cross-cortical coherence. To illustrate this idea, we simulated two patches of integrate-and-fire neurons, each connected to the other (fig. 6.1.1). White noise and constant-current inputs were tuned to give neurons in both patches firing rates of 10 Hz on average. One patch (PRR) received an additional 20 Hz sin-wave drive (see Appendix for computational methods). This small asymmetric drive was sufficient to produce a significant difference in the population LFP spectra, and cross-cortical spike-LFP coherence. The inputs from PRR to PMd were sufficient to cause a coherent oscillation in the PMd LFP, but not enough to cause synchronization between PMd spikes and the original PRR LFPs.

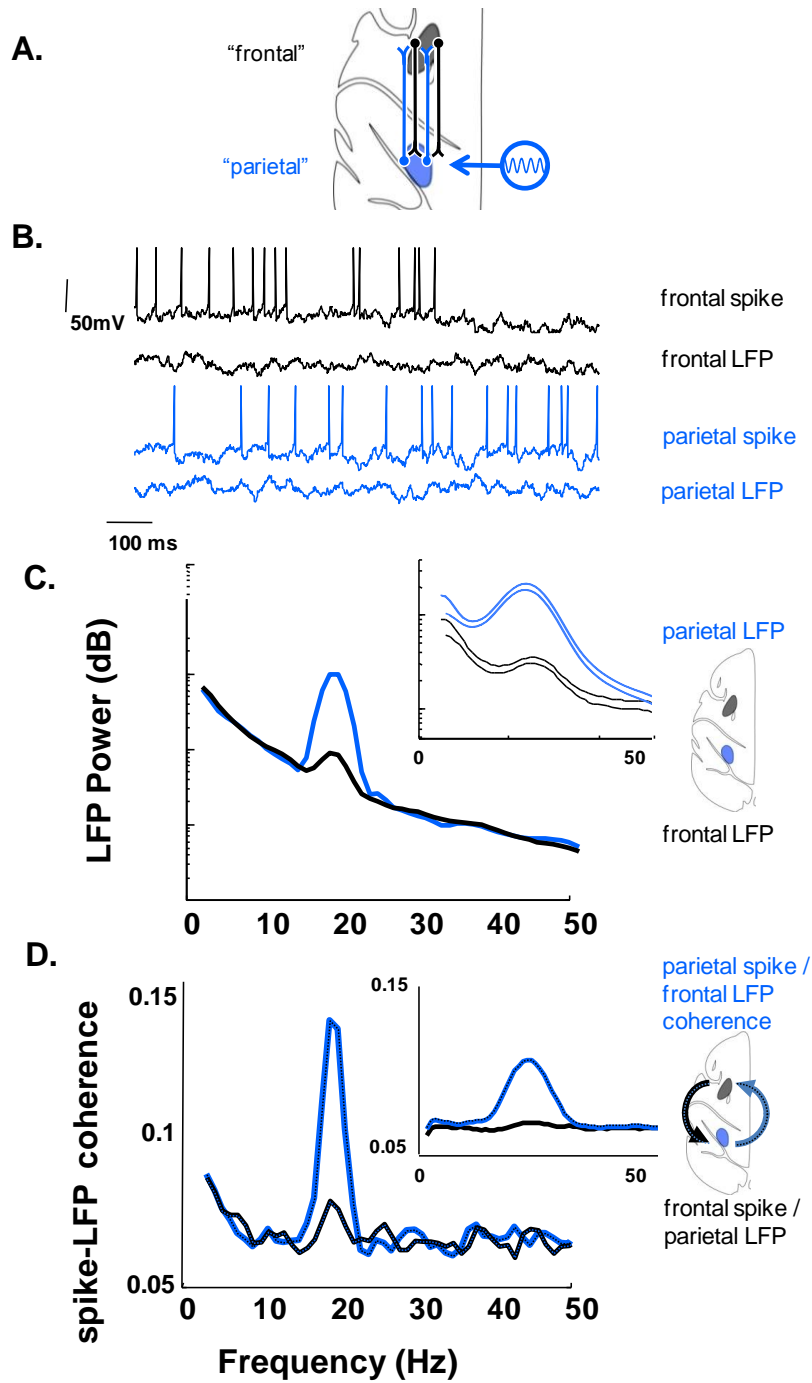


**Figure 6.1.1:** Computational illustration of a mechanism underlying asymmetric spike-LFP coherence. Oscillations in one group of cells extend to the other group, such that spikes from the former become coherent with LFPs from the latter. However, stochasticity in spiking

prevents spiking in the second area from being coherent with LFPs in the first. **A.** Identical patches of cells are connected via cross-cortical excitatory projections, and driven by gaussian white noise. One patch is also driven by an additional 20 Hz signal (the "PRR" patch, A). **B.** Example spikes and LFPs from each patch. LFPs are simulated by averaging over all membrane potentials in a patch. **C.** LFP power spectra. **D.** Cross-cortical spike-LFP coherence

## 6.2 Coherence and mutual information

Neuronal oscillations may provide a carrier signal by which distant brain areas can synchronize for the purpose of communication. This theory predicts a relationship between spike timing and information content across brain regions. The more a spike synchronizes with a distant brain region, the more information it should share with spikes in that distant region. We tested this prediction by comparing two independent cross-cortical measures: spike-field coherence, and spike-spike mutual information.

The natural behavior of the animal provided a brain state which acted as an ideal probe for this question. As the animal waited to begin the task, he would periodically close his eyes for more than 30 seconds at a time. During these phases of pre-sleep, cross-cortical coherence was especially strong in the alpha band. As in previous sections, partial spike-LFP coherence is calculated between the spike and the distant LFP with respect to the local LFP, with the goal of filtering out the common driver. We calculated the multi-taper spike-LFP coherence, using 3 Slepian tapers, adding smoothness in frequency space at the cost of some frequency resolution. Coherence was normalized on a window-by-window basis (section 1.5.2, eq. 3). As before, stacks of 200 windows

at a time were formed. We further transformed this number into a z-score, in order to bring the baseline distribution of coherence closer to a normal distribution, for the purposes of calculating correlations.

To calculate the cross-cortical mutual-information, we selected cells from the same electrode as the distant LFP. We summed the spiking for each cell within the same windows used to make the partial coherence. This left us with an array of 200 spike counts for each cell. We calculated the mutual information between the spike-count array and each cell recorded on the remote LFP's electrode. This left us with a mutual information number for each pair of cells in separate cortical regions, as well as a spike-LFP coherence associated with each one. At each frequency, we calculated the correlation between spike-LFP coherence at that frequency and mutual information of the associated spikes.

Figure 6.2.1 shows the results. Mutual information positively correlates with cross-cortical spike-LFP coherence. In other words, spikes that cohere with distant LFPs are also more likely to be informative about distant cells.

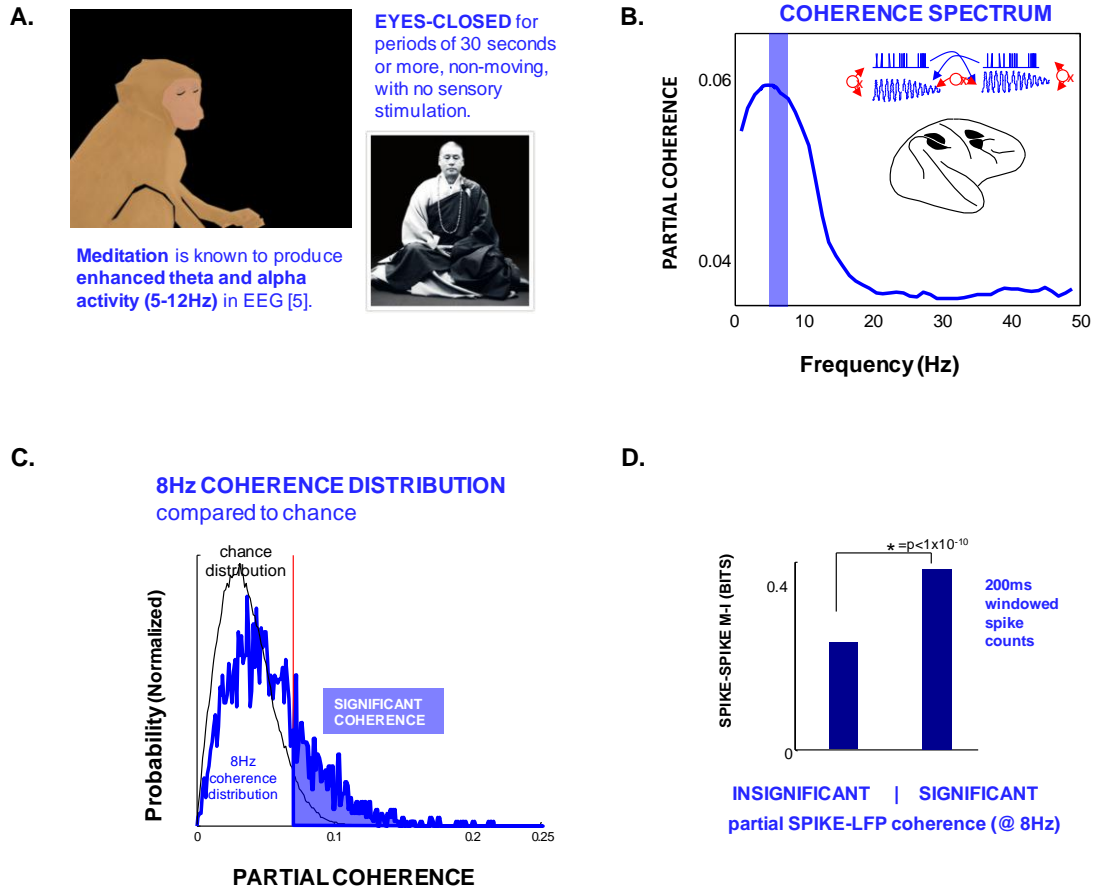


**Figure 6.2.1.** **A.** Sleep-like state produces **(B.)** low-frequency cross-cortical coherence. **C.** Distribution of partial coherence values at 8 Hz (blue bar in **B**). Cells were grouped into significantly (filled blue) and non-significantly (empty) coherent. For each group, the average mutual information with cross-cortical cells was calculated. **D.** Highly coherent cells tend to be more informative about other cells in the same region as the distant LFP.

### 6.3 Connectivity between PRR and PMd

Connections between intraparietal and prefrontal areas, when they exist, are generally thought to be reciprocal. However, this symmetry may not be reflected in the literature. We conducted a meta-analysis of connectivity papers by polling the macaque anatomy database CoCoMac [Stephan et al., 2001]. Five retrograde tracer studies were returned identifying connections from MIP and Area 5 (the nearest locations to the region we name “PRR”) to PMd. In contrast, no studies were returned featuring connections in the opposite direction. These data may indicate a researcher bias to look for connections in one direction. Moreover, it is impossible to know whether any experiments have been conducted searching for anatomical connections in the other direction with negative results. While new tools such as diffusion tensor imaging are promising for understanding anatomical connections, they are unable to indicate directionality, and so we must still rely on retrograde tracer studies. While these asymmetrical anatomical results should be interpreted with caution, it is possible that they indicate an asymmetry in strength of connectivity of parieto-frontal connections, which could help explain the asymmetry in spike-LFP coherence found in these data (section 5).

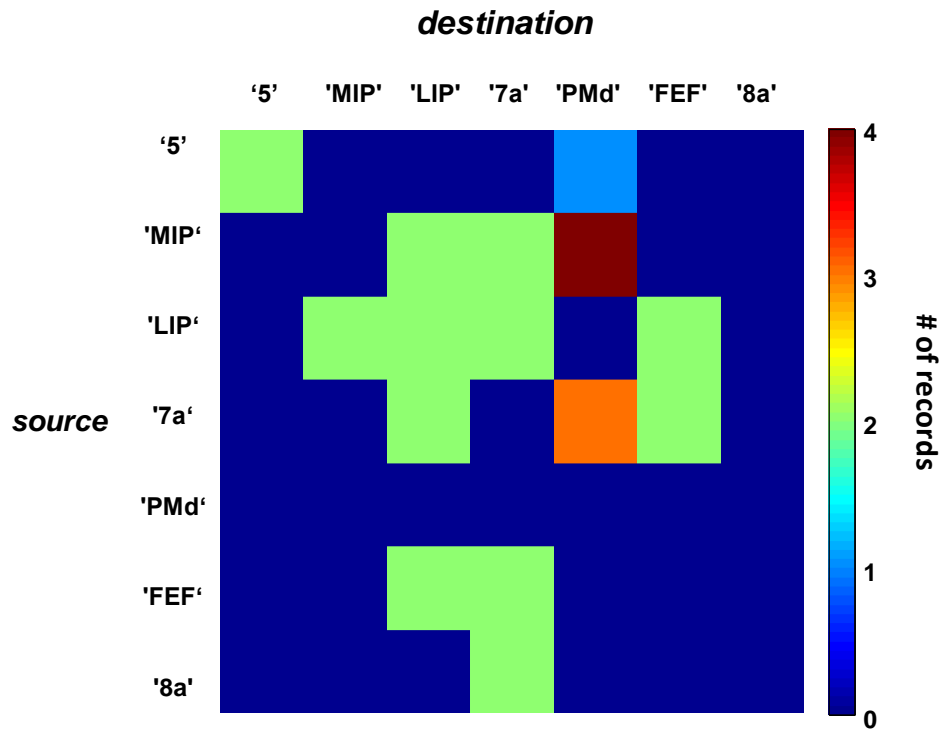
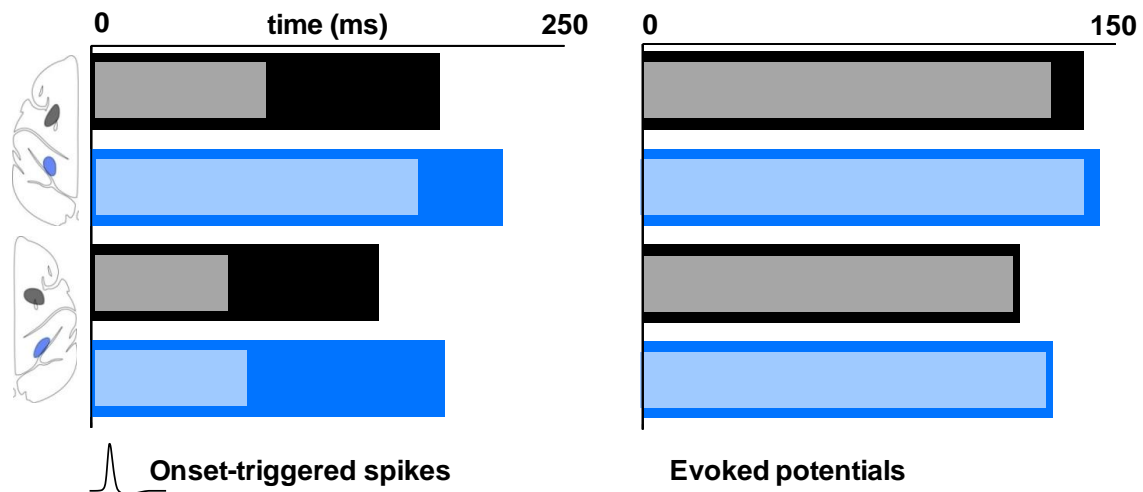


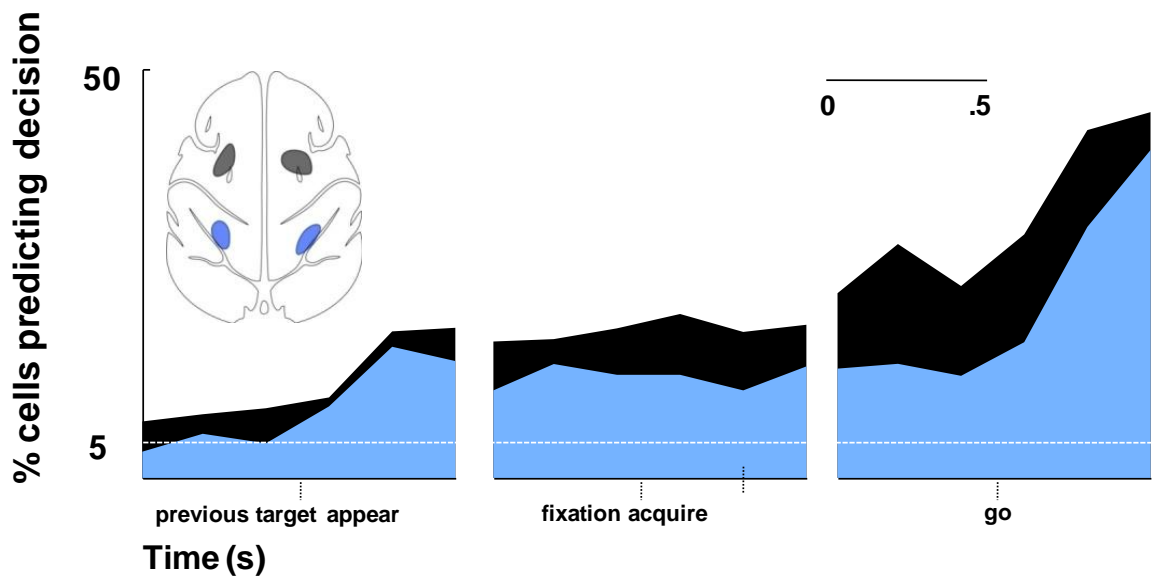
**Figure 6.4.1.** Meta-analysis of connectivity from the literature. Five records exist which implicate PRR (here, encapsulated MIP and Area 5) as projecting to PMd [Colby et al., 1988; Caminiti et al., 1999; Tanne-Gariepy et al., 2002]. However, no projections were described from PMd back to PRR.

## 7 Conclusion: Planning-Related Interaction of PRR and PMd

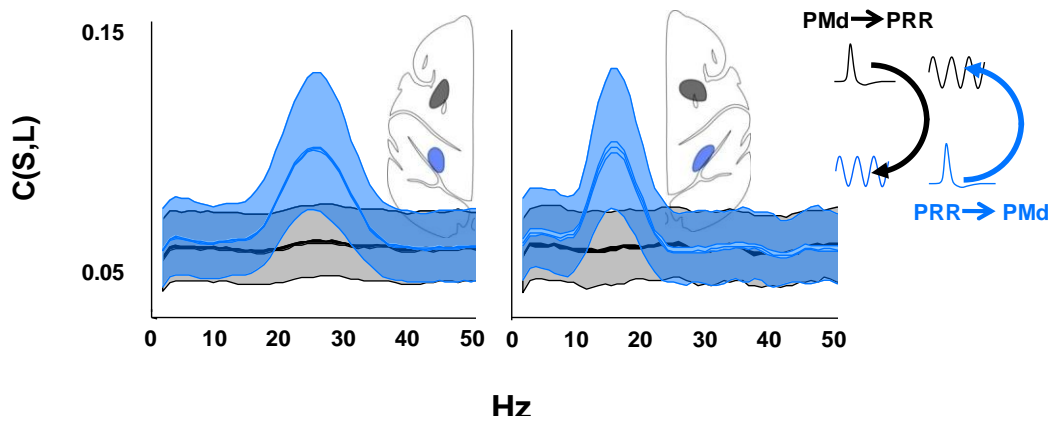
The goal of these experiments was to understand the interaction between frontal and parietal planning regions. PRR and PMd have similar functional properties (figs. 1.5.4–6; also fig. 2.1.5), but they may occupy different positions in the sensorimotor pathway, and therefore respond to stimuli with different timing. After the brain regains steady state, the coherence between spiking and LFP activity may indicate the extent and direction of these areas' interaction during planning. The results of these experiments are summarized in the following figures:



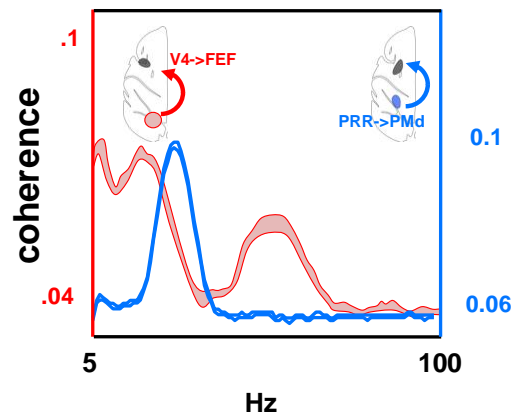
**Summary Figure 7.1:** Dorsal premotor cortex (PMd, black) responds sooner to visual targets than does parietal reach region (PRR, blue). Number of milliseconds to the peak (inner bars) and mean (outer bars) of the onset time distributions for spikes (left) and evoked potentials (right) in the left hemisphere (top rows) and right (bottom two) are shown above (see figs. 2.1.1–2). PMd also indicates sooner the target direction (fig. 2.1.5) and the instructed effector (fig. 2.1.4).



**Summary Figure 7.2:** In a task with no visual stimulus, both premotor (PM) and intraparietal (IPS) areas begin to predict an animal's decisions before the trial even begins, indicating a previously unknown commonality between premotor and intraparietal cortices. PM shows stronger predictive power than IPS, though whether drives the latter with decisions generated from the frontal lobe, or instead accepts input from IPS as one of a number of inputs, the spiking data alone cannot report.

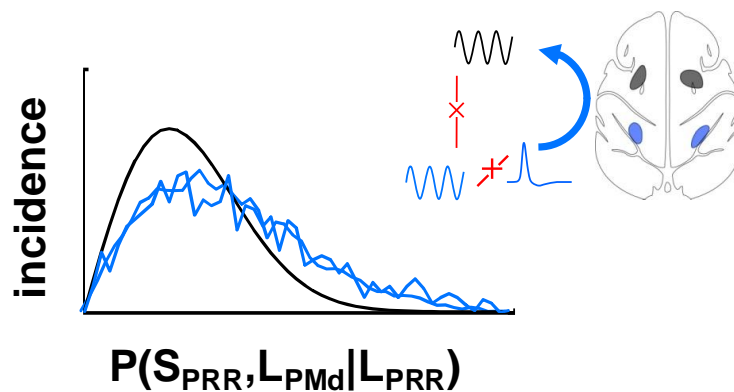


**Summary Figure 7.3:** Spike-LFP coherence, which has been proposed to indicate influence (Section 1.5), is significant between spikes in PRR and LFPs in PMd, but not vice-versa (Section 5.3). These data may indicate that in the absence of stimuli, PRR drives PMd at 15–30Hz.

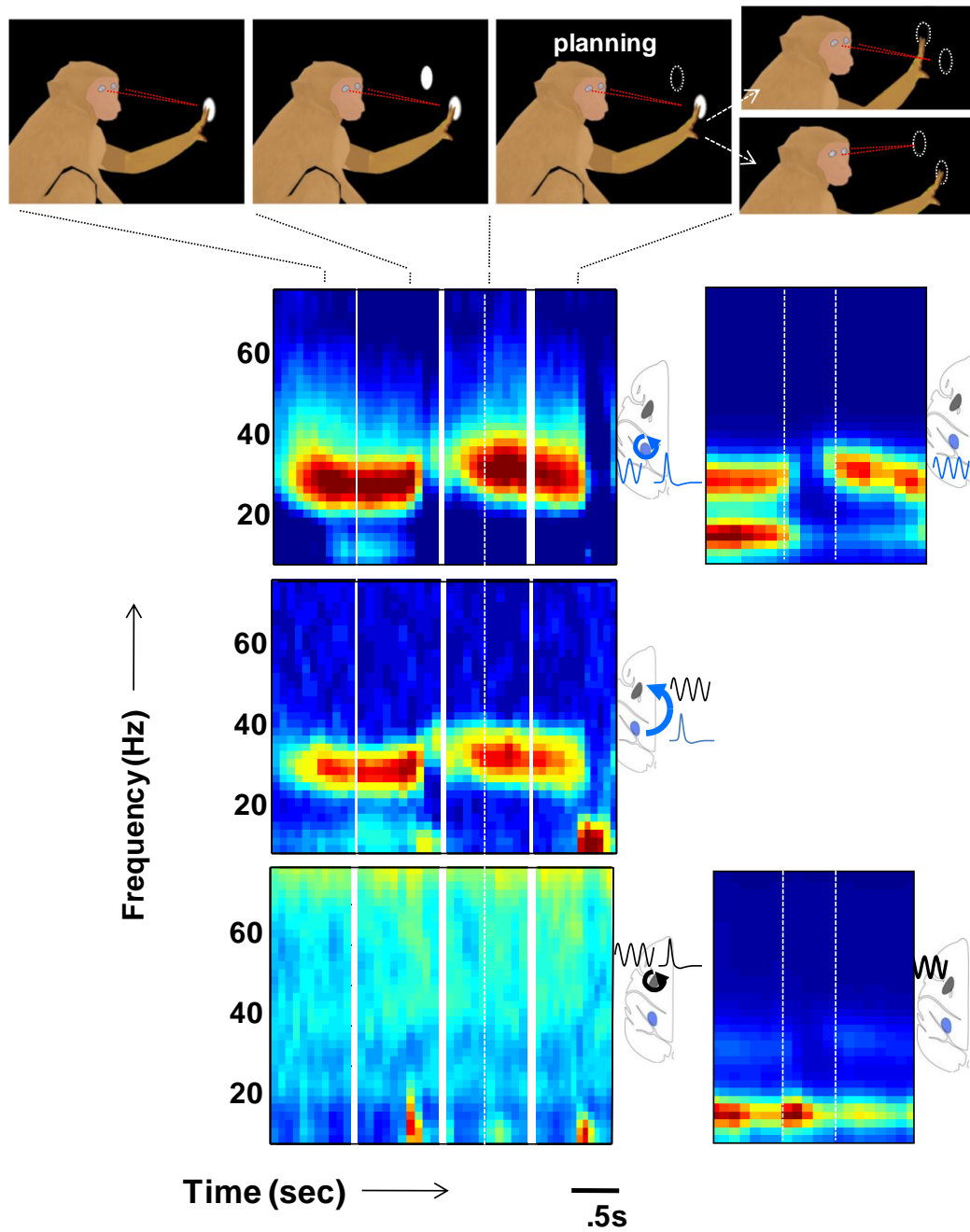


**Summary Figure 7.4:** Cross-cortical coherence is concentrated in the beta-band. Even where significant power or synchrony exists locally in other frequency bands (e.g., alpha-band patterns; figs. 4.2.1, 4.2.4), it is not communicated across cortex in these data. Whereas previous reports on cross-cortical coherence describe interaction in a range of frequencies (e.g., Gregoriou et al., [2009], adapted here, V4 → FEF spike-LFP

coherence during attention, red), PRR-PMd data during the planning period (blue) select only the beta-band. Beta is unlikely to be driven by the high-frequency coupling of parvalbumin interneurons known to drive gamma oscillations, and may represent a unique and spatially extended cortical phenomenon in its own right.

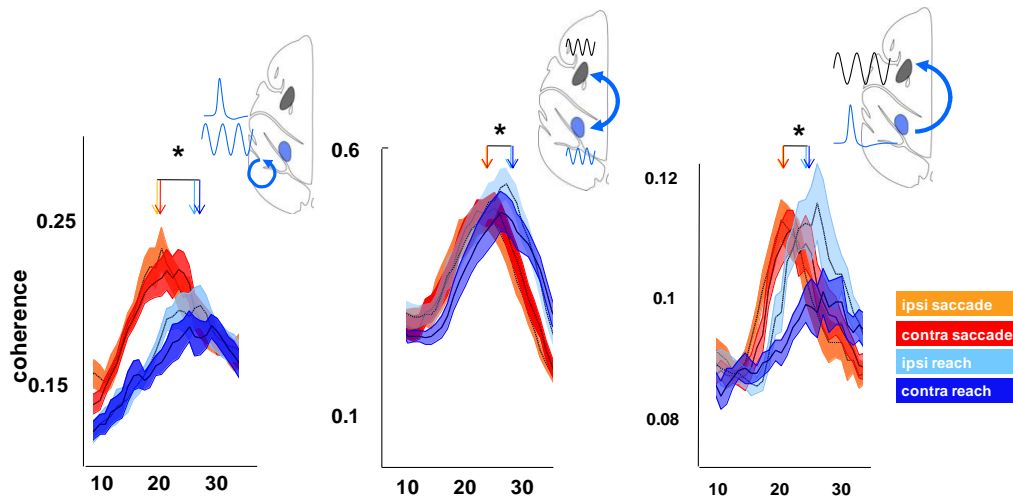


**Summary Figure 7.5:** PRR-PMd spike-LFP coherence is not simply an epiphenomenon of local coupling within each area to a globally broadcast signal, as indicated by the partial coherence treatment (fig. 5.3.1). Shown above are the partial coherence chance (black) and measured (blue, one curve per hemisphere) distributions at the peak coherence level (one curve for each hemisphere). These data indicate a relationship between PRR spikes and PMd LFPs which cannot be explained by other signals. Whatever the exact interpretation of the meaning of the cross-cortical spike-LFP coherence, it should be examined in its own right, and not eclipsed by studies of cross-cortical LFP-LFP coherence.

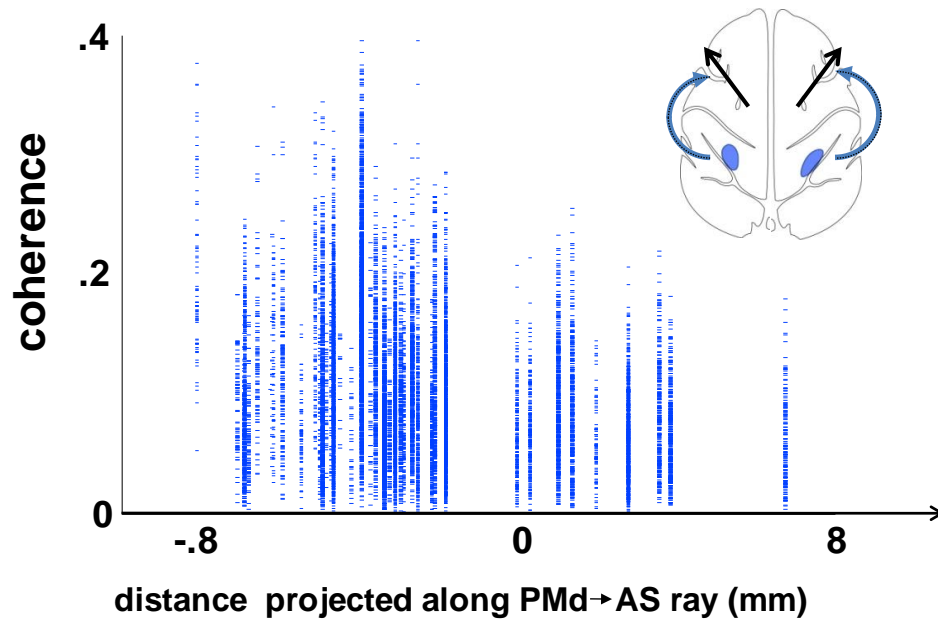


**Summary Figure 7.6:** The general pattern of beta-band activity — strong during periods of preparation and planning, extinguished by visual input and action generation — is largely conserved across PRR spectra, spike-LFP coherence, and PRR-PMd

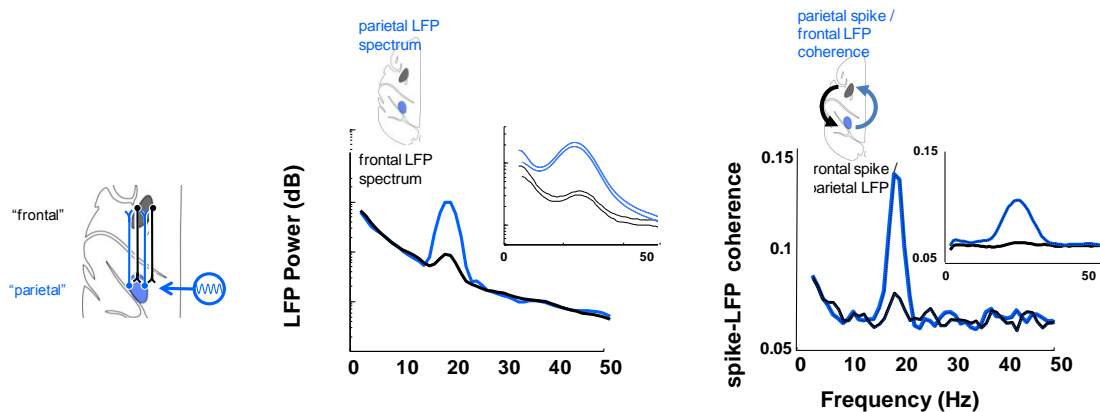
cross-cortical spike-LFP coherence (first 3 plots). PMd spike-LFP coherence and LFP power spectra show a somewhat different temporal evolution.



**Summary Figure 7.7:** Cross-cortical coherence encodes planned actions (figs. 5.3.3–4), albeit weakly. While the general encoding pattern is not consistent across monkeys, it seems to be conserved among different measures within monkeys. That is, PRR-PRR spike-LFP coherence (left plot), PRR-PMd LFP-LFP coherence (center), and PRR-PMd spike-LFP coherence (right) all increase in frequency in advance of a reach in monkey L. In contrast, monkey R does not show this frequency bias in any measure of synchrony, though coherence in some cells still codes for the action plan (fig. 5.3.3).



**Summary Figure 7.8:** Cross-cortical spike-LFP coherence is anatomically-dependent (fig. 5.3.5, as is LFP-LFP coherence, fig. 5.3.1). That is, PRR spikes are more likely to cohere with LFPs in PMd than FEF, to which it is not known to project. This implies either that coherence interacts over the direct projections from PRR to PMd, or that PRR and PMd are simultaneously and exclusively driven by a third region.



**Summary Figure 7.9:** Figure 7.6 may indicate that beta-band power and synchrony throughout planning areas is a monolithic phenomenon, of which these measures used in this report are all different aspects. While within-area and across-area synchrony and power spectra are often reported independently [Gregoriou et al., 2009; Buschmann and Miller, 2007; Womelsdorf et al., 2008], in the case of beta-band activity these measures may all represent a single process. A simple way to explain figs. 7.6 and 7.8 is that beta-band in PMd arises from PRR, at least in part. A simulation illustrates that a single source for beta-band activity, centered in the parietal lobe, can explain not only the LFP power difference but also the asymmetry in cross-cortical spike-LFP coherence.

If spike-LFP coherence does indeed subserve communication (section 1.2), then these data suggest that PRR drives PMd, but only at certain times. PMd, which responds tens of milliseconds earlier to visual stimuli than does PRR (section 2), has no need of PRR input in order to generate an immediate response to a visual stimulus. In fact, PMd may drive PRR at low frequencies immediately after visual input (fig. 5.3.6). But when a movement plan must be stored in working memory, strongly asymmetric PRR-PMd coherence may occur represent a "broadcasting" of relevant state information from the

parietal lobe. The parietal lobe has been interpreted, among other functions, to maintain a real-time state representation of the body and the world outside [Mulliken et al., 2008; Husain et al., 1997; Desmurget et al., 2009]. While both parietal and frontal neurons show similar behavior during working memory tasks (section 1.5), the asymmetry in parieto-frontal coupling may indicate different roles in maintaining an internal representation of state. This state information may include not just the direction of the intended reach or the intended effector, but other variables such as the current state of the eye and the arm, or the expectancy of an upcoming cue. The asymmetric coherence appears across disparate measures (sections 4–5) as a sharp peak in the beta-band, which seems likely to represent a unique cortical phenomenon in its own right. If this asymmetric coherence could be enhanced or interrupted, communication of spiking information between PRR and other brain areas might be altered.

## 8 Appendix: Methods for Neurophysiology

**Recording methods:** Two male rhesus monkeys (*Macaca mulatta*) participated in the experiments. PMd and PRR were anatomically localized using structural MRI scans. We recorded single-unit and LFP activity from PMd and PRR using Pt/W electrodes, impedance between .5 and 1 MOhm, controlled by multiple-electrode microdrives (3- and 5-channel, Thomas Recordings). Spiking events and local field potentials were recorded (Plexon, Texas) on separate channels, with LFPs low-pass filtered at 200 Hz and subsampled at 1 kHz. The transfer function for the entire recording system was determined by passing a sin wave (100  $\mu$ V) with a chirped profile over the relevant frequencies (1–200Hz), with periodic simulated spikes inserted to test for any phase offset between the slow-wave and event-recordings. The transfer function reflected the low-pass filtering used for LFPs (3 db at 200 Hz), as well as a low-frequency filter (3 db at 3 Hz), however there was no appreciable filtering in our frequencies of interest (10–100 Hz), nor any appreciable phase offset. During a recording day, electrodes were simultaneously guided to both target locations. After isolating cells in both targets, we allowed the electrodes to settle into the tissue. We did not select cells based on task-relatedness, opting instead to record from all cells in which we could maintain in isolation.

**Behavioral methods:** We employed several variants of a reach/saccade planning task. The basic structure of the task for both monkeys progressed as follows: after fixating on a central lit spot with eye and hand for .5–1.5 seconds (.8–1.5 for monkey R), the “fixation” period, we showed the monkey a target in the right or left of his visual space for .5 s. After the target disappeared, the monkey was required to maintain fixation for .5–1.5 s, the “planning period”, after which the lit fixation spot disappeared, which was the

monkey's cue to move. If the target had been colored red, the monkey was rewarded for saccading to the remembered target. If it had been colored green, the monkey was rewarded for reaching to the remembered target. These were termed ordinary instructed-effector trials. Examples of spiking during ordinary instructed-effector trials can be seen in fig. 1.5.3 and 1.5.5. For some recording days, we added the following variations: If the target were colored both red and green, the monkey was free to decide whether to reach or saccade. In these effector-decision trials, we encouraged the monkey to randomize his choice of effectors [Barraclough et al., 2004]. In an attempt to localize decision-related signals to the planning period, we interleaved effector-decision trials with trials in which the target color corresponding to the desired effector (red for reaches, green for saccades; see Cui and Andersen, 2007) remained lit after the normal visual target disappeared, until the fixation spot disappeared to provide the "Go" cue. The latter interleaved-delayed-instructed trials were only run for monkey R, and were not included in the analysis due to their lack of planning period. Finally, in an effort to improve trial resolution for these trials, we replaced interleaved-delayed-instructed trials with trials in which the colored cue indicating instructed effector lasted only 50ms, followed by a planning period. These trials were called "interleaved-planning-instructed" trials, and were only run for monkey L; the overall distributions of trial types for each monkey were: 18% ordinary instructed, 41% effector-decision, 41% interleaved-planning-instructed for monkey L, and 100% effector-decision for monkey R (with an equal number of interleaved-delay-instructed trials for monkey R, which were excluded due to their lack of a planning period). All of these trial types involved fixation, target presentation, and a planning period, as described above. Because we found no significant differences in the planning period coherence among these different trial types, we combined them in order to have more trial resolution.

**Data analysis methods:** Because of the relatively low SNR we expected to achieve for cross-cortical spike-LFP coherence, calculating a coherence value required on the order of hundreds of trials. We could not maintain isolation in all of our cells over this period, and even the best -isolated cells exhibited some change in waveform shape over several hours. We therefore designed special spike-sorting software, based on cluster-analysis in PCA space, which allowed us to define cells only over the time period in which they were well-isolated, and allowed us to track them over slow changes in their shape. Single-units were classified as those cells which had qualitatively well-separated clusters and waveforms, and  $< 1\%$  of inter-spike-intervals  $< 2$  ms. Each single unit had a time period over which it was considered to be well-isolated. Outside of this time period, a spike was never included in the analysis. Similarly, LFPs experienced large and infrequent noise artifacts, caused most often by the monkey's movements. These events, identified via a threshold of 2 mV and buffered by a windowed of a minimum of 1 s, were likewise excluded from all analyses.

We calculated the coherence by dividing time courses of spiking and LFP activity into windows, and calculating the individual spectra and cross-spectra for each window. We then averaged the normalized cross-spectra (as opposed normalizing the averaged cross spectra with the averaged individual spectra, as in, for example, Gregoriou et al., [2009]). Our method of calculating coherence, while less conventional, removes window-by-window power correlations. Therefore, in this study, coherence can be interpreted to mean phase locking between spikes and LFPs at a given frequency.

We calculated the coherence on a by-brain-state and by-cell basis. For a given brain state, for a given cell and LFP pair, we collected "stacks" of 200 windows of 200 ms each, and calculated coherence across these windows. Where the data were numerous

for more than one stack, or where multiple LFPs were available in a given site, we averaged across stacks and LFPs, such that we arrived at a single coherence value for each cell. We did not detect significant differences between this method, compared to collecting the stacks by time-within-trial (for the cell with the highest cross-cortical coherence,  $p=73\%$ , t-test btw. planning period coherence stacked by time vs. time-within-trial). Also, we found that if a given cell cohered with a distant LFP, it was much more likely to cohere with other distant LFPs, hence our averaging coherence over multiple cross-cortical LFPs. We always calculated within-area coherence from LFPs taken from a different electrode than the spike in question, so as not to pollute the coherence measure with the residual of the spike in the LFP measured on the same electrode. If this measure is not employed, a large amount of spurious high-frequency coherence appears between spikes and LFP, increasing in magnitude with increasing frequency. We found multi-unit activity (MUA) to have a similar distribution of cross-cortical coherence to single-cell activity, and so unless otherwise labeled, we added MUA spikes in order to increase our resolution for these behavioral and anatomical questions.

Granger causality [Baccala and Sameshima, 2001] has often been employed in order to understand cross-cortical functional interactions [Verhoef et al., 2011; Brovelli et al., 2004]. However, we felt that these oscillatory relationships (between spikes and LFPs) were likely to be highly reciprocal, and the autoregression step of Granger causality, which is designed to reveal single-directional "causal" relationships, was likely to add complication without extra knowledge.

When reporting LFP or spiking power spectra, we use arbitrary units because of the difficulty in interpreting the meaning of a unit such as  $(\text{spk/s})^2/\text{Hz}$ . Power spectra, to be

correctly labeled, must be normalized for the window size used in estimating the spectrum, since twice the window size incorporates twice as much energy into the estimate. For better or worse, reporting power in arbitrary units has become a standard in neuroscience [Pesaran, 2008]. This is permissible if the sole intention of reporting power spectra is to compare between behavioral conditions.

**Computational methods:** To illustrate our explanation for the cross-cortical coherence asymmetry, we simulated a group of 256 integrate-and-fire neurons (threshold -40 mV, reset -60 mV, voltage floor -80 mV), connected via all-to-all excitatory projections to an equal number of integrate-and-fire neurons “across the cortex”. Each neuron was driven by Gaussian white noise, tuned so that their mean firing rate would be ~ 10 Hz (DC drive .06 mV/ms, noise std = 2.7 mV). One population was additionally driven by 20 Hz sine wave at a lower power than the noise input (std = .1 mV). Spikes in one region elicited immediate voltage fluctuations in the other of .065 mV. The computational illustration did not include within-area connections, either excitatory or inhibitory, conduction delays, or extended, excitatory post-synaptic potentials. We think it is likely that a more biophysically realistic network would exhibit similar oscillation and coherence properties given similar inputs, but we believe the point is illustrated most clearly with the simplest possible network. Power spectra and coherence values were calculated as with the experimental data.

## References:

- Akam T, Kullmann DM. Neuron. Oscillations and filtering networks support flexible routing of information. *Neuron*. 2010 Jul 29;67(2):308–20.
- Albo Z, Di Prisco GV, Chen Y, Rangarajan G, Truccolo W, Feng J, Vertes RP, Ding M. Is partial coherence a viable technique for identifying generators of neural oscillations? *Biol Cybern*. 2004 May;90(5):318–26. PMID: 15221392
- Anastassiou C, Perin R, Markram H, Koch C. Ephaptic coupling of cortical neurons. *Nature Neuroscience*. 2011 14: 217–223 doi:10.1038/nn.2727
- Andersen, R. A., Asanuma, C., Essick, G, and Siegel, R.M. (1990). "Corticocortical connections of anatomically and physiologically defined subdivisions within the inferior parietal lobule." *J. Comp. Neurol*. 296: 65–113.
- Averbeck BB, Battaglia-Mayer A, Guglielmo C, Caminiti R. Statistical Analysis of Parieto-Frontal Cognitive-Motor Networks. *J Neurophysiol*. 2009 Sep;102(3):1911–20.
- Azouz R, Gray CM. Adaptive coincidence detection and dynamic gain control in visual cortical neurons in vivo. *Neuron*. 2003 Feb 6;37(3):513–23.
- Badre, D., Hoffman, J., Cooney, JW, D'Esposito, M. Hierarchical cognitive control deficits following damage to the human frontal lobe. *Nature Neuroscience* 12, 515–522 (2009)
- Baccalá LA, Sameshima K. Partial directed coherence: a new concept in neural structure determination. *Biol Cybern*. 2001 Jun;84(6):463–74.
- Baldauf, D., Cui, H., and Andersen, R.A. (2008). "The Posterior Parietal Cortex Encodes in Parallel Both Goals for Double-Reach Sequences". *The Journal of Neuroscience* . 28(40):10081–10089
- Barraclough DJ, Conroy, M.L., and Lee, D. (2004). Prefrontal cortex and decision making in a mixed-strategy game. *Nat. Neurosci*. 7, 404–410
- Bendat JS, Piersol AG. *Random Data: Analysis & Measurement Procedures*. Wiley-Interscience. 2000
- Berens P, Keliris GA, Ecker AS, Logothetis NK, Tolias AS. Comparing the feature selectivity of the gamma-band of the local field potential and the underlying spiking activity in primate visual cortex. *Front Syst Neurosci*. 2008;2:2. Epub 2008 Jun 17.
- Bisley JW; Goldberg ME. Neuronal activity in the lateral intraparietal area and spatial attention. *Science*. 2003 Jan 3;299(5603):81–6.
- Brovelli A, Ding M, Ledberg A, Chen Y, Nakamura R, Bressler SL. Beta oscillations in a large-scale sensorimotor cortical network: directional influences revealed by Granger causality. *Proc Natl Acad Sci U S A*. 2004 Jun 29;101(26):9849–54.

- Buschman TJ, Miller EK. Top-down versus bottom-up control of attention in the prefrontal and posterior parietal cortices. *Science*. 2007 Mar 30;315(5820):1860–2.
- Buzsaki, G. *Rhythms of the Brain*. Oxford University Press, 2006. ISBN: 0195301064
- Caminiti R, Genuvesio A, Marconi B, Battaglia-Mayer A, Onorati P, Ferraina, S. Early coding of reaching: frontal and parietal association connections of parieto-occipital cortex. *Eur J Neurosci*. 1999 Sep;11(9):3339–45.
- Chafee, MV, Goldman-Rakic, PS. Matching patterns of activity in primate prefrontal area 8a and parietal area 7ip neurons during a spatial working memory task. *J Neurophysiol*. 1998 Jun;79(6):2919–40.
- Cisek P, Kalaska JF. Neural correlates of reaching decisions in dorsal premotor cortex: specification of multiple direction choices and final selection of action. *Neuron*. 2005 Mar 3;45(5):801–14.
- Colby CL, Gattass R, Olson CR, Gross CG. Topographic organization of cortical visual afferents to extrastriate visual area PO in the Macaque: A dual tracer study. *J Comp Neurol*. 1988 Mar 15;269(3):392–413.
- Cui H, Andersen RA. Posterior parietal cortex encodes autonomously selected motor plans. *Neuron*. 2007 Nov 8;56(3):552–9. PMID: 17988637
- Curtis CE, Lee D.. Beyond working memory: the role of persistent activity in decision making. *Trends Cogn Sci*. 2010 May;14(5):216–22. Epub 2010 Apr 8.
- Desmurget M, Reilly KT, Richard N, Szathmari A, Mottolese C, Sirigu A. Movement intention after parietal cortex stimulation in humans. *Science*. 2009 May 8;324(5928):811–3.
- Felleman DJ, Van Essen DC. Distributed hierarchical processing in the primate cerebral cortex. *Cereb Cortex*. 1991 Jan–Feb;1(1):1–47. PMID: 1822724
- Fisher NI, *Statistical Analysis of Circular Data*, Cambridge University Press, 1993. ISBN 0-521-35018-2
- Fries P. A mechanism for cognitive dynamics: neuronal communication through neuronal coherence. *Trends Cogn Sci*. 2005 Oct;9(10):474–80.
- Fries P, Reynolds JH, Rorie AE, Desimone R. Modulation of oscillatory neuronal synchronization by selective visual attention. *Science*. 2001 Feb 23;291(5508):1560–3.
- Gazzaniga MS. *The Cognitive Neurosciences IV*. Bradford Books, 2009. ISBN 0-262-01341-X
- Gersch W, Goddard GV, Epileptic focus location: spectral analysis method. *Science*. 1970 Aug 14;169(946):701–2.
- Gnadt JW, Andersen RA. Memory related motor planning activity in posterior parietal cortex of macaque. *Exp Brain Res*. 1988;70(1):216–20.

- Goodale MA, Milner AD. Separate visual pathways for perception and action. *Trends Neurosci.* 1992 Jan;15(1):20–5.
- Gold JI, Shadlen MN. Representation of a perceptual decision in developing oculomotor commands. *Nature.* 2000 Mar 23;404(6776):390–4.
- Granger, CWJ., Investigating causal relations by econometric models and cross-spectral methods. *Econometrica* 1969 37 (3), 424–438.
- Gray, C.M. and Singer, W., Stimulus-specific neuronal oscillations in orientation columns of cat visual cortex. *Proc Natl Acad Sci U S A.* 1989 Mar;86(5):1698–702.
- Graziano MS, Taylor CS, Moore T. Complex movements evoked by microstimulation of precentral cortex. *Neuron.* 2002 May 30;34(5):841–51.
- Gregoriou GG, Gotts SJ, Zhou H, Desimone R. High-frequency, long-range coupling between prefrontal and visual cortex during attention. *Science.* 2009 May 29;324(5931):1207–10.
- Hwang EJ, Andersen RA. Brain control of movement execution onset using local field potentials in posterior parietal cortex. *J Neurosci.* 2009 Nov 11;29(45):14363–70.
- Hwang EJ, Andersen RA. Effects of visual stimulation on LFPs, spikes, and LFP-spike relations in PRR. *J Neurophysiol.* 2011 Apr;105(4):1850–60. Epub 2011 Feb 9.
- Husain M, Shapiro K, Martin J, Kennard, C. Abnormal temporal dynamics of visual attention in spatial neglect patients. *Nature.* 1997 Jan 9;385(6612):154–6.
- Hutchison WD, Dostrovsky JO, Walters JR, Courtemanche R, Borud T, Goldberg J, Brown P. Neuronal oscillations in the basal ganglia and movement disorders: evidence from whole animal and human recordings. *J Neurosci.* 2004 Oct 20;24(42):9240–3. PMID: 15496658
- Huxter J, Burgess N, O'Keefe J. Independent rate and temporal coding in hippocampal pyramidal cells. *Nature.* 2003 Oct 23;425(6960):828–32.
- Jarvis MR, Mitra PP. Sampling properties of the spectrum and coherency of sequences of action potentials. *Neural Comput.* 2001 Apr;13(4):717–49.
- Janssen P, Shadlen MN (2005). A representation of the hazard rate of elapsed time in macaque area LIP. *Nat Neurosci.* 2005 Feb;8(2):234–41.
- Katzner S, Nauhaus I, Benucci A, Bonin V, Ringach DL, Carandini M. Local Origin of Field Potentials in Visual Cortex. *Neuron.* 2009 Jan 15;61(1):35–41.
- Lepage KQ, Kramer MA, Eden UT. The dependence of spike-LFP coherence on expected intensity. *Neural Comput.* 2011 Sep;23(9):2209–41. Epub 2011 Jun 14.
- Lindén H, Tetzlaff T, Potjans TC, Pettersen KH, Grün S, Diesmann M, Einevoll GT. Modeling the Spatial Reach of the LFP. *Neuron.* 2011 Dec 8;72(5):859–72.

Lynch JC, Hoover JE, Strick PL. Input to the primate frontal eye field from the substantia nigra, superior colliculus, and dentate nucleus demonstrated by transneuronal transport. *Exp Brain Res.* 1994;100(1):181–6. PMID: 7813649

von der Malsburg, C. *The correlation theory of brain function.* Springer-Verlag. 1981

McCarthy MM, Moore-Kochlacs C, Gu X, Boyden ES, Han X, Kopell N. Striatal origin of the pathologic beta oscillations in Parkinson's disease. *Proc Natl Acad Sci U S A.* 2011 Jul 12;108(28):11620–5. Epub 2011 Jun 22.

Mitzdorf U. Current source-density method and application in cat cerebral cortex: investigation of evoked potentials and EEG phenomena. *Physiol Rev.* 1985 Jan;65(1):37–100.

Mulliken GH. *Continuous Sensorimotor Control Mechanisms in Posterior Parietal Cortex: Forward Model Encoding and Trajectory Decoding.* Thesis, California Institute of Technology. 2008

Mulliken GH, Musallam S, and Andersen, RA. Forward estimation of movement state in posterior parietal cortex. *Proc Natl Acad Sci U S A.* 2008 Jun 17;105(24):8170–7.

Mulliken GH, Musallam S, Andersen RA. Decoding trajectories from posterior parietal cortex ensembles. *J Neurosci.* 2008 Nov 26;28(48):12913–26.

Musallam S, Corneil BD, Greger B, Scherberger H, Andersen RA. Cognitive Control Signals for Neural Prosthetics. *Science.* 2004 Jul 9;305(5681):258–62.

Pesaran B, Nelson MJ, Andersen RA. Free choice activates a decision circuit between frontal and parietal cortex. *Nature.* 2008 May 15;453(7193):406–9. Epub 2008 Apr 16.

Pesaran B, Pezaris JS, Sahani M, Mitra PP, Andersen RA. Temporal structure in neuronal activity during working memory in macaque parietal cortex. *Nat Neurosci.* 2002 Aug;5(8):805–11

Pesaran, B. (2008) Spectral Analysis for Neural Signals In: *Neural Signal Processing: Quantitative Analysis of Neural Activity.* (Mitra P, ed) pp. 1–12. Washington, DC: Society for Neuroscience.

Platt ML, Glimcher PW. Neural correlates of decision variables in parietal cortex. *Nature.* 1999 Jul 15;400(6741):233–8.

Poulet JF, Petersen CC. Internal brain state regulates membrane potential synchrony in barrel cortex of behaving mice. *Nature.* 2008 Aug 14;454(7206):881–5.

Quiñero R, Snyder LH, Batista AP, Cui H, Andersen RA. Movement Intention Is Better Predicted than Attention in the Posterior Parietal Cortex. *J Neurosci.* 2006 Mar 29;26(13):3615–20.

Rao RP, Ballard DH. Predictive coding in the visual cortex: A functional interpretation of some extra-classical receptive-field effects, *Nat Neurosci.* 1999 Jan;2(1):79–87.

Shannon, C. *A Mathematical Theory of Communication.* The Bell System Technical Journal. July, October, 1948. Vol. 27, pp. 379–423, 623–656

- Scherberger H, Jarvis MR, Andersen RA. Cortical local field potential encodes movement intentions in the posterior parietal cortex. *Neuron*. 2005 Apr 21;46(2):347–54.
- Schoffelen JM, Oostenveld R, Fries P. Neuronal coherence as a mechanism of effective corticospinal interaction. *Science*. 2005 Apr 1;308(5718):111–3
- Snyder LH, Batista AP, Andersen RA. Coding of intention in the posterior parietal cortex. *Nature*. 1997 Mar 13;386(6621):167–70.
- Stephan KE, Kamper L, Bozkurt A, Burns GA, Young MP, Kötter R. Advanced database methodology for the Collation of Connectivity data on the Macaque brain (CoCoMac). *Philos Trans R Soc Lond B Biol Sci*. 2001 Aug 29;356(1412):1159–86.
- Sugrue LP, Corrado GS, Newsome WT. Matching behavior and the representation of value in the parietal cortex. *Science*. 2004 Jun 18;304(5678):1782–7.
- Tanné-Gariépy J, Rouiller EM, Boussaoud D. Parietal inputs to dorsal versus ventral premotor areas in the macaque monkey: evidence for largely segregated visuomotor pathways. *Exp Brain Res*. 2002 Jul;145(1):91–103.
- Traub RD, Whittington MA, Stanford IM, Jefferys JG. A mechanism for generation of long-range synchronous fast oscillations in the cortex. *Nature*. 1996 Oct 17;383(6601):621–4
- Ungerleider, L. G., Mishkin, M. 1982. Two cortical visual systems. In *The Analysis of Visual Behavior*, ed. D. J. Ingle, R. J. W. Mansfield, M. S. Goodale, pp. 549–86. Cambridge, Mass: MIT Press
- Van Der Werf J, Jensen O, Fries P, Medendorp WP. Neuronal Synchronization in Human Posterior Parietal Cortex during Reach Planning. *J Neurosci*. 2010 Jan 27;30(4):1402–12.
- Verhoef BE, Vogels R, Janssen P. Synchronization between the end stages of the dorsal and the ventral visual stream. *J Neurophysiol*. 2011 May;105(5):2030–42.
- Vinck M, Battaglia FP, Womelsdorf T, Pennartz C. Improved measures of phase-coupling between spikes and the Local Field Potential. *J Comput Neurosci*. 2011 Dec 21. DOI: 10.1007/s10827-011-0374-4
- Volgushev M, Chistiakova M, Singer W. Modification of discharge patterns of neocortical neurons by induced oscillations of the membrane potential. *Neuroscience*. 1998 Mar;83(1):15–25.
- Wilke M, Logothetis NK, Leopold DA. Local field potential reflects perceptual suppression in monkey visual cortex. *Proc Natl Acad Sci U S A*. 2006 Nov 14;103(46):17507–12.
- Wise SP, Boussaoud D, Johnson PB, Caminiti R. Premotor and parietal cortex: corticocortical connectivity and combinatorial computations. *Annu Rev Neurosci*. 1997;20:25–42.

Womelsdorf T, Schoffelen JM, Oostenveld R, Singer W, Desimone R, Engel AK, Fries P. Modulation of neuronal interactions through neuronal synchronization. *Science*. 2007 Jun 15;316(5831):1609–12

Zhang Y, Chen Y, Bressler SL, Ding M. Response preparation and inhibition: the role of the cortical sensorimotor beta rhythm. *Neuroscience*. 2008 Sep 22;156(1):238–46. Epub 2008 Jul 8.